https://doi.org/10.15388/vu.thesis.381
https://orcid.org/0000-0002-3069-5734

VILNIUS UNIVERSITY

Mindaugas Lesanavičius

Reduction mechanisms of prooxidant xenobiotics by flavin-containing dehydrogenases – electrontransferases

DOCTORAL DISSERTATION

Natural sciences,
Biochemistry N 004

Vilnius 2022

The dissertation was prepared between 2017 and 2022 in Vilnius University, Life Sciences Center, Institute of Biochemistry. The research was supported by Lithuanian – French Programme "Gilibert" (P-LZ-19-10) and the European Social Fund (measure No. 09.33-LMT-K-712, grant No. DOTSUT-34/09.3.3-LMT-K712-01-0058/LSS-600000-58).

Academic supervisor –
Habil. Dr. Narimantas Čėnas (Vilnius University, Natural Sciences, Biochemistry, N 004).

This doctoral dissertation will be defended in a public meeting of the Dissertation Defence Panel:

Chairman – Prof. Habil. Dr. Albertas Malinauskas (Center for Physical Sciences and Technology, Natural sciences, Chemistry, N 003)
Members:
Dr. Gintautas Bagdžiūnas (Vilnius University, Natural Sciences, Biochemistry, N 004)
Prof. Dr. Rimantas Daugelavičius (Vytautas Magnus University, Natural Sciences, Biochemistry, N 004)
Prof. Dr. Jean-Pierre Jacquot (Université de Lorraine, Nancy, France, Natural Sciences, Biochemistry, N 004)
Dr. Lidija Tetianec (Vilnius University, Natural Sciences, Biochemistry, N 004)

The dissertation shall be defended at a public meeting of the Dissertation Defence Panel at 14:30 on the 29th September 2022 in Room R-104 of the VU LSC (7 Saulėtekio ave., LT-10257, Vilnius, Lithuania).
Tel. +370 5 223 4419; e-mail info@gmc.vu.lt

The text of this dissertation can be accessed at the library of Vilnius University as well as on the website of Vilnius University:
www.vu.lt/lt/naujienos/ivykiu-kalendorius

https://doi.org/10.15388/vu.thesis.381
https://orcid.org/0000-0002-3069-5734

VILNIAUS UNIVERSITETAS

Mindaugas Lesanavičius

Prooksidantinių ksenobiotikų redukcijos flavininėmis dehidrogenazėmis – elektrontransferazėmis mechanizmai

DAKTARO DISERTACIJA

Gamtos mokslai,
Biochemija N 004

Vilnius 2022

Disertacija rengta 2017 – 2022 metais Vilniaus universiteto Gyvybės mokslų centro Biochemijos institute.
Mokslinius tyrimus rėmė Lietuvos – Prancūzijos programa "Žiliberas" (P-LZ-19-10) ir Europos socialinis fondas (paraiškos numeris 09.33-LMT-K-712, granto nr. DOTSUT-34/09.3.3-LMT-K712-01-0058/LSS-600000-58, „Aromatinių nitrojunginių ir *N*-oksidų redokso chemija, biochemija ir citotoksiškumas: nauji požiūriai").

Mokslinis vadovas –
habil. dr. Narimantas Čėnas (Vilniaus universitetas, gamtos mokslai, biochemija, N 004).

Gynimo taryba:
Pirmininkas – prof. habil. dr. Albertas Malinauskas (Fizinių ir technologijos mokslų centras, gamtos mokslai, chemija, N 003)
Nariai:
dr. Gintautas Bagdžiūnas (Vilniaus universitetas, gamtos mokslai, biochemija, N 004)
prof. dr. Rimantas Daugelavičius (Vytauto Didžiojo universitetas, gamtos mokslai, biochemija, N 004)
prof. dr. Jean-Pierre Jacquot (Lorraine universitetas, Prancūzija, gamtos mokslai, biochemija N 004)
dr. Lidija Tetianec (Vilniaus universitetas, gamtos mokslai, biochemija, N 004)

Disertacija ginama viešame Gynimo tarybos posėdyje 2022 m. rugsėjo mėn. 29 d. 14:30 val. Vilniaus universiteto Gyvybės mokslų centro R-104 auditorijoje. Adresas: Saulėtekio al. 7, LT-10257, Vilnius, Lietuva.
Tel. +370 5 223 4419; el. paštas info@gmc.vu.lt

Disertaciją galima peržiūrėti Vilniaus universiteto bibliotekoje ir VU interneto svetainėje adresu:
https://www.vu.lt/naujienos/ivykiu-kalendorius

CONTENTS

ABBREVIATION LIST

$AcADP^+$ - 3-acetylpyridine adenine dinucleotide phosphate (oxidized)
AcADPH – 3-acetylpyridine adenine dinucleotide phosphate (reduced)
Adx – adrenodoxin
AdxR – adrenodoxin reductase
*An*FNR – *Anabaena nostoc* FNR
ArN→O – aromatic *N*-oxide
$ArNO_2$ – nitroaromatic compound
*Bs*FNR – *Bacillus subtilis* FNR
CaM – calmodulin
CTC – charge transfer complex
cyt *c* – cytochrome *c*
E_7^1 – single-electron reduction midpoint potential at pH 7.0
FAD – flavin adenine dinucleotide
Fcb2 – flavocytochrome b_2
Fd – ferredoxin
Fld – flavodoxin
FMN – flavin mononucleotide
FNR – ferredoxin:$NADP^+$ oxidoreductase
GrxR – glutathione reductase
H_4B – tetrahydrobiopterin
Hq – hydroquinone
k_{cat} – catalytic constant
k_{cat}/K_m – bimolecular rate constant
K_d – dissociation constant
K_i – inhibitory constant
K_m – Michaelis constant
eNOS – endothelial NO synthase
iNOS – inducible NO synthase
nNOS – neuronal NO synthase
NOS – nitric oxide synthase
Ox – oxidized
P-450R – NADPH:cytochrome P-450 reductase
PD – plasmodione
*Pf*Fd – *Plasmodium falciparum* ferredoxin
*Pf*FNR – *P. falciparum* FNR
Q – quinone
Red – reduced
*Rp*FNR – *Rhodopseudomonas palustris* FNR

ROS – reactive oxygen species
SOD – superoxide dismutase
*So*Fd – spinach (*Spinacia oleracea*) ferredoxin
*So*FNR – spinach FNR
Sq – semiquinone
σ – substituent constant
TPZ – 3-NH_2-1,2,4-benzotriazine dioxide (tirapazamine)
TrxR – thioredoxin reductase

INTRODUCTION

Flavoenzymes comprise some 3% of all enzymes, they are found in all groups of living organisms and have functions as diverse as reducing equivalent transfer in photosynthesis, DNA repair, detoxification of environmental pollutants and xenobiotics, apoptosis, cell signalling and more. For detailed recent reviews, the reader is referred to [1–5]. As the name implies, these enzymes contain a flavin moiety in the form of a flavin mononucleotide (FMN) or flavine adenine dinucleotide (FAD), which is usually bound noncovalently.

Flavoenzymes are often concerned with redox reactions where they usually play a role in transferring electrons further down the path. Aside from natural electron acceptors, a wide variety of nonphysiological electron acceptors are able to oxidize the flavins in such enzymes. These can be various environmental pollutants or xenobiotics, with nitroaromatic compounds ($ArNO_2$) belonging mostly to the former group, and quinones (Q) and aromatic *N*-oxides (ArN→O) being representative of the later one. Another important facet of flavoenzymes is the ability of their flavin prosthetic group to transform between one- and two-electron reduction.

Prooxidant xenobiotics (chemical substances found in an organism yet not naturally produced by it) can be reduced enzymatically with dehydrogenases – electrontransferases-performed catalysis taking the central role. Single-electron enzymatic reduction of these low-potential oxidants yields radical anion species which is then reoxidized by oxygen in a futile redox cycle thus forming the basis of their oxidative stress-based cytotoxicity.

The three enzymes studied in this work are representative of two distinct groups belonging to the dehydrogenase – electrontransferase family of flavoenzymes based on their physiological redox partners, namely acting on Fe-S proteins (ferredoxin:$NADP^+$ oxidoreductases from *Plasmodium falciparum* and *Rhodopseudomonas palustris*, (*Pf*FNR and *Rp*FNR, respectively)) or heme proteins (neuronal NO synthase, (nNOS)). Their reactions with nonphysiological oxidants and xenobiotics are the basis of mechanistic studies presented here that provide general insight into the mechanisms of enzymatic xenobiotic reduction and highlight specific features of each enzyme relevant to these processes.

GOAL AND TASKS OF THE THESIS

The goal of the thesis is the characterization of specific aspects of electron transfer mechanisms in two distinct subgroups of dehydrogenases –

electrontransferases, an arbitrary group of flavoenzymes, namely Fe-S protein reductases (*Pf*FNR, *Rp*FNR) and heme protein reductases (nNOS), and evaluation of one-electron reduction catalyzed by these enzymes.

The tasks to achieve the goal were as follows:

1. The evaluation of *Pf*FNR- and *Rp*FNR-catalyzed reduction of xenobiotics in light of other extensively studied ferredoxin:$NADP^+$ oxidoreductases from *Anabaena* and spinach (*An*FNR and *So*FNR, respectively);
2. The characterization of redox properties of a novel thioredoxin reductase-type (TrxR-type) *Rp*FNR with emphasis on its semiquinone state;
3. The analysis of nNOS-catalyzed reduction of xenobiotics with emphasis on the activating role of calmodulin (CaM) and the possible involvement of heme moiety in these reactions;
4. Evaluation of the applicability of rate constants of dehydrogenase – electrontransferase catalyzed single-electron reduction of xenobiotics in estimating their single-electron reduction potentials and electron transfer distances in these reactions.

IMPORTANCE AND SCIENTIFIC NOVELTY

1. It was shown that the reactivity of nNOS in terms of k_{cat}/K_m in the bioactivation of xenobiotics may be similar to that of cytochrome P-450 reductase (P-450R). It was shown for the first time that the heme moiety of nNOS, namely the Fe^{2+}-NO complex, may have a role in the reduction of external oxidants.
2. The electron transfer distances in the reactions of these dehydrogenases – electrontransferases calculated according to the outer sphere model of electron transfer show good agreement with data reported in earlier studies of homologous enzymes e.g., nNOS with P-450R and *Pf*FNR and *Rp*FNR with other FNRs.
3. It was shown that dehydrogenases – electrontransferases can be used for approximate determination of single-electron reduction potential of $ArNO_2$ and ArN→O with the calculated potential values being within 30 mV of the measured values.
4. *Pf*FNR, localized in the apicoplast of *P. falciparum*, could be a potential target for novel quinodal antimalarial agents. The results presented here provide general insights into the reduction mechanisms of prooxidant xenobiotics that could be considered as exerting oxidative stress on the protozoan upon their single-electron reduction.
5. Redox reactions catalyzed by a novel TrxR-like *Rp*FNR from a model organism *R. palustris* were investigated in depth, and quantitative analysis

of the obtained results was enabled by the determination of the redox potentials and semiquinone stabilization that are comparable to those of plastidic-type *So*FNR and *An*FNR.

STATEMENTS

1. Dehydrogenases – electrontransferases reduce quinones, nitroaromatics and aromatic *N*-oxides in a single-electron way according to a *ping-pong* mechanism. In all of these cases the reactivity of oxidants (log k_{cat}/K_m) increases with their single-electron reduction potential (E_7^1). The reactivity of nitroaromatics is systematically lower than that of quinones and aromatic *N*-oxides of analogous E_7^1. The rate limiting step is the oxidative half-reaction;
2. The enzyme-catalyzed reactions are in line with the outer sphere electron transfer model and the reactivity can be used to calculate approximate electron transfer distances;
3. The steady-state rate constants for single-electron reduction of certain classes of oxidants can be employed for an approximate assessment of their single-electron reduction potentials.

1. LITERATURE REVIEW

1.1. Flavoenzymes: general characteristics and classification

The extraordinary versatility of flavoenzymes stems from the nature of the flavin cofactor. It is a derivative of riboflavin (vitamin B_2) which is comprised of a tricyclic isoalloxazine ring system connected to a ribityl side chain at N-10 (Fig. 1). While the usual case is a tight noncovalent bond with the protein, there are some cases of the prosthetic group being bound covalently, usually at the 8-α or 6- positions [6]. In some cases a flavoenzyme will use a modified isoalloxazine or the ribityl side-chain.

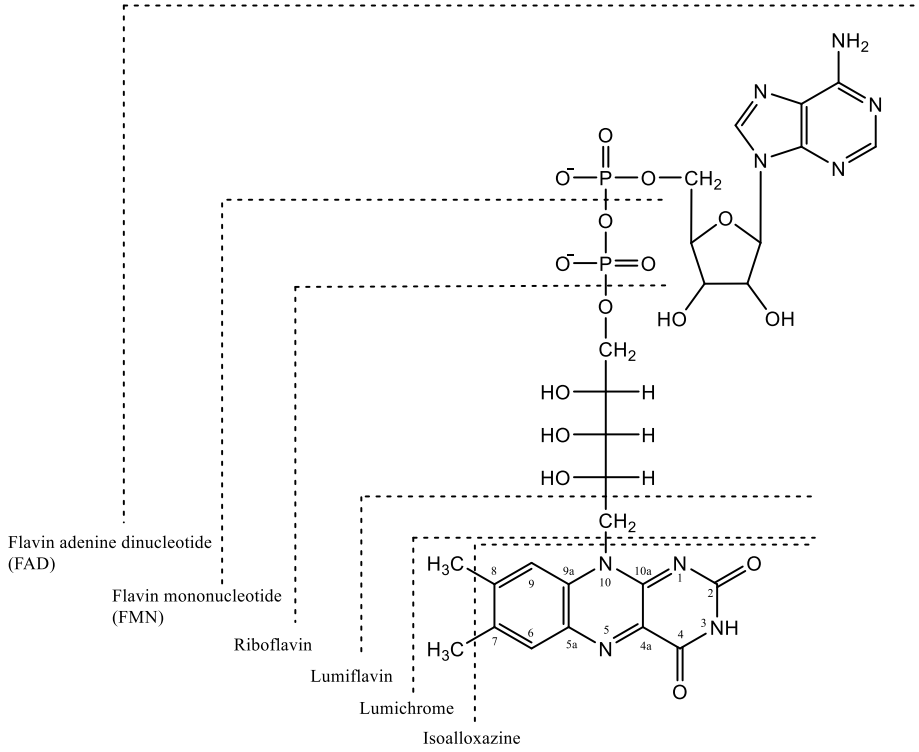

Figure 1. The structure of flavin species and the numbering system for isoalloxazine ring [7].

The isoalloxazine ring confers the chemical activity to the flavins: it is capable of one- and two-electron reduction and a nucleophilic attack is possible at both N-5 and C-4a atoms. A one-electron reduction yields a semiquinone (Sq), which can be either anionic or neutral, and a two-electron reduction produces a hydroquinone (Hq) form (Fig. 2). Although there are 9

possible redox states of flavins, at least six of them are possible under physiological conditions on the basis of pK_a values. The semiquinone form of free flavins and majority of flavoproteins is typically unstable but some proteins, e.g., flavodoxins, stabilize up to 90% of the semiquinone.

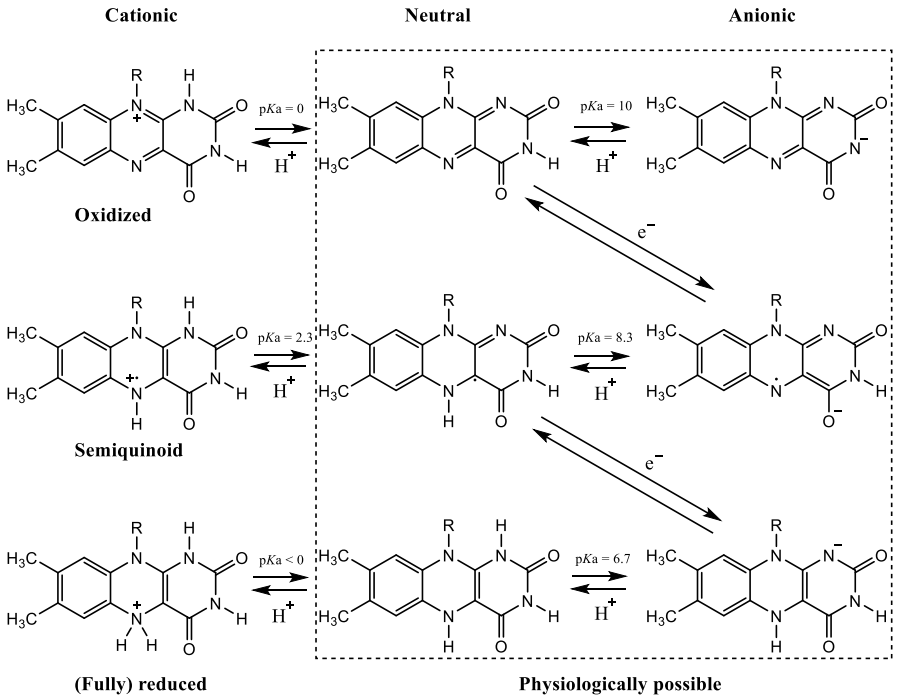

Figure 2. The chemical states of flavins [7].

According to the definition in encyclopedia of biophysics, redox potential is a measure of the propensity of a chemical or biological species to either acquire or lose electrons through ionization [8]. Thus, the reduction potential E^0 is a thermodynamic parameter characterizing an electron transfer process and measuring the tendency of an oxidized molecule to become reduced. The difference in reduction potentials between any two species ΔE is related to equilibrium constant K_{eq} and the standard free energy change for the reaction ΔG^0 according to Eqs. 1 and 2

$$\Delta E^0 = -\frac{\Delta G^0}{nF} = \frac{RT}{nF}\ln K_{eq} \quad (1)$$

$$\Delta E = \Delta E^0 - \frac{RT}{nF}\ln\left(\frac{a_{A_{red}} a_{B_{ox}}}{a_{A_{ox}} a_{B_{red}}}\right) \quad (2)$$

where ΔE^0 is the standard reduction potential, n is the number of electrons in the reaction, F is the Faraday constant, R is the universal gas constant, T is temperature and a is the activity of the reacting species A and B.

The value of the reduction potential can be influenced by various factors, namely the protein *per se* and the surrounding solution. The chemical nature of ligands, coordination geometry and noncovalent interactions, including steric effects and electrostatic interactions are exerted by the protein, whereas the solvent influence stems from temperature, pH and ion effects. Any such arising modifications will inevitably translate into changes in the kinetics of an electron transfer reaction. The two-electron reduction (standard) potential of a free flavin at pH 7.0 (E_7^0) is −207 mV, but due to the effects of apoprotein it can reach as low as −495 mV for Sq/Hq pair and +40 mV for Ox/Hq pair in proteins.

Most typically, flavoenzymes exhibit *ping-pong* kinetics. A *ping-pong* reaction is characterized by both the oxidant and the reductant binding to either the same reaction center or to reaction centers that overlap sufficiently. In other words, the k_{cat}/K_m value for one substrate does not depend on the concentration of the second substrate, i.e., the k_{cat}/K_m of a reductant does not depend on the concentration of the oxidant. The oxidative and reductive half-reactions seen in the enzymatic cycle are accompanied by typical shifts in absorbance. An oxidized isoalloxazine cofactor exhibits absorbance maxima (λ_{max}) at ~360 nm and ~450 nm, the later falling sharply upon reduction. While free FMN and FAD exhibit extinction coefficient (ε) of 12.5 and 11.3 $mM^{-1}cm^{-1}$, respectively, their binding to a protein affects the value [9]. The semiquinone resulting from one-electron reduction can be neutral (protonated, blue) or anionic (deprotonated, red) and have distinct absorbances. The neutral semiquinone exhibits a broad peak in the ~580 – 620 nm region ($\varepsilon \approx 3.8 – 5.0$ $mM^{-1}cm^{-1}$), while the anionic semiquinone absorbs at 380 ($\varepsilon \approx 16$ $mM^{-1}cm^{-1}$) with an additional sharp peak at 400 nm [10,11]. These spectral characteristics are then employed in the studies of rapid kinetics of the flavoenzyme catalyzed reactions, the binding of substrates and inhibitors or insights into the flavin environment in the protein.

It should come as no surprise that the ever-increasing amount of new information about flavoenzymes and various novel examples among them make a rigid albeit overarching classification both difficult and quite necessary. A classification proposed by Hemmerich and Massey remains the predominant one in this field even though it should not be regarded as absolute [11,12]. Flavoenzymes are divided into five classes according to whether their

activity is exerted through hydrogen transfer alone or electron transfer alone or a combination of the two, as follows:

1) Transhydrogenases do not exert one-electron transfer or oxygen activation and are further subdivided because of the restrictive nature of the historical use of the term:
   a) Carbon – carbon transhydrogenases. 2 electrons are transferred between the carbon centers while pyridine nucleotides act as electron donors, acceptors or both;
   b) Carbon – sulfur transhydrogenases. 2 electrons are transferred between a pyridine nucleotide and a disulphide – dithiol pair;
   c) Carbon – nitrogen transhydrogenases employ electron transfer flavoproteins (ETFs) as redox partners;
   d) Nitrogen – nitrogen transhydrogenases catalyse two-electron transfer with ETFs.
2) Dehydrogenases – oxidases perform a two-electron reduction of O_2 by dehydrogenating the substrate, with a concomitant production of H_2O_2; the flavin accepts two electrons.
3) Dehydrogenases – oxygenases catalyze the consumption of four redox equivalents from O_2 without the liberation of H_2O_2, i.e., an oxygen atom is reduced to water while the other oxygen atom is incorporated into the substrate as a hydroxyl group.
4) Dehydrogenases – electrontransferases act as transformers between two-electron and one-electron transfer. While the flavin is reduced by two electrons, its reoxidation proceeds in a stepwise manner with a one-electron reduction of electron acceptors such as cytochromes or iron – sulfur proteins.
5) Pure electrontransferases (flavodoxins) are the simplest flavoproteins, the flavin is reduced and reoxidized during a one-electron transfer without the catalysis of an enzymatic reaction.

While there are various other attempts to classify flavoenzymes based on different properties, none seem to be satisfactory [13]. For example, C – O transhydrogenases such as NAD(P)H:quinone oxidoreductase (NQO1, DT-diaphorase) and nitroreductases were not considered originally, yet there are examples of flavoenzymes falling under this category [14]. One recent attempt to revise the classification is worth mentioning, since the flavoenzymes are grouped into four groups according to the amount of electrons transferred during the reductive and oxidative half-reactions [7]. Accordingly, dehydrogenases – electrontransferases could then be considered as class 2/1 enzyme.

1.2. Single-electron reduction of redox active xenobiotics (quinones, nitroaromatic compounds, aromatic *N*-oxides) by flavoenzymes

Quinones, nitroaromatics and aromatic *N*-oxides are structurally distinct classes of compounds, comprising several important groups of redox active xenobiotics with sometimes similar functions, such as anticancer agents (quinones and aromatic *N*-oxides), antibacterial and antiparasitic drugs (nitroaromatics and aromatic *N*-oxides), explosives and pesticides (nitroaromatics). These compounds can undergo reduction in various ways and accept from up to two (quinones) to six (nitroaromatics) electrons.

In the case of quinones, their net reduction is a reversible two-step process with the formation of an unstable semiquinone radical intermediate:

$$Q + e^- \rightleftharpoons Q^{\bullet -} + e^- + 2H^+ \rightleftharpoons QH_2 \qquad (3)$$

The standard (two-electron reduction) reduction potential (E_7^0) for a Q/QH_2 couple varies from −0.30 V to 0.28 V [15], but is generally higher than the E_7^1 values for respective couples, i.e., $E_7\left(Q/Q^{\bullet -}\right) < E_7\left(Q^{\bullet -}/QH_2\right)$, thus explaining the low stability of a semiquinone. Moreover, there exists a partial correlation between one- and two-electron reduction potentials of quinones with the deviations being pronounced in quinones with halogen substituents, ionized substituents, and in the case of intramolecular hydrogen bond formation [16]. Electron donating substituents and the number of aromatic rings in the system are factors decreasing the E_7^1 values, which in the case of common relatively simple quinones range from −0.46 V (2-CH_3-3-OH-1,4-naphthoquinone, phthiocol) to 0.09 V (1,4-benzoquinone, *p*-quinone) (table 1) [15,17].

Table 1. The decrease in redox potential due to electron-donating substituents or increase in the aromatic ring system [17,18].

Quinone	E_7^1**, V**
1,4-benzoquinone	0.09
2,5-$(CH_3)_2$-1,4-benzoquinone	−0.07
$(CH_3)_4$-1,4-benzoquinone	−0.26
1,4-naphthoquinone	−0.15
9,10-anthraquinone	−0.445
2-CH_3-3-OH-1,4-naphthoquinone	−0.46

Quinones can be reduced in single-electron, two electron or mixed (single- and two-electron) way by flavoenzymes. Dehydrogenases – electrontransferases usually perform one-electron reduction and a common theme for these enzymes is them having natural single-electron acceptors

(cytochromes, Fe-S proteins), for example NADPH:cytochrome P-450 reductase (P-450R), NO synthase (NOS), ferredoxin:$NADP^+$ oxidoreductase (FNR), NADH:ubiquinone oxidoreductase, NADH:cytochrome b_5 reductase. Generally, there is a flavin cofactor (FMN or FAD), that is reduced by two electrons coming from an electron donor, NAD(P)H. Two successive single-electron transfer steps follow, with the now-reduced enzyme reducing two molecules of a quinone. The resulting semiquinone radicals can be rapidly reoxidized by oxygen, with reoxidation resulting in a regeneration of the quinone; this redox cycling also leads to the formation of reactive oxygen species, namely superoxide anion and hydrogen peroxide (Eqs. 4 and 5) with the subsequent formation of a hydroxyl radical in a Fenton reaction (Eqs. 6 and 7). These reactions are the basis of cytotoxicity of quinones due to the oxidative stress.

$$Q^{\bullet -} + O_2 \rightleftharpoons Q + O_2^{\bullet -} \tag{4}$$

$$2O_2^{\bullet -} + 2H^+ \rightleftharpoons H_2O_2 + O_2 \tag{5}$$

$$O_2^{\bullet -} + Fe^{3+} \rightleftharpoons O_2 + Fe^{2+} \tag{6}$$

$$Fe^{2+} + H_2O_2 \rightleftharpoons Fe^{3+} + OH^- + OH^{\bullet} \tag{7}$$

While two-electron reduction of quinones is outside of the scope of this work, a brief outline will be given. In a model reaction, nonenzymatic reduction of quinones by NADH [19,20], a two-electron reduction proceeds concomitantly with the transfer of two protons and may thus be considered a net hydride and H^+ transfer:

$$NADH + Q + H^+ \longrightarrow NAD^+ + QH_2 \tag{8}$$

The two most common models are a single step (H^-) and a three-step (e^-, H^+, e^-) hydride transfer mechanisms (Eqs. 9 and 10):

$$NADH + Q \longrightarrow NAD^+ + QH^- \xrightarrow{+H^+} NAD^+ + QH_2 \tag{9}$$

$$NADH + Q \underset{k_{-1}}{\overset{k_1}{\rightleftharpoons}} NAD^{\bullet +} \cdots QH^{\bullet -} \xrightarrow{k_H} NAD^{\bullet} \cdots Q^{\bullet} \longrightarrow NAD^+ + QH^- \tag{10}$$

Taken together, it is possible to devise a simplistic unified scheme for the single-, two- and mixed single- and two-electron reduction of quinones by flavoenzymes. The formation of flavin/quinone ion-radical pair happens after the first electron transfer; this pair can then either undergo a sequential (steps a and d) or a concerted proton and second electron transfer (step b) or dissociate (step c) with the product of step c then undergoing an oxidation by a second molecule of quinone (Fig. 3) [21].

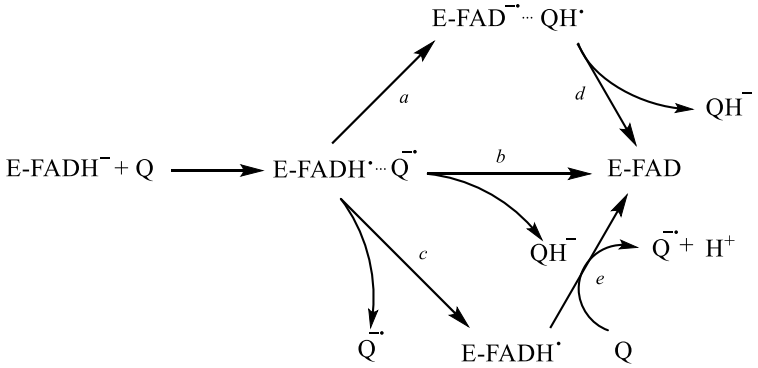

Figure 3. The single- and two-electron reduction of quinones by flavoenzymes [21].

Nitroaromatic compounds can be reduced in various ways. In general, a nitroaromatic compound is reduced by a single electron to yield an anion radical and a general scheme of reduction is given in Eq. 11:

$$ArNO_2 \xrightarrow{e^-} ArNO^{\bullet -} \xrightarrow[-H_2O]{e^-, 2H^+} ArNO \xrightarrow{2e^-, 2H^+} ArNHOH \xrightarrow[-H_2O]{2e^-, 2H^+} ArNH_2 \quad (11)$$

The resulting nitroradicals are then reoxidized by oxygen with the formation of a superoxide radical, which is converted into hydrogen peroxide and a hydroxyl radical, leading to futile redox cycling and oxidative stress according to Eqs. 4 – 7. Under aerobic conditions polynitroaromatic compounds, frequently used as explosives, are reduced analogously. The log k_{cat}/K_m values for these compounds increase with increasing E_7^1, and the high reactivity is the result of single-electron reduction energetics, which is influenced by electron-accepting substituents, rather than the structure of a compound *per se*. The high reactivity of polynitroaromatics as a function of energetics rather than structure is further supported by quantum mechanical calculations [22,23].

Dehydrogenase – electrontrasferase-catalyzed quinone or nitroaromatic compound reduction can be considered an example of the outer-sphere electron transfer model [24]. An electron transfer event occurring between chemical species that remain separate over its duration is considered to be outer sphere, i.e., the interaction between the reagents is weak. According to the Marcus theory, the thermodynamic driving force is responsible for the electron transfer rate; moreover, this transfer rate is inversely proportional to the so-called reorganization energy. It then follows that a one-electron transfer rate constant k_{12} is dependent on the electron self-exchange rate constants of the reagents, k_{11} and k_{22} and an equilibrium constant K:

$$k_{12} = \sqrt{(k_{11} \times k_{22} \times K \times f)} \quad (12)$$

$$\log K = \frac{\Delta E^1}{0.059\text{V}} \tag{13}$$

$$\log f = \frac{(\log K)^2}{4\log\left(\frac{k_{11} \times k_{22}}{Z^2}\right)} \tag{14}$$

where ΔE^1 is the 1 e^- transfer potential and Z is the frequency factor, 10^{11} $M^{-1}s^{-1}$ [24]. Thus for a series of homologous compounds (k_{22} = constant), log k_{12} will be characterized by a parabolic (quadratic) dependence on ΔE^1 with a characteristic slope of 8.45 V^{-1} at $\Delta E^1 = \pm 0.15$ V for quinones. The $k_{22} = \sim 10^8$ $M^{-1}s^{-1}$ for quinones [25] and aromatic *N*-oxides [26] and is 100-fold higher than that of nitroaromatics, where $k_{22} = \sim 10^6$ $M^{-1}s^{-1}$ [27]. The later are usually characterized by a linear dependence and their reactivity is an order of magnitude lower than that of quinones. Such interrelationships have been documented for various dehydrogenases – electrontransferases, including P-450R, FNR and NOS [21,28,29].

Aromatic *N*-oxides are reduced enzymatically with concomitant free radical generation with 3-NH_2-1,2,4-benzotriazine-1,4-dioxide (tirapazamine, TPZ) being the most comprehensively studied (Fig. 4):

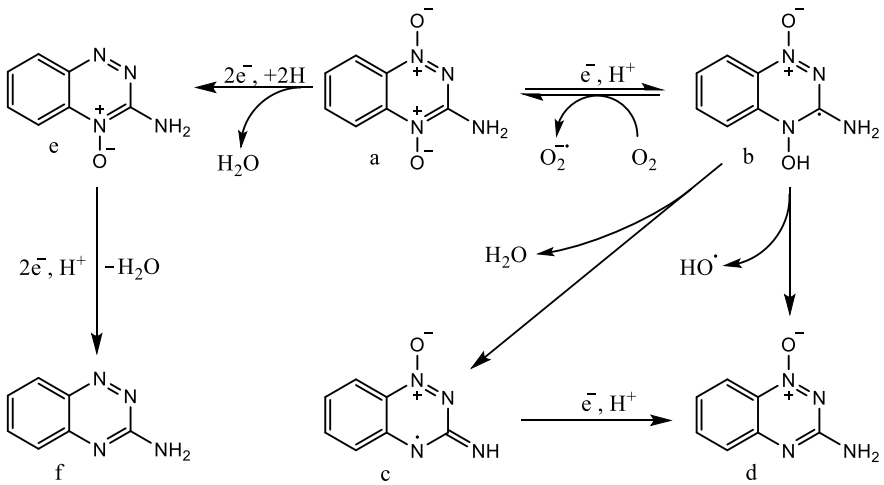

Figure 4. The mechanism of tirapazamine reduction.

Upon enzymatic reduction of TPZ (a) in a single-electron way to a free radical (b) under hypoxic conditions, a DNA damaging species, namely an oxidizing hydroxyl radical [30–32] and/or a reactive benzotriazinyl radical (c) forms. The relatively nontoxic final metabolites of TPZ are its mono-*N*-oxide (d) and its nor-oxide (f) [30,31,33]. The aerobic cytotoxicity of ArN→O is typically

attributed to redox cycling with oxidative stress due to the formation of superoxide $O_2^{\bullet-}$ [30,34].

Redox cycling is an intrinsic property of Qs, $ArNO_2$ and ArN→O which means that oxidative stress is an obligatory process under aerobic conditions [35]. Enzymatic formation of the anion radical and redox cycling are considered to be the main factors in cytotoxicity, which can then be described by a quantitative structure-activity relationship (QSAR) (Eq. 15):

$$\log cL_{50} = a + bE_7^1 + c\log P(\log D) \qquad (15)$$

where cL_{50} is compound concentration causing 50% cell death or analogous quantitative parameter, log*P* is octanol/water partition coefficient and log*D* is octanol/water distribution coefficient at pH 7.0 [36–41] with these dependences mirroring log (rate constant) *vs.* E_7^1 relationships in single-electron reduction by dehydrogenases – electrontransferases.

Dehydrogenases – electrontransferases known to participate in the single-electron reduction of xenobiotics can be arbitrarily grouped as reacting with iron-sulfur (Fe-S) proteins or heme proteins according to different roles of their redox partners in the reduction of xenobiotics rather than different redox properties. Their mechanisms of action will be considered in the following chapters.

1.3. Electrontransferases reacting with iron-sulfur proteins

Flavoenzymes Fe-S reductases either have Fe-S proteins as redox partners or perform the intramolecular electron transfer to a Fe-S redox center. The direction of electron transfer is not uniform as there are examples of enzymes transferring electrons either to or from the Fe-S centers (Fig. 5). Some of the examples of enzymes belonging to this subclass are $NADP^+$:ferredoxin oxidoreductase (FNR) (recently extensively reviewed in [42], NADPH:adrenodoxin reductase (AdxR) and NADH:ubiquinone reductase (CoQR, complex I).

1.3.1. NADPH:adrenodoxin reductase

NADPH:adrenodoxin reductase (AdxR, EC 1.18.1.6) is a monomeric 51 kD FAD containing enzyme first isolated from bovine adrenal cortex. It functions as the first enzyme in the mitochondrial P-450 systems catalyzing essential steps in steroid hormone biosynthesis. The FAD coenzyme is reduced by two electrons coming from NADPH and they are then transferred to the Fe_2S_2 13 kD protein adrenodoxin (Adx) one at a time. Electrostatic interactions between the positively charged amino acid residues of AdxR and

negatively charged residues of Adx determine the AdxR-Adx complex formation.The redox potential of FAD/$FADH_2$ couple is calculated to be between −0.250 V and −0.274 V while E_7^1(FAD/$FADH^{\bullet}$) = −0.320 V [43]. The redox potential for free Adx is −0.260 V. The reduction of AdxR by NADPH is characterized by a maximal rate of 28 s^{-1} at pH 7.0 [44]. The reduction of AdxR by NADPH proceeds via the formation of a $FADH_2$-$NADP^+$ charge-transfer complex (CTC) ($K_d \approx 10^{-8}$ M). Reaction product $NADP^+$ can bind to the oxidized or semiquinone form of AdxR, however the affinity is lower.

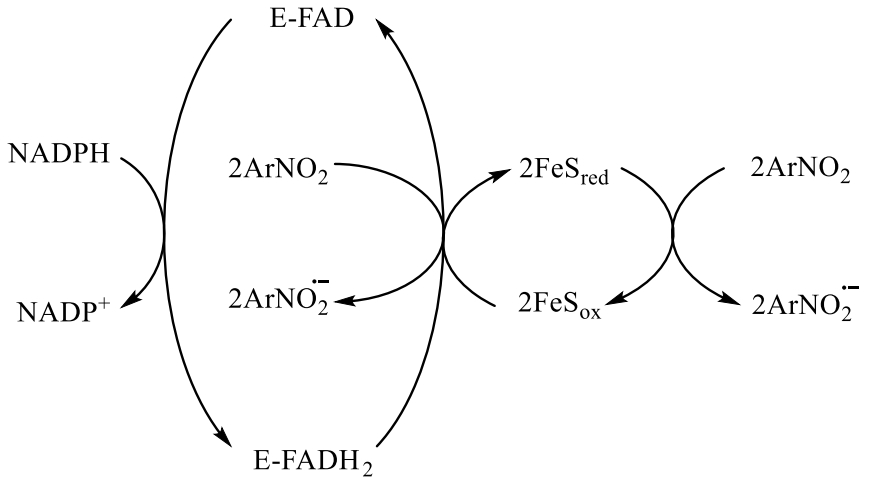

Figure 5. The principal scheme of a Fe-S reductase-catalyzed reduction of nitroaromatic compounds.

The steady-state reactions of quinone or $ArNO_2$ reduction by AdxR proceed with a k_{cat} value of 20 – 25 s^{-1}, which is close to the maximal rate of enzyme reduction by NADPH [45]. The k_{cat}/K_m values for the AdxR catalyzed reduction of nitrofurans extrapolated to [NADPH] = 0 are low, reaching 4.0 × 10^3 $M^{-1}s^{-1}$ [46]. NADPH was found to exert inhibitory action with respect to oxidants and K_i = 5.0 – 6.0 μM. An explanation was given that quinones and $ArNO_2$ are able to oxidize both the free enzyme form and its complexes with NADPH and $NADP^+$, although these are oxidized at slower rates. AdxR-catalyzed $ArNO_2$ reduction was stimulated by Adx, i.e., the inhibition by NADPH diminished and an alternative more efficient reductive pathway via reduced Adx appeared with k_{cat}/K_m values becoming much higher. The dependence of log k_{cat}/K_m values on the E_7^1 of oxidants is supportive of an outer-sphere electron transfer mechanism with quinones being more reactive than nitroaromatics of similar E_7^1 values.

1.3.2.Ferredoxin:$NADP^+$ oxidoreductases

Ferredoxin:$NADP^+$ oxidoreductases (FNRs, EC 1.18.1.2) are dehydrogenases – electrontransferases utilizing a non-covalently bound FAD as a prosthetic group for electron transfer in plastids, mitochondria and bacteria. FNR catalyzed two electron transfer from two equivalents of reduced ferredoxin (Fd) to $NADP^+$ (Eq. 16) is the final step of electron transfer in photosynthesis. The generated NADPH is used for CO_2 fixation by plants and cyanobacteria [47]:

$$2Fd_{red} + NADP^+ + H^+ \rightleftharpoons 2Fd_{ox} + NADPH \quad (16)$$

FNR participation in various other redox processes, such as nitrogen fixation or isoprenoid biosynthesis, is characterized by electrons transported in the opposite direction with the reduction of Fd and/or another electron acceptor following the oxidation of NADPH. Thus, the general reaction in FNR catalysis proceeds in two steps

$$NADPH + H^+ + FNR_{ox} \rightleftharpoons NADP^+ + FNRH_2 \quad (17)$$

$$FNRH_2 + nA_{ox} \rightleftharpoons FNR_{ox} + nA_{red} \quad (18)$$

with a FAD semiquinone forming after the transfer of a single electron to the oxidant (A) during the second step (Eq. 18).

FNRs can be classified into two protein families that are phylogenetically and structurally unrelated, namely plant-type and glutathione reductase-type FNRs, which are then further subdivided (Fig. 6). Classification of FNRs is based on the comparisons of the three-dimensional structures and amino acid sequences, hence the further subdivisions. Moreover, plant-type FNRs differ among themselves in the environment of the active site, the conformation of the coenzyme and the catalytic efficiency. Plant type FNRs are best characterized, whereas glutathione reductase-type FNRs can be considered novel. Bacterial-type FNRs are the most divergent group of plant-type FNRs. They differ from plastidic-type FNRs functionally, since they are concerned with nitrogen fixation and detoxification of reactive oxygen species. In addition to ferredoxin, bacterial-type FNRs can use flavodoxin (Fld), an FMN-containing electron transfer protein. Moreover, bacterial-type FNRs all exhibit k_{cat} values that are two orders of magnitude lower than that of the plastidic-type FNRs [48].

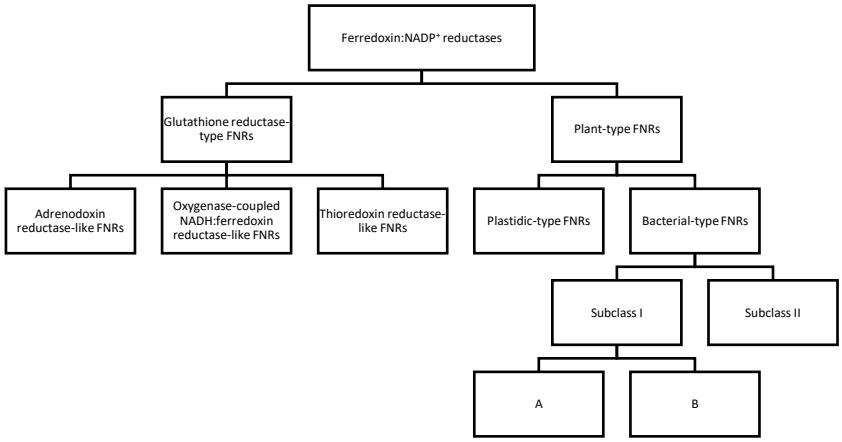

Figure 6. The classification of FNRs.

FNRs of either family are composed of distinct FAD- and NADP-binding domains, both of which are composed of approximately 150 amino acids. The topology of NADP-binding domain is the same in both families, whereas there are differences in the FAD-binding domain. Plant-type FNR FAD-binding domain is composed of the *N*-terminal part of the polypeptide chain, however it is formed from two discontinuous segments in the glutathione reductase-type FNRs. While most of known FNRs are monomeric, the glutathione reductase-type FNRs are distinct from the plant-type FNRs in being homodimeric. The *N*- terminal domain adopts the β barrel structure and the *C*- terminal domain has a characterstic α-helix/β-strand fold. Residues for NADP(H) binding are situated in the *C*-terminal domain. The isoalloxazine ring of FAD is shielded from the environment by the bulky terminal Tyr stacked on the *re*- face and likely displaced upon $NADP^+$ binding. However, the edge of the dimethylbenzene ring is exposed to the solvent thus enabling it to transfer electrons to other protein substrates.

FNRs belonging to the plastidic-type have a conserved Tyr residue at the *C*- terminus of the molecule. The prosthetic group is bound in an extended conformation and a second Tyr residue interacts with the adenine moiety. A common amino acid cluster corresponds to the protruding sheet-loop-sheet fragment that interacts with 2′-P-AMP region of FAD in plastidic-type FNRs whereas it is absent in bacterial-type FNRs where FAD consequently adopts a twisted conformation [49].

The nicotinamide ring of the electron donor must be in close proximity to the isoalloxazine moiety during the enzyme catalysis for direct hydride transfer to occur [50–53]. Substrate entry is facilitated by a reorientation of

the *C*- terminal amino acid residue [52]. 2′-P-AMP of NADP(H) first interacts with a preformed binding site, however the nicotinamide is distant to the catalytic site, which means that the nucleotide is bound in an unproductive conformation to the enzyme. After the initial binding, the nicotinamide is then positioned close to the isoalloxazine ring and a productive conformation is established. However, this is based on the findings in mutagenesis structures, where the terminal Tyr is replaced by a Ser [50,54].

As mentioned earlier, FNRs are found in a variety of organisms and participate in several different processes. FNR catalyzed reaction in photosynthesis is one of the rate-limiting steps and the enzyme functions in controlling the balance between the demand for reducing equivalents and photosynthetic activity [55,56]. The transhydrogenase reaction *in vivo* is speculated to be responsible for the intrachloroplastic NADH generation [57].

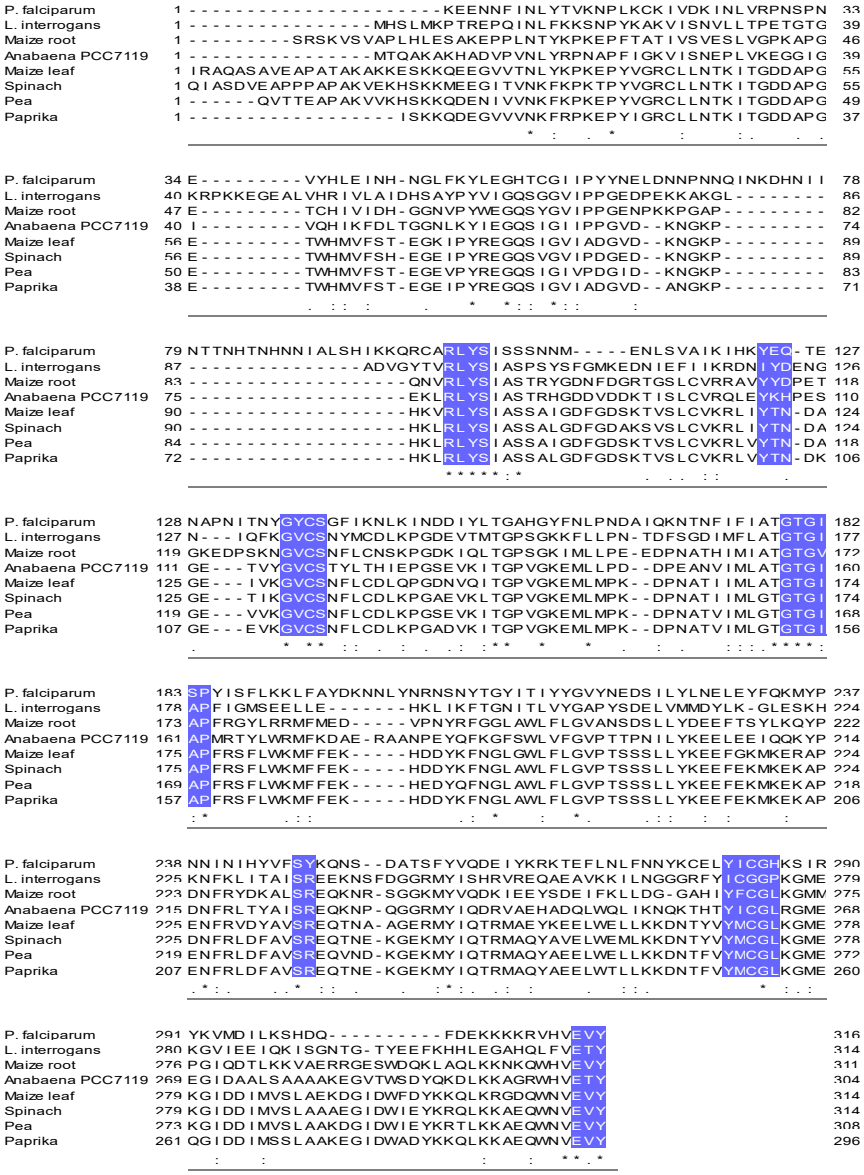

Figure 7. Multiple sequence alignments of plastidic-type FNRs. Sequence motifs are presented in boxes. * indicates positions with a fully conserved residue, : and . indicate groups with strongly and weakly similar properties, respectively. Accession codes in https://www.rcsb.org/ are as follows: 2OK8 (*P. falciparum*), 2RC5 (*Leptospira interrogans*), 3LO8 (maize root), 1GJR (*Anabaena* PCC7119), 1GAW (maize leaf), 1FNB (spinach), 1QG0 (pea), 1SM4 (paprika).

The electron transfer from reduced Fd to $NADP^+$ is thought to occur via the formation of a ternary complex (Fig. 8) [58,59]. Upon $NADP^+$ binding to FNR, a molecule of reduced Fd binds to and reduces FNR to the semiquinone. The oxidized Fd then dissociates and a second molecule of Fd binds to the FNR-$NADP^+$ complex; the semiquinone is then reduced to hydroquinone with a final transfer of two reducing equivalents from the enzyme to $NADP^+$. Steady-state kinetics measurements show that diaphorase and transhydrogenase activities proceed via a *ping-pong* mechanism [60–62]. The optimum pH for FNR is 7.5 – 8.0 [63,64], whereas the pI is in the range of 5.5 – 6.8 [65].

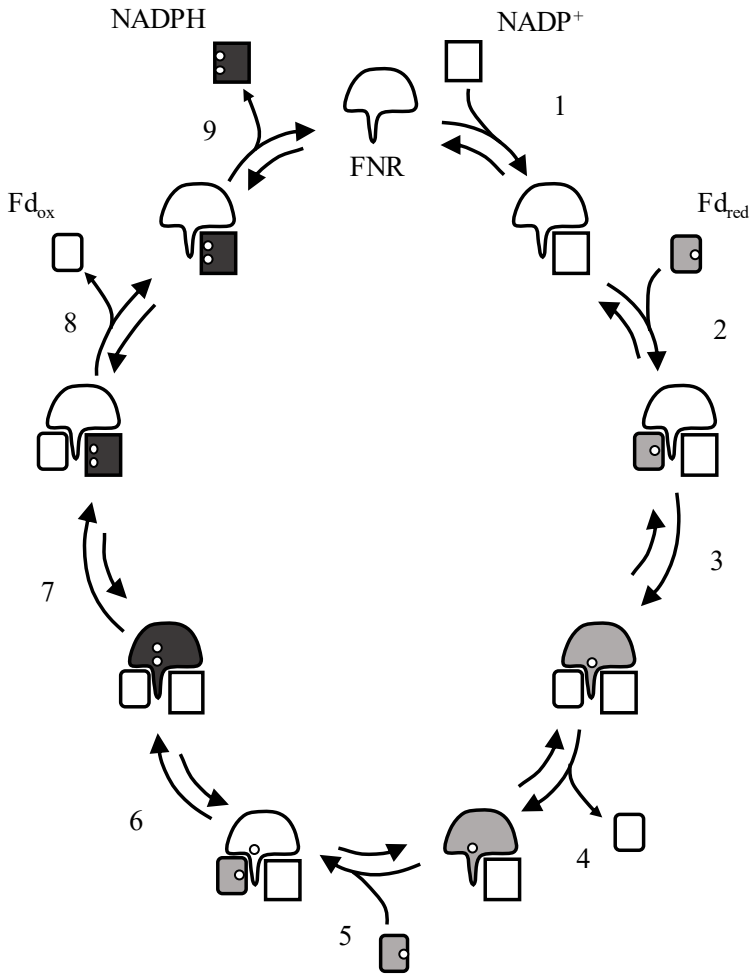

Figure 8. The electron transfer mechanism of FNR. Adapted from [58].

Table 2. Kinetic and binding parameters for various activities and interactions of FNR [58].

Reaction	Source of FNR					
	K_m or K_d (μM)			k_{obs} or k_{cat} (s^{-1})		
	S. oleracea	*Anabaena*	*E. coli*	*S. oleracea*	*Anabaena*	*E. coli*
Binding						
FNR_{ox}-$NADP^+$	15	6		-	-	-
FNR_{ox}-Fd_{ox} (Fld_{ox})	<1	4 (3)[a]	0.5 (2)[a]	-	-	-
Electron transfer						
Fd_{red} → FNR → $NADP^+$	10[b]			600	>200	
	1[b]					
Fd_{red} (Fld_{red}) → FNR_{ox}		10		>600[c]	6200 (>600)[c,a]	8 (25)[a]
				60[c]	250 (>600)[c,a]	(8)[a]
FNR_{red} → $NADP^+$				500	>600	
NADPH → FNR → Fd_{ox} → cyt *c*	10[b]	6[b]	4[b]	250	225	20
	1[b]	15[b]	2[b]			
NADPH → FNR → Fld_{ox} → cyt *c*			4		23 – 80	5
		33	7			
NADPH → FNR_{ox}	<2		<5	>600[d]	>600[d]	22
				200[d]	>140[d]	
FNR_{red} → Fd_{ox} (Fld_{ox})			<5 (<5)[a]		>600 (3)[a]	2 (0.01)[a]
NADPH → FNR → $K_3Fe(CN)_6$	30[b]	23[b]	10[b]	550	225 – 520	27
	100[b]	170[b]	24[b]			

[a] – values in parentheses are those for Fld; [b] – the upper and lower numerals indicate K_m estimates for electron donors and acceptors, respectively; [c] – the upper and lower values are for the rates of transfer of the first and second e^-, respectively; [d] – the upper and lower numerals show the rates of formation of CTC and rates of hydride transfer, respectively.

1.3.3. FNRs from spinach and *Anabaena*

Spinach FNR was crystallized for the first time by Shin and coworkers and given the name of ferredoxin-TPN reductase in 1962 [66] and its purification followed an intense period of studies of ferredoxin and photosynthesis in general. The enzyme is composed of two domains of approximately equal length. An antiparallel β barrel composes the core of the FAD domain, with it being flattened and having distinct edges [67]. The flavin of the prosthetic group is inserted at the domain boundary with ribose and adenine parts of the molecule being exposed while making only limited contact with Leu118 and Tyr120. However, hydrogen bond-enabled stabilization is seen for the pyrophosphate with Arg93, Ser133 and three peptide amides from residues 131 – 137 [67]. Gly130 facilitates a close approach between the α helix and the pyrophosphate, whereas Tyr95 forms a hydrogen bond with the ribityl 3′-hydroxyl.

The NADP domain is made of five parallel β strands and six α helices. Data about this domain is obtained using 2′-P-AMP, a competitive inhibitor of $NADP^+$, as its binding places the NADP binding site at the *C*- terminal edge of the sheet. Gln248 carbonyl forms hydrogen bonds with adenine [68], while the 2'-phosphate forms four hydrogen bonds with Ser234, Arg235, Lys244 and Tyr246 [67,68]. These hydrogen bonds are thought to be responsible for the discrimination between NAD^+ and $NADP^+$ [69]. Tyr246, Leu274 and Gly203-Val204-Pro205 form nonpolar contacts with the 2′-P-AMP after some movement. Upon binding, the nicotinamide ring displaces Tyr314 thus facilitating the N-5 to C-4 hydride transfer from FAD. Nicotinamide moiety also establishes contacts with Cys272 and Glu312; however, if the former is important in catalysis based on mutagenesis studies [70], the latter is dubious because of the proposed movement of a neighboring Tyr314. Ser96 interacts with the N5 atom of the flavin, which is responsible for the catalytic activity. The *si*-face is covered by the hydrogen-bond forming amino acid residues from the FAD domain, while the *re*-side is facing the NADP domain with terminal Tyr314 covering it. Ser75, Leu94 and Glu312 make up the surface around the solvent-exposed edge of the dimethyl benzyl ring.

Ferredoxin makes contact with FNR in the shallow cleft formed between the two domains, where the dimethylbenzene part of FAD is exposed. The complex between *So*FNR and *So*Fd forms via crosslinks between FNR 72-91/Fd 53-97 and, to a minor extent, FNR 2-15/Fd 5-40 with FNR residues being the amino donors due to Lys85 and/or Lys88 [71]. The *C*-terminal region of ferredoxin has several negatively charged glutamic acid residues

(Glu92-Glu94), with Glu92 being the most likely. Leu92, Leu94, Val151, Val311 and Val313 are thought to be contributing to the binding strength of the two proteins due to their hydrophobicity [68]. The crosslink between the *N*- terminal parts of the proteins is postulated to be formed by −COOH donating Asp20, Asp21 or Asp26 in *So*Fd and the $-NH_2$ of Ile2 in *So*FNR with no internal crosslinks in ferredoxin or reductase [71]. In case of the major crosslink, one has to note that there is a cluster of positive charges, namely Lys85, Lys88, His90, Lys91 and Arg93.

*So*FNR can be considered an oxygen sensitive nitroreductase. When acting on tetryl, nitrite is released. K_m for tetryl is 130 μM (20 mM Tris, pH 8.6) and it is transformed to *N*-methylpicramide upon reduction [72]. Upon aerobic conditions, the release of nitrite was inhibited by 60 – 65%. This, together with the necessity of tetryl for oxygen consumption by FNR and diminishing oxygen uptake upon addition of superoxide dismutase or catalase points to a nitroanion radical formation.

FNR was found to reduce various anthracyclines, including daunomycin, aclacinomycin A, nogalamycin and their respective 7-deoxyanthracyclinones, that are antitumor antibiotics having a quinone moiety that is presumed to be responsible for their oxidative effect [73]. The intrinsic oxidase activity of *So*FNR was measured to be 0.12 s^{-1} (0.1 M Tris/HCl, pH 7.4, 30 °C), and the addition of anthracyclines increases the consumption of O_2 16 to 35 times, however the K_m value for various anthracyclines is around 75 μM. Moreover, both anthracyclines and their respective 7-deoxyanthracyclinones may contribute to the production of O_2^- and H_2O_2 *in vivo* [73]. These compounds were shown to inactivate *So*FNR, presumably via the modification of an essential thiol due to the oxidizing effect of the produced H_2O_2.

Another example of a thoroughly examined plastidic FNR comes from a filamentous cyanobacteria of the genus *Anabaena* (*An*FNR), with 3D structure for *A. nostoc* strain PCC7119 available [74]. Structurally and functionally *An*FNR is very similar to *So*FNR, as can be inferred from Fig. 7, with sequences being 50% homologous, and table 2, with kinetic parameters being similar. The enzyme follows a *ping-pong* mechanism and the partly rate-limiting step is the oxidative half-reaction, with rates reaching up to 100 s^{-1}. The addition of the natural electron acceptor ferredoxin caused stimulation of quinone reductase activity at low quinone concentrations, evidenced by biphasicity in Lineweaver – Burk plots [75], which is similar to that seen in AdxR/Adx pair [45].

Similarly to *So*FNR, there is no significant structural specificity for nitroaromatics or quinones in the *An*FNR-catalyzed single-electron reduction [75]. A hydrogen bond formed between Glu301 and Ser80 was found to be

responsible for a negative electrostatic charge, yet it does not exert influence on the binding of $NADP^+$ [76,77]. Ser80, Cys261 and Glu301 form a highly conserved catalytic triad among plastidic-type FNRs [78–81]. A Ser80Ala mutation has a profound effect on the semiquinone stabilization [78]. A Glu301Ala mutation, while destabilizing the FAD semiquinone (48% wtFNR *vs*. 8% Glu301AlaFNR stabilization), does not induce any structural selectivity for oxidizing quinones [21]. However, the destabilization causes quinone reduction to proceed in a partially two-electron way with the stability of flavin/quinone ion-radical pair ($E\text{-}FADH^{\bullet}\cdots Q^{\bullet-}$) assuming the main role. All of this leads the authors to argue that a two-electron character of quinone-reduction is inducible by the destabilization of flavin semiquinone rather than being an intrinsic property of flavoenzymes [21]. Moreover, there is evidence pointing to the hydrogen bond network between Ser80, Glu301, Tyr303 and N5 of the isoalloxazine [67,82] being responsible for the stabilization of the semiquinone [78].

1.3.4.*Plasmodium falciparum* FNR

Plasmodium falciparum ferredoxin:$NADP^+$ reductase (*Pf*FNR) is a plastidic-type enzyme found in the apicoplast of the parasite [83]. The apicoplast is an organelle reminiscent of plastids and specific to a group of disease-causing protists *Apicomplexa*, which include malaria causing *Plasmodium* spp., toxoplasmosis causing *Toxoplasma gondii*, coccidiosis causing *Emeria* and several others. It is thought that the apicoplast is representative of an endosymbiotic event where an *Apicomplexa* ancestor engulfed an algal cell [84]. Some of the functions performed by the apicoplast include biosynthesis of isoprenoids and fatty acids, thus making it vital for the survival of the parasites and making these enzymes attractive targets for the development of novel drugs. *Plasmodium falciparum* caused malaria is responsible for more than a million deaths yearly. The emerging treatment resistant forms of *Plasmodia* is another cause of concern as the go-to drug artemisinin becomes less effective and new antimalarial compounds are needed [85–88].

The 30 kD monomeric protein forms a redox system with a Fe_2S_2 protein ferredoxin (*Pf*Fd). *Pf*FNR consists of a *N*-terminal FAD binding domain (residues 1 – 160) and *C*-terminal $NADP^+$ binding domain (residues 166 – 316). The FAD binding domain is composed of two perpendicular three-stranded antiparallel β sheets and a single α helix. *C*-terminal domain is made up of a five-stranded parallel β sheet that is surrounded by seven α helices. Five disordered surface regions are also found in the protein [89]. Sequence

homology with other plant-type FNRs is low, there are unique insertions and deletions (Fig. 9). The absorbance spectrum of *Pf*FNR is typical of flavoproteins, peaks are at 394 and 454 nm and $\varepsilon_{454} = 10\ mM^{-1}cm^{-1}$ [89].

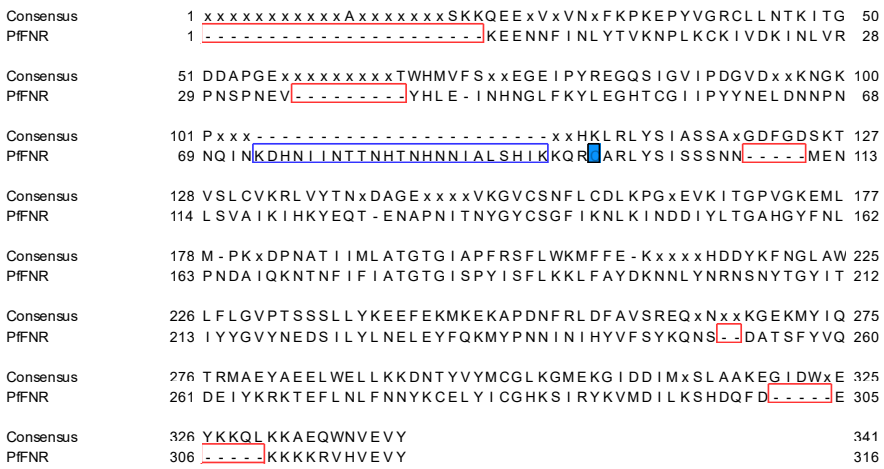

Figure 9. Multiple sequence alignments of a consensus sequence of plastidic FNRs from higher plants and *Pf*FNR. Insertions and deletions are denoted by blue and red boxes, respectively. *Pf*FNR unique Cys99 is colored light blue.

The isoalloxazine ring of FAD is inserted in a pocket between a terminal Tyr316 and a cluster of amino acid residues of the β4 chain. FAD forms hydrogen bonds with Arg101, Leu102, Tyr103, Ser104, Ala117, Lys119, His121, Tyr123, Tyr137, Cys138, Ser139 and Tyr316. Two water molecules interact with O2 and O4 carbonyl oxygen atoms thus mediating interactions between the protein and isoalloxazine. Additionally, the phenolic ring of Tyr123 stacks with the adenine ring. Two striking sequence differences in the $NADP^+$ domain should also be mentioned. When compared to other plant-type FNRs there is a lack of two basic amino acid residues, namely Ser256 in place of Arg/Lys and Tyr248 instead of Arg. Plasmodial Cys99 also appears a unique amino acid among plant-type FNRs.

*Pf*FNR is characterized by $E_7^0 = -0.28$ V [90], while its natural electron acceptor *Pf*Fd has a $E_{7.5}^0 = -0.26$ V. The protein complex formation is attributed to the electrostatic interactions between the basic residues of *Pf*FNR and acidic residues of *Pf*Fd. FAD semiquinone is thought to be highly destabilized and the long-wavelength band extending over 800 nm under anaerobiotic conditions is ascribed to charge transfer complex between fully reduced FAD and $NADP^+$ [90]. However, the quantitative characteristics of

its stability are unavailable. A K_d value between 0.1 and 0.5 μM for *Pf*FNR-*Pf*Fd complex was found under physiological ionic strength which then extrapolates to nanomolar range at 0 ionic strength [90]. *Pf*Fd was also preventive in dimerization.

A *Pf*FNR-specific feature is the formation of a dimer via Cys99 under oxidizing conditions; the dimerization inactivates the enzyme almost completely whereas full reactivity is restored upon disulfide reduction. The dimerization is thought to be brought on by induced-fit changes due to binding of $NADP^+$ or its analogues [89]. A *Pf*FNR-specific His286 is important in binding the substrate since diaphorase activity exhibits 3 to 5 times greater catalytic efficiency at pH 7.0 when compared to the plant-type FNRs' optimal pH 8.2 [90]. The later have an aliphatic Leu in this position, whereas His286 is protonated at pH 7.0. A higher catalytic efficiency at neutral pH was also seen in the physiological reaction with *Pf*Fd, i.e., a 2-times lower k_{cat}, lower K_m for NADPH (11-fold) and *Pf*Fd (3-fold) and higher k_{cat}/K_m for NADPH (6-fold) and *Pf*Fd (2-fold) when compared to pH 8.2. The k_{cat} values were, however, about 5 times lower than those of other plastidic-type FNRs. Rapid kinetic studies show hydride transfer from NADPH to FAD being rate limiting in the ferricyanide reductase reaction.

In an earlier study on the quinone reductase activity of *Pf*FNR the authors found a parabolic dependence of log k_{cat}/K_m *vs*. E_7^1 of the oxidant [91]. The reaction proceeds in a single-electron way. However, the net two-electron reduction takes place under partial anaerobiosis, ($[O_2] = 40 – 50$ μM) [91]. On the other hand, the data on the reduction of other types of redox active compounds by *Pf*FNR is absent.

Concerning the other aspects of *Pf*FNR as a potential target of antiplasmodial agents, its −SH groups are sensitive to organomercurials and carmustine, a nitrosourea that acts as an inhibitor of *Pf*FNR. Its putative target is in the active site of the enzyme, since the addition of $NADP^+$ or *Pf*Fd slows the inhibition [92]. Dihydroartemisinin, the active form of antimalarial drug artemisinin, exhibits a partially inhibitory effect towards diaphorase activity of *Pf*FNR and *in silico* analysis has shown it to bind in the same site as 2′,5′-ADP, so the resulting competition might be responsible for the lowered enzymatic affinity towards NADPH [93], however the authors conclude that *Pf*Fd is unlikely to be a direct target of dihydroartemisinin, even though the resistance to artemisinin in *P. falciparum* has been linked to Asp97Tyr mutation in *Pf*Fd [94]. This mutation inhibits diaphorase activity with lower concentration of *Pf*Fd and there is a possibility that *Pf*Fd and *Pf*FNR acting together play a role in protecting the parasite from ROS that are generated by artemisinin [93]. Methoxyamino chalcone derivatives inhibit the *Pf*FNR-*Pf*Fd

interaction up to 50%, probably through an electrostatic interaction with acidic residues of *Pf*Fd [95].

1.3.5. *Rhodopseudomonas palustris* FNR

Rhodopseudomonas palustris is a Gram-negative purple nonsulfur bacterium exhibiting the ability to switch its metabolism between four different modes, namely photoautotrophic, photoheterotrophic, chemoautotrophic and chemoheterotrophic [96]. Moreover, it can grow with and without oxygen and it can use various alternative forms of inorganic electron donors, carbon and nitrogen. Its ability to degrade plant biomass and various pollutants and to generate hydrogen because of nitrogen fixation makes it a valuable model organism when one is concerned with single cell-confined metabolic reactions and their changes due to changes in light, electron sources or other experimentally controlled factors.

Rhodopseudomonas palustris FNR (*Rp*FNR, EC 1.18.1.2) is encoded by *rpa*3954 and is a member of a novel thioredoxin reductase-like (TrxR) subfamily of FNRs belonging to the glutathione reductase-like (GrxR) family. As the name implies, *Rp*FNR is structurally and sequence-wise similar to TrxRs, however it is unable to reduce thioredoxin due to lack of a catalytic CXXC motif [79,97]. Contrary to almost all other FNRs, TrxR-like FNRs are homodimeric. A protomer is made of two domains and there are Rossmann-like three-layer ββα sandwich nucleotide binding folds for FAD and NADP(H). The NADP(H) binding domain is inserted between the FAD domain that is made of two segments, and the two domains are connected by a hinge region. The domain rotation along the hinge region is thought to be important for the catalysis: in the case of *Bacillus subtilis* TrxR-like FNR (*Bs*FNR, YumC), the distance between bound $NADP^+$ and FAD is more than 15 Å [98].

TrxR-like FNRs also exhibit a flexible *C*-terminal region (amino acids 319 – 344 for *Rp*FNR). This subdomain stretches over the FAD cofactor of the other monomer [99]. FAD cofactor is stabilized by π-π interactions and hydrogen bonds from an aromatic residue and hydroxyl-containing aliphatic residues [98–100]. The aromatic residue is stacked opposite to FAD, and in the case of *Rp*FNR this *re*- facing FAD stacking Tyr328 is supposed to act as a shield preventing FAD from being exposed to the solvent, similarly to the terminal Tyr residues in plastidic FNRs. Moreover, the *C*-terminal helix may possibly act in substrate binding, electron transfer and hydride transfer [101,102]. While *Bs*FNR exhibits higher reactivity to Fe_4S_4 type ferredoxin (Fd), which is unique among FNRs, there is no reactivity of *Rp*FNR towards

Fe_4S_4 Fd reported and its reactivity with Fe_2S_2 Fd is low [103]. For a more thorough recent review on TrxR-like FNRs the reader is referred to [104].

The reduction of *Rp*FNR by NADPH and reoxidation by $NADP^+$ proceeds in several phases and the fastest ones exceed 500 s^{-1} [105], similarly to other TrxR-like FNRs, i.e., *Bs*FNR and *Chlorobaculum tepidum* FNR (*Ct*FNR) [106,107]. Mutation of Tyr328 leads to a decrease in both K_m and K_d for $NADP^+$ and NADPH in the steady-state assays, possibly due to the weakening of interaction that is required for catalytic turnover. In other words, tyrosine destabilizes the charge transfer complex (CTC) thus enhancing the overall catalytic turnover. The *C*-terminal tyrosine has a similar role as in plant-type FNRs [50,52].

1.4. Electrontransferases reducing heme

These flavoenzymes have heme as a redox partner, which is situated either in the same protein, for example in NO synthase, or constitutes another protein (NADPH:cytochrome P-450 reductase/cytochrome P-450 pair).

1.4.1.NADPH:cytochrome P-450 reductase

NADPH:cytochrome P-450 reductase (P-450R, EC 1.6.2.4) is a *ca.* 80 kD membrane bound diflavin reductase using NADPH as an electron donor to transfer electrons to FAD and FMN [108–110] and located in the endoplasmic reticulum. P-450R is of critical importance to the microsomal cytochromes P-450 (P-450) providing them with reducing equivalents from NADPH for drug, xenobiotic and steroid hormone metabolism [111]. The FMN, FAD and NADPH binding domains are highly conserved among different species and exhibit similarity with respective domains of FNRs and NOSs [67,112,113].

A relatively short hydrophobic *N*-terminal segment binds P-450R to the membrane of the endoplasmic reticulum. Glu90, Thr91, Thr93, Thr142 and Tyr143 in the FMN binding domain were found to be absolutely conserved across a number of species [111]. A short, *ca*. 10 – 12 amino acid long flexible hinge region connects the FMN domain and FAD domain. During catalysis redox equivalents are transferred along the pathway of NADPH → FAD → FMN → P-450. Upon binding NADPH, a conformational change in both FAD and FMN domains occurs so that NADPH is situated closer to isoalloxazine of FAD. The bulky aromatic Trp679 (human P-450R) potentially serves in differentiating between NADPH and $NADP^+$ and shielding the isoalloxazine

[114] while mutagenesis studies show NADPH being able to come closer to isoalloxazine [115].

The distance between isoalloxazine rings of FMN and FAD is 3.5 – 4.5 Å. The complex between P-450R and P-450 forms between the negatively charged FMN binding domain of the former and a hydrophobic membrane binding domain of the later. Redox potentials are as follows: −0.325 V (FAD/FADH$^{\bullet}$), −0.372 V (FADH$^{\bullet}$/$FADH_2$), −0.068 V (FMN/FMNH$^{\bullet}$) and −0.246 V (FMNH$^{\bullet}$/$FMNH_2$) at pH 7.4 [116] with large difference in values between the first and second electron transfers pointing to a highly stabilized semiquinone. The proposed catalytic cycle involves one-, two- and three-electron reduced states of P-450R with $FMNH_2$ acting as the principal electron donor [117].

P-450R reduces nitroaromatic compounds, quinones and aromatic *N*-oxides in a single-electron way with a linear (for nitroaromatics) or quadratic (for quinones) dependence of logarithms of reaction rate on E_7^1 [118,119]. This, together with a systematically lower reactivity of $ArNO_2$ when compared to quinones of similar E_7^1 values, support the outer sphere ET model [24,26,119]. The P-450R redox partner P-450 exhibits oxygen reductase activity resulting in ROS generation and xenobiotic reductase activity [120].

1.4.2.Nitric oxide synthase

Nitric oxide synthase (NOS, EC 1.14.13.39) is a dimeric flavohemoprotein catalyzing the conversion of *L*-arginine to NO$^{\bullet}$ and citrulline at the expense of NADPH via an enzyme bound *N*-hydroxy-*L*-arginine intermediate [121]. The produced nitric oxide (NO) acts as a signalling molecule and an immune response agent. There are three mammalian NOS isoforms – neuronal, inducible and endothelial (nNOS, iNOS and eNOS, respectively). nNOS is expressed in neural cells and skeletal and cardiac myocites, iNOS is expressed in the cells of the immune system and eNOS is expressed in blood vessel lining with functions being as diverse as nerve signalling, blood vessel dilation, inhibition of blood clotting and acting bacteriocidally. The differences between various isoforms at the amino-acid sequence level are illustrated in Fig. 10:

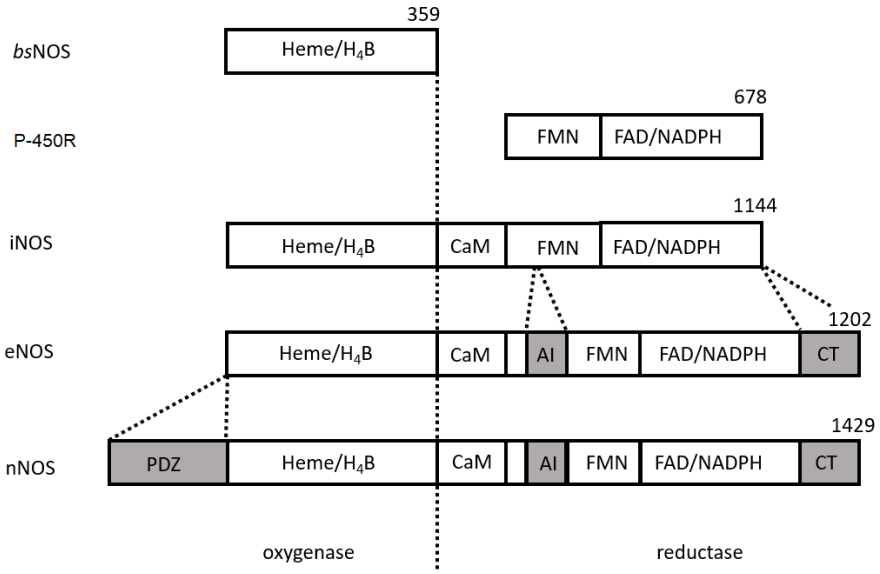

Figure 10. Block gene alignment of NO synthases and related enzymes indicating the binding sites for heme, H_4B, CaM, FMN, FAD, NADPH and domain boundaries. PDZ – PDZ domain; Al – autoinhibitory loop; CT – *C*-terminal extension; *bs*NOS – *Bacillus subtilis* NO synthase. Adapted from [122].

The enzymes are homodimeric, each subunit consisting of an *N*-terminal oxygenase domain and a *C*-terminal reductase domain. The latter is related to NADPH-dependent microsomal cytochrome P-450 reductase [123,124]. The domains are linked by a calmodulin (CaM) binding sequence [121,125]. The active homodimer forms upon interaction between two oxygenase domains. There are a total of four redox cofactors in a NOS subunit, two in each domain: FAD and FMN are situated in the reductase domain and heme (iron protoporphyrin IX) and 6*R*-tetrahydrobiopterin (H_4B) in the oxygenase domain. During the catalysis redox equivalents are transferred along the pathway of NADPH → FAD → FMN → heme with electrons from FMN of one subunit transferred to the oxygenase domain of another subunit [126–128]. The reductase domain of NOS cycles between one- and three-electron reduced states during the turnover [129–131].

The multistep NO synthesis involves the formation of several heme Fe^{3+}/Fe^{2+} complexes and electron exchange between heme and H_4B (Fig. 11) [125,132]. Only a part of NO synthesized by NOS is released with a significant fraction of Fe^{2+}-NO complex engaging in a futile redox cycling with no accompanying $NO^{\bullet}$ dissociation. The catalysis of NOS involves the

movement of reductase domain and there is complex regulation by the concerted action of binding of CaM, NADP(H) and the interdomain electrostatic interactions.

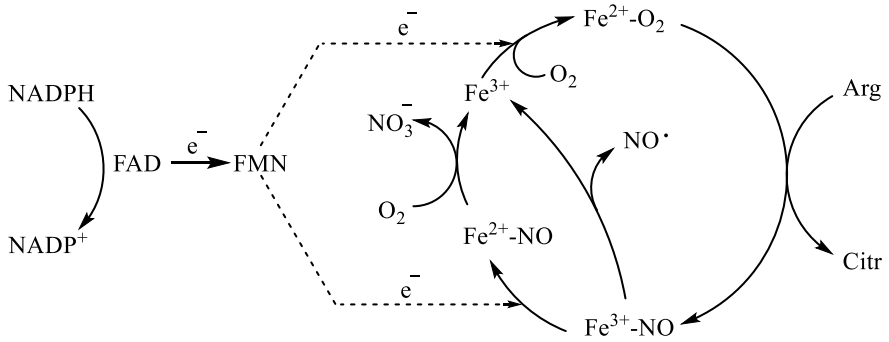

Figure 11. A simplified scheme of catalysis of nNOS. Adapted from [125,133,134].

Structurally, the reductase domain of nNOS is very similar to that of P-450R [123,124] and the distance between the two flavin cofactors is only 5 Å. The CT and Al inserts (Fig. 10) increase the area of contact between the FAD and FMN domains. The peptide constituting CaM binding site that connects the reductase and oxygenase domains has been determined in the case of eNOS [135].

Similarly to FNRs, an aromatic residue (Phe1395 in the case of nNOS) stacking with the isoalloxazine ring of the flavin is displaced towards FMN thus allowing a direct hydride ion transfer from NADPH to N5 of FAD [136,137]. The aromatic residue promotes NAD(P)H selectivity, facilitates $NADP^+$ dissociation and prevents simultaneous binding of two nucleotides [136,137]. FAD is reduced in a two-electron way and the hydroquinone then transfers an electron to FMN. The FMN semiquinone is neutral and extremely stable, oxidation in air is slow [138,139]. Therefore FMN constantly changes between hydroquinone and semiquinone while FAD attains all three oxidation states intermittently [136,139]. As mentioned, the distance between FAD and FMN is 5 Å meaning a rapid electron transfer from FAD to FMN. However, an effective interaction of FMN with heme would require substantial movement which is speculated to be brought on by a hinge region connecting the FAD and FMN domains in the reductase domain.

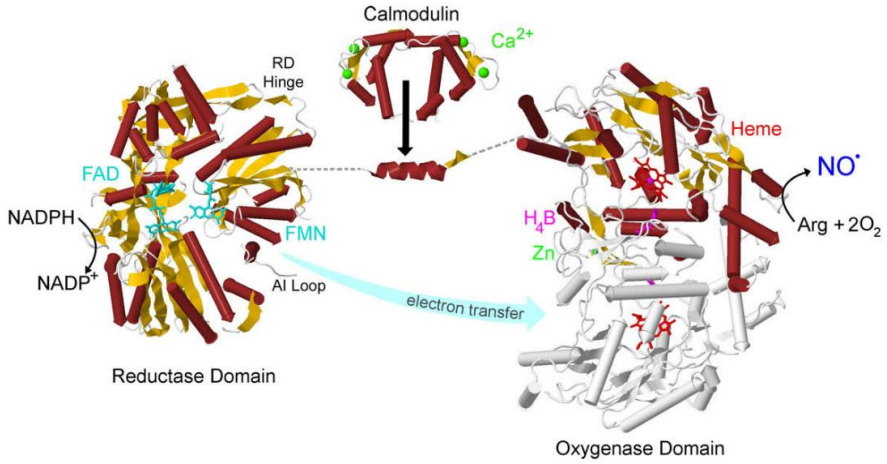

Figure 12. Structures of the different fragments of NO synthase aligned in order of amino-acid sequence [122].

The intracellular Ca^{2+} concentration is the regulating factor of NOS due to induced binding of CaM to the enzyme [122,140,141] and NO synthesis is induced upon CaM binding to the recognition sequence in an antiparallel orientation [142]. CaM primarily acts as an electronic switch activating electron transfer from FMN to heme [143,144] while also increasing the rate of flavin reduction by NADPH and the steady-state reduction of electron acceptors [29,144,145].

NO synthase is known to reduce quinones, aromatic *N*-oxides and nitroaromatic compounds in a single-electron way [29,130,146–149]. As in the case of other dehydrogenases – electrontransferases, the radicals of these compounds undergo redox cycling which may contribute to the oxidative stress-type cytotoxicity. nNOS is known to play a key role in doxorubicin induced toxicity to neurons and it is thought to be involved in the neurotoxic action of dinitrobenzenes [150,151]. The overexpression in astrocytic tumors renders nNOS a potential target for anticancer agents [152]. iNOS was found to be partly responsible in the reductive activation of anticancer agents 2-nitroimidazole EF5 and benzotriazine-*N*-oxide SN30000 [153]. Finally, it is possible that $NO^{\bullet}$ formation is inhibited by the redox cycling of quinones and nitroaromatics due to the rapid reaction between $NO^{\bullet}$ and the forming superoxide [151,154]. It is thought that nNOS reduces redox cycling xenobiotics via $FMNH_2$ and, possibly, $FADH_2$ without the involvement of heme based on the kinetic studies of reductase domain and the insensitivity of holo-nNOS quinone- and nitroreductase activity to NO_2-arginine, binding to heme [130,146,148,149,153].

1.5. CONCLUDING REMARKS

While there exists a massive body of research into the mechanisms of action of dehydrogenases – electrontransferases and their structural peculiarities enabling their action, single-electron reduction of redox cycling species, such as quinones and nitroaromatics, are often overlooked, regardless of these substances being potent drug candidates or them being widely spread in the environment in the form of pollutants. It was thus attempted to further characterize the one-electron transfer mechanisms underlying representative enzymes of both groups, namely Fe-S proteins (*Pf*FNR, *Rp*FNR) and heme proteins (nNOS).

2. MATERIALS AND METHODS

2.1. Enzymes and reagents

Plasmodium falciparum ferredoxin:NADP$^+$ oxidoreductase (*Pf*FNR) and ferredoxin (*Pf*Fd) were a generous gift from Dr. Alessandro Aliverti (Università degli Studi di Milano, Italy). They were prepared as previously described [90]. The concentrations were determined spectrophotometrically according to ε_{454} = 10.0 $mM^{-1}cm^{-1}$ and ε_{424} = 9.68 $mM^{-1}cm^{-1}$, respectively.

Rhodopseudomonas palustris ferredoxin:NADP$^+$ oxidoreductase (*Rp*FNR) was a generous gift from Dr. Daisuke Seo (Kanazawa University, Japan) and was prepared as described, the concentration was determined spectrophotometrically according to ε_{466} = 10.8 $mM^{-1}cm^{-1}$ [101].

Rat neuronal nitric oxide synthase (nNOS) was a generous gift from Dr. Jean-Luc Boucher (Université Paris Descartes, France) and was prepared as previously described [148]. The concentration was determined spectrophotometrically according to ε_{393} = 100 $mM^{-1}cm^{-1}$ [155], and activity of nNOS determined in Dr. J.-L. Boucher's laboratory according to the assay of [^{3}H]-*L*-citrulline formation was equal to 280 ± 50 nmol × min^{-1} × mg $protein^{-1}$ [148].

Multiple sequence alignments of enzymes were performed using Clustal Omega (https://www.ebi.ac.uk/Tools/msa/clustalo/) [156]. Consensus sequence was generated using the EMBOSS Cons tool (https://www.ebi.ac.uk/Tools/msa/emboss_cons/) [157]. Sequence alignments were analysed and annotated using Jalview. The 3D structures used are available at RCSB PDB and their IDs are as follows: 2OK8 (*Pf*FNR), 2RC5 (*Leptospira interrogans* FNR), 3LO8 (maize root FNR), 1GAW (maize leaf FNR), 1GJR (*An*FNR), 1FNB (*So*FNR), 1GQ0 (pea FNR), 1SM4 (paprika FNR).

NADP(H), AcADP$^+$, 2′,5′-ADP, cytochrome *c* (from horse heart), bovine superoxide dismutase, glucose-6-phosphate, glucose-6-phosphate dehydrogenase from *Leuconostoc mesenteroides*, *L*-ascorbate, dithiothreitol, *L*-arginine, N^{ω}-NO_2-*L*-arginine, calmodulin (CaM, from bovine testis), $CaCl_2$, (6R)-5,6,7,8-tetrahydrobiopterin (H_4B), benzylviologen (BVG), Fe(EDTA)$^-$, ferrycianide (FeCya), quinones (Q) and nitroaromatic compounds ($ArNO_2$) except for those mentioned below were purchased from Sigma-Aldrich (St. Louis, MO, USA) and used as received.

Aromatic *N*-oxides, *N*-methylpicramide, 2,4,6-trinotrotoluene, tetryl, pentryl, nitrofurans, nitrobenzimidazolones, 5-nitrothiophene-2-carbonic acid morpholide were a generous gift from Dr. Jonas Šarlauskas (Vilnius

University, Lithuania) and they were synthesized as described [23,158–161]. CB-1954 was a generous gift from Dr. Vanda Miškinienė (Vilnius University, Lithuania) and was synthesized as described [40]. All synthesized compounds were characterized by their melting points, ^{1}H-NMR and IR spectra. The purity of the compounds determined using HPLC-MS (LCMS-2020, Shimadzu, Kyoto, Japan) was ≥98%. 3-[4-(trifluoromethyl)benzyl]-menadione (plasmodione, PD) and its derivatives were generous gifts from Dr. Elisabeth Davioud-Charvet (Université de Strasbourg, France) and they were synthesized as described [162]. Log*D* values were calculated using a log*D* predictor (https://chemaxon.com). The structural formulae of nontrivial oxidants are given in Fig. 13.

2.2. Steady-state kinetic studies

Steady-state kinetic measurements were performed using Cary60 UV-Vis (Agilent Technologies, Santa Clara, CA, USA) or PerkinElmer Lambda 25 (PerkinElmer, Waltham, MA, USA) spectrophotometer. Standard buffer compositions for the experiments with different enzymes are given in table 3 and apply for each respective case unless noted differently.

Table 3. Buffer compositions for different enzymes

Enzyme	Buffer
*Pf*FNR	0.1 M K_2HPO_4/KOH + 1 mM EDTA, pH 7.0
*Rp*FNR	0.02 M Hepes/NaOH + 1 mM EDTA, pH 7.0
nNOS	0.1 M Tris/HCl + 1 mM EDTA + 0.1 M NaCl, pH 7.0

The steady-state parameters of the reactions, namely the catalytic constants k_{cat} and the bimolecular rate constants (or catalytic efficiency constants k_{cat}/K_m) of the oxidants at fixed concentrations of NADPH were obtained by fitting the kinetic data to the parabolic expression using Mathematica (Wolfram Research, Inc., Mathematica, Version 12.0, Champaign, IL, USA) or SigmaPlot (Systat Software, Sigmaplot, Version 14.0, San Jose, CA, USA). They correspond to the reciprocal intercepts and slopes of the Lineweaver – Burk plots, [E]/*v vs.* 1/[oxidant], respectively, where *v* is the reaction rate and [E] is the enzyme concentration. k_{cat} represents the number of molecules of NADPH oxidized by a single active center of the enzyme per second under saturating concentration of the substrate. The concentrations of enzymes used in these experiments were 5 – 50 nM. The statistical analysis was performed using using Statistica (StatSoft Inc., Statistica, Version 10, Tulsa, OK, USA).

The rates of enzyme-catalyzed NADPH oxidation in the presence of quinones, nitroaromatic compounds or aromatic *N*-oxides were determined using the value $\Delta\varepsilon_{340}$ = 6.2 $mM^{-1}cm^{-1}$. The rates were corrected for the intrinsic NADPH-oxidase activities. In experiments where 50 μM cytochrome *c* was added to the reaction mixture, its organic oxidant-mediated reduction was measured using the value $\Delta\varepsilon_{550}$ = 20 $mM^{-1}cm^{-1}$. The rate of ferricyanide reduction was determined using the value $\Delta\varepsilon_{420}$ = 1.02 $mM^{-1}cm^{-1}$. The rate of tetryl reduction was corrected for the increase in absorbance due to *N*-methylpicramide, $\Delta\varepsilon_{340}$ = 12.8 $mM^{-1}cm^{-1}$ [163]. The reduction rate for $AcADP^+$ was determined using the value $\Delta\varepsilon_{363}$ = 5.6 $mM^{-1}cm^{-1}$ [164]. AcADPH, the reduced form of $AcADP^+$, was prepared by *in situ* reduction with 10 mM glucose 6-phosphate and 0.01 mg/ml glucose 6-phosphate dehydrogenase. AcADPH concentration was determined according to ε_{365} = 7.8 $mM^{-1}cm^{-1}$ [164].

For quinone reduction by flavoenzymes the single-electron flux is defined as a ratio of the rate of 1,4-benzoquinone-mediated reduction of the added cytochrome *c* to the doubled rate of 1,4-benzoquinone-mediated NAD(P)H enzymatic oxidation at pH < 7.2 [165]. This approach is based on the fast reduction of cytochrome *c* by 1,4-benzosemiquinone ($k_{cat} \approx 10^6$ $M^{-1}s^{-1}$) and its slow reduction by the hydroquinone form.

Stock solutions of organic compounds were prepared in DMSO, the final volume of DMSO in the reaction mixture was 1%. All measurements were performed at 25 °C. The initial concentrations of electron acceptors were 50 – 1000 μM, with 6 – 8 separate measurements for each compound with the concentration lowered 1.5× each time. All measurements were performed at least twice.

The kinetic parameters of steady-state reactions according to a *ping-pong* mechanism were calculated according to Eq. 19:

$$\frac{v}{[\mathrm{E}]} = \frac{k_{cat}[\mathrm{NADPH}][\mathrm{Q}]}{K_m^{\mathrm{NADPH}}[\mathrm{Q}] + K_m^{\mathrm{Q}}[\mathrm{NADPH}] + [\mathrm{NADPH}][\mathrm{Q}]} \qquad (19)$$

where *v* is the reaction rate, [E] is the enzyme concentration and Q stands for the electron acceptor. Inhibition constants K_i were calculated according to Eq. 20 for competitive inhibition of $NADP^+$ or 2′,5′-ADP *vs*. NADPH and Eq. 21 for uncompetitive inhibition *vs*. an oxidant and Eq. 22 for noncompetitive inhibition:

$$\frac{v}{[\mathrm{E}]} = \frac{k_{cat}^{app}[\mathrm{S}]}{K_m^{\mathrm{S}}\left(1 + \frac{[\mathrm{I}]}{K_i}\right) + [\mathrm{S}]} \qquad (20)$$

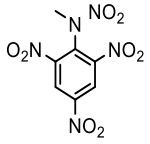

Tetryl

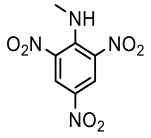

N-methylpicramide

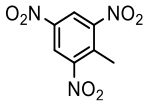

2,4,6-trinitrotoluene

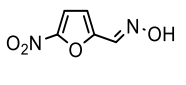

Nifuroxime

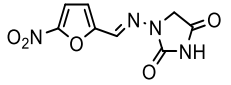

Nitrofurantoin

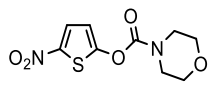

5-nitrothiophene-2-carbonic acid morpholide

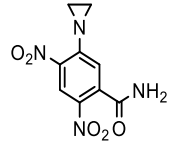

CB1954

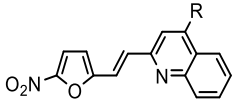

Vinylquinoline-substituded nitrofurans (table 4, 14 – 16)

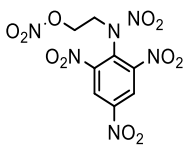

Pentryl

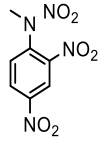

2,4-dinitrophenyl-*N*-methylnitramine

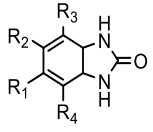

Nitrobenzimidazolones

R_1= $-N_2O$; R_2=R_3=R_4= $-H$

R_1=R_2= $-N_2O$; R_3=R_4= $-H$

R_1=R_2=R_3= $-N_2O$; R_4= $-H$

R_1=R_2=R_3=R_4= $-N_2O$

R_1= $-NH_2$; R_2=R_4= $-N_2O$; R_3= $-H$

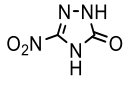

NTO

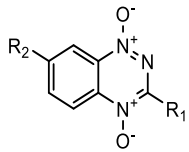

Aromatic di-*N*-oxides (tirapazamine (TPZ) derivatives)

R_1=R_2= -H

R_1= $-NH_2$; R_2= -H (TPZ)

R_1= $-NH_2$; R_2= -CF3

R_1= $-NH_2$; R_2= -Cl

R_1= $-NH_2$; R_2= -F

R_1= $-NH_2$; R_2= $-CH_3$

R_1= $-NH_2$; R_2= $-OC_2H_5$

R_1= $-NH_2$; R_2= $-OCF_3$

R_1= $-NHCHOCH_3$; R_2= -H

R_1= $-NHCOOCH_3$; R_2= -H

R_1= $-NHSO_2CF_3$; R_2= -H

R_1= $-NHSO_2CH_3$; R_2= -H

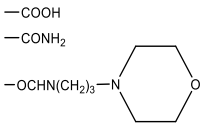

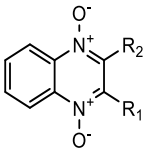

Quinoxaline dioxides

R_1=R_2= -H

R_1= -H; R_2= $-CF_3$

R_1= -CN; R_2= $-NH_2$

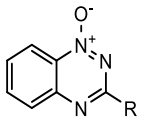

Aromatic *N*-oxides

R= -H

R= $-NH_2$

R= $-NHCOCH_3$

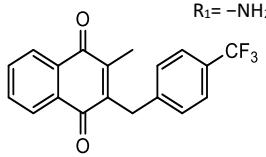

Plasmodione (PD)

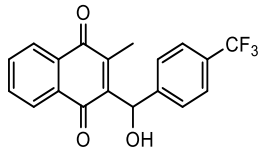

PD-bzol

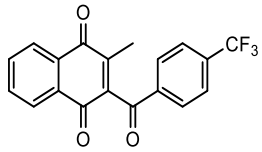

PDO

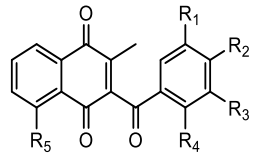

Table 6, compounds 4 - 11:

(4) R_1=R_3=R_5= -H; R_2= $-CF_3$; R_4= -F

(5) R_1=R_4= $-OCH_3$; R_2=R_3=R_5= -H

(6) R_1=R_3= $-OCH_3$; R_2=R_4=R_5= -H

(7) R_1=R_2=R_4=R_5= -H; R_3= $-NO_2$

(8) R_1=R_3=R_4=R_5= -H; R_2= $-NO_2$

(9) R_1=R_3=R_4=R_5= -H; R_2= -CCH

(10) R_1=R_3=R_4=R_5= -H; R_2= -Br

(11) R_1=R_3=R_4= - H; R_2= -Br; R_5= -OH

Figure 13. Structural formulae of nontrivial compounds used throughout this work.

$$\frac{v}{[\mathrm{E}]} = \frac{k_{\mathrm{cat}}^{\mathrm{app}}[\mathrm{Q}]}{K_{\mathrm{m}}^{\mathrm{Q}} + [\mathrm{Q}]\left(1 + \frac{[\mathrm{I}]}{K_{\mathrm{i}}}\right)} \quad (21)$$

$$\frac{v}{[\mathrm{E}]} = \frac{k_{\mathrm{cat}}^{\mathrm{app}}}{1 + \frac{[\mathrm{I}]}{K_{\mathrm{i}}}} \quad (22)$$

where S stands for NADPH, Q stands for electron acceptor and I stands for inhibitor. In the transhydrogenase reaction, S stands for $AcADP^+$ and I stands for NADPH.

PfFNR

The intrinsic NADPH-oxidase activity was 0.12 s^{-1}. Ionic strength variation was achieved by using different concentrations of K_2HPO_4. For experiments with varying pH, KOH was used to set pH from 5.5 to 8.0 in the increments of 0.5. NADPH regeneration system was used (50 μM NADPH, 10 mM glucose-6-phosphate, 50 U/ml glucose-6-phosphate dehydrogenase) when monitoring the reduction rates of nitroaromatic compounds in the absence of external oxygen supply.

RpFNR

The intrinsic NADPH-oxidase activity was 0.12 s^{-1}.

nNOS

The intrinsic NADPH-oxidase activity was 0.1 s^{-1}. In the experiments with varied ionic strength, different concentrations of NaCl were added to 0.03 Tris/HCl. In some experiments, the reaction medium was enriched with 10 μg/mL calmodulin and 1.0 mM $CaCl_2$, or with CaM-Ca^{2+} and H_4B (5.0 μM) or with CaM-Ca^{2+}, H_4B and *L*-arginine (200 μM). In this case, the rates were corrected for the intrinsic NADPH-oxidase activity of nNOS, which reached 1.0 – 1.7 s^{-1}. In some experiments the reaction mixture additionally contained 1.0 mM dithiothreitol or 1.0 mM N^{ω}-NO_2-*L*-arginine.

2.3. Presteady-state kinetic studies

Enzyme rapid kinetic studies were performed using a SX20 stopped-flow system (Applied Photophysics, Leatherhead, UK) under aerobic conditions and the data analyzed with the accompanying software package (ProData SX v2.5.0, Applied Photophysics, Leatherhead, UK).

PfFNR

The enzyme reduction by NADPH and its reoxidation was monitored at 460 nm and 600 nm, respectively, at 25 °C. Spectra of reaction intermediates were recorded at various wavelengths in the 460 – 800 nm range and assessed at different times of the reaction. During turnover studies, *Pf*FNR in syringe 1 (6.0 – 7.0 μM) was mixed with the contents of syringe 2 (50 μM NADPH and 100 – 500 μM CH_3-1,4-benzoquinone). All measurements were performed in triplicates. Concentrations are reported after mixing. The multiple turnover data were analyzed according to Eq. 23 [166]:

$$k_{ox} = \frac{[\mathrm{NADPH}]_0}{[\mathrm{E_{red}}]_{max} \times t_{1/2(off)}} \quad (23)$$

where k_{ox} is the apparent first-order rate constant of enzyme reoxidation, $[NADPH]_0$ is the initial concentration of NADPH, $[E_{red}]_{max}$ is the maximum concentration of the reduced enzyme formed during the turnover and $t_{1/2(off)}$ is the time interval between the formation of the half-maximum amount of E_{red} and its decay to the half-maximum value.

RpFNR

Enzyme reduction by NADPH and its reoxidation was monitored at 460 nm and 600 nm, respectively, at 25 °C. Spectra of reaction intermediates were recorded at various wavelengths in the 460 – 800 nm range and assessed at different times of the reaction. During turnover studies, *Rp*FNR in syringe 1 (4 – 5 μM) was mixed with the contents of syringe 2 (50 μM NADPH or NADPH and varied concentrations of duroquinone or 250 μM duroquinone (for the reaction intermediates spectra)). All experiments were performed in triplicates. Concentrations are reported after mixing. Reoxidation kinetics were analyzed according to Eq. 23.

nNOS

Enzyme rapid kinetic studies were performed under aerobic conditions in 0.1 M Tris/HCl (pH 7.0) buffer, containing 1 mM EDTA, 0.1 M NaCl, 3% (v/v) glycerol at 25 °C. Syringe 1 contained either nNOS (2.0 μM) or nNOS, CaM, $CaCl_2$ and H_4B (2.0 μM, 5.0 μM, 1.0 mM and 5.0 μM, respectively), while syringe 2 contained NADPH (30 μM) or NADPH and varied concentrations of duroquinone, or NADPH and *L*-arginine (200 μM), or NADPH, *L*-arginine and duroquinone. In separate experiments, superoxide dismutase was added to syringe 2. All experiments were performed in triplicates. Concentrations are reported after mixing. The kinetic traces at 485, 436 and 397 nm were analyzed using the accompanying software package by

fitting the data to single- or double-exponential equations. The multiple turnover data were analyzed according to Eqs. 23 and 24 [166]:

$$k_{red} = \frac{k_{ox}}{\left(\frac{[E]_t}{[E_{red}]_{max}} - 1 \right)} \quad (24)$$

where k_{red} is the rate constant of enzyme reduction by NADPH, k_{ox} is the rate constant of reoxidation at particular duroquinone concentration and $[E]_t$ is the total enzyme concentration.

2.4. Oxygen consumption studies

Oxygen consumption studies were performed using a Digital Model 10 (Rank Brothers Ltd., Bottisham, UK) Clark electrode with the assumption that the concentration of O_2 at the beginning of the reaction is 250 μM by measuring the current of oxygen reduction. The rates of oxygen consumption were monitored under identical conditions to the respective steady-state kinetics measurements, i.e., NADPH regeneration system and no external oxygen supply. The bimolecular rate constants of ascorbate oxidation by quinones (k), expressed as

$$k = \frac{v_0}{[Q][\text{ascorbate}]} \quad (25)$$

were calculated from the initial rates of O_2 consumption in the presence of 1.0 mM asorbate and various concentrations of quinones [167].

2.5. Photoreduction studies

The photoreduction studies of *Rp*FNR (16 – 17 μM) were performed according to a modified procedure [168] under anaerobic conditions in 0.02 M Hepes buffer, pH 7.0, using 5-deaza-FMN (0.125 μM) and EDTA (8 mM) as photosensitizers. Before protein introduction from a concentrated stock solution, the solution in a sealed spectrophotometer cell was flushed with O_2-free argon for 60 min. Subsequent to the protein introduction, the cell was illuminated for short periods at 20 °C with a 100 W incandescent lamp at a distance of 20 cm; the progress of the reaction was followed spectrophotometrically for 1 – 1.5 h. The maximal amount of neutral semiquinone (E-FADH•) formed under illumination was assumed to be defined by the inflection point of the A_{600} vs. A_{466} plot. The FAD semiquinone concentration was calculated according to ε_{600} = 5.0 $mM^{-1}cm^{-1}$ [169]. The difference between two single-electron transfer potentials ΔE_7^1 was further

calculated from the semiquinone formation constant K_s according to Eqs. 26 and 27:

$$\frac{[\text{E-FADH}^{\bullet}]_{max}}{[\text{E-FAD}]_{tot}} = \frac{\sqrt{K_S}}{\left(2+\sqrt{K_S}\right)} \tag{26}$$

$$\Delta E_7^1 = E_7^{\text{E-FAD/E-FADH}^{\bullet}} - E_7^{\text{E-FADH}^{\bullet}/\text{E-FADH}^{-}} = 0.059\text{V} \times \log K_S \tag{27}$$

where $[\text{E-FADH}^{\bullet}]_{max}$ is the maximal amount of formed semiquinone, E_7 (E-FAD/E-FADH$^{\bullet}$) is the potential of oxidized/semiquinone FAD couple, E_7 (E-FADH$^{\bullet}$/E-FADH^{-}) is the potential of semiquinone/reduced FAD couple and $[\text{E-FAD}]_{tot}$ is the total enzyme concentration [170].

3. RESULTS AND DISCUSSION

The results and discussion section will be presented in three parts according to different enzymes studied.

3.1. Mechanisms of reduction of nonphysiological electron acceptors by *Plasmodium falciparum* ferredoxin:$NADP^+$ oxidoreductase

3.1.1. Steady-state kinetic studies and oxidant specificitiy of *Pf*FNR

3.1.1.1. Reactions of *Pf*FNR with oxidants with characterized single-electron reduction potentials

It had previously been established that one of the most active nonphysiological electron acceptors of *Pf*FNR is 5-OH-1,4-naphthoquinone (juglone) [91]. A series of parallel lines obtained in double reciprocal plots at varied concentrations of juglone and fixed concentrations of NADPH indicate a *ping-pong* mechanism of the quinone reductase reaction catalyzed by *Pf*FNR that is common for electrontransferases – dehydrogenases. According to Eq. 19 the k_{cat} value for juglone reduction at infinite NADPH concentration is equal to 63.2 ± 4.1 s^{-1}, and the values of bimolecular rate constants (k_{cat}/K_m) for NADPH and juglone are 6.0 ± 0.4 × 10^5 $M^{-1}s^{-1}$ and 1.1 ± 0.1 × 10^6 $M^{-1}s^{-1}$, respectively (Fig. 14).

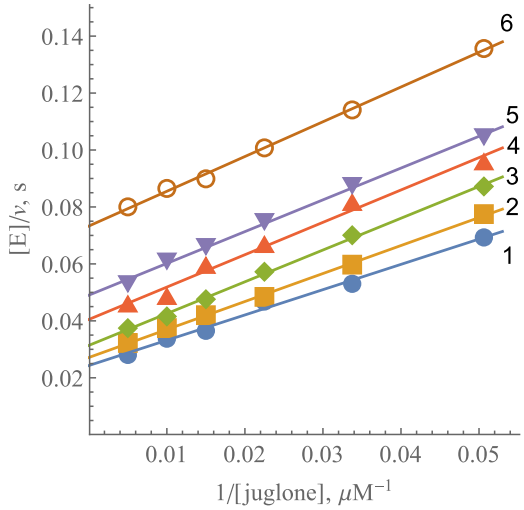

Figure 14. Steady-state kinetics of reduction of juglone by NADPH catalyzed by *Pf*FNR. NADPH concentrations are200 μM (1), 150 μM (2), 100 μM (3), 75 μM (4), 50 μM (5) and 25 μM (6).

Building on the fact that *Pf*FNR reduces quinones in a single-electron way [91], it was investigated whether the same applies for nitroaromatic compounds ($ArNO_2$) and aromatic *N*-oxides (ArN→O). *Pf*FNR-catalyzed single-electron reduction of $ArNO_2$ was demonstrated by the addition of cytochrome *c* (cyt *c*) since it cannot be reduced by *Pf*FNR directly. Cytochrome *c* was reduced in the presence of 3,5-dinitrobenzoic acid, *p*-dinitrobenzene, *N*-methylpicramide and tetryl, and the rate of reduction was equal to 140 – 195% that of NADPH oxidation. Moreover, 100 U/ml superoxide dismutase (SOD) inhibited the reduction of cyt *c* by 15 to 25%. Further proof of redox cycling of $ArNO_2$ came from the consumption of excess oxygen during the reaction (Fig. 15). However, it is also important to note that *Pf*FNR-catalyzed formation of stable products of $ArNO_2$ reduction starts at $[O_2]$ = 40 – 50 μM and does not need complete O_2 exhaustion (Fig. 15A).

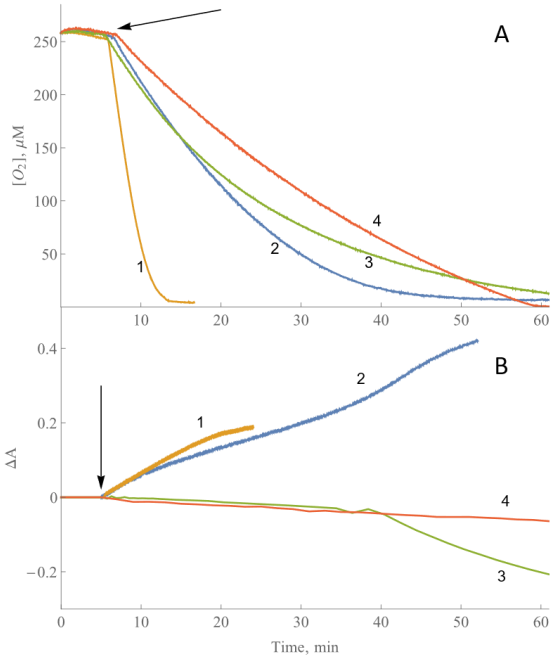

Figure 15. (A) Time course of oxygen consumption and (B) spectral changes during the reduction of tetryl (1), p-dinitrobenzene (2), nitrofurantoin (3) and N-methylpicramide (4) by 50 nM PfFNR in the presence of NADPH regeneration system and the absence of external oxygen supply. Compound concentrations were 50 μM monitored at 420 nm (tetryl and nitrofurantoin), 340 nm (p-dinitrobenzene) and 343 nm (*N*-methylpicramide). The arrows indicate the introduction of *Pf*FNR.

In the case of tirapazamine, an aromatic *N*-oxide representative, the *Pf*FNR-catalyzed oxidation of NADPH by 100 – 200 μM of it was accompanied by oxygen consumption with the rate being close to that of NADPH oxidation. The addition of 50 μM cyt *c* to the reaction mixture results in its reduction at the rate representing 180 – 190% that of NADPH oxidation. 100 U/ml SOD inhibited the reduction of cyt *c* by 40 – 65%. Thus, the single-electron flux in the *Pf*FNR-catalyzed reduction of ArN→O is equal to 90 – 95% and cytochrome *c* is reduced by their radicals which form a steady-state with the $O_2/O_2^{\bullet-}$ couple.

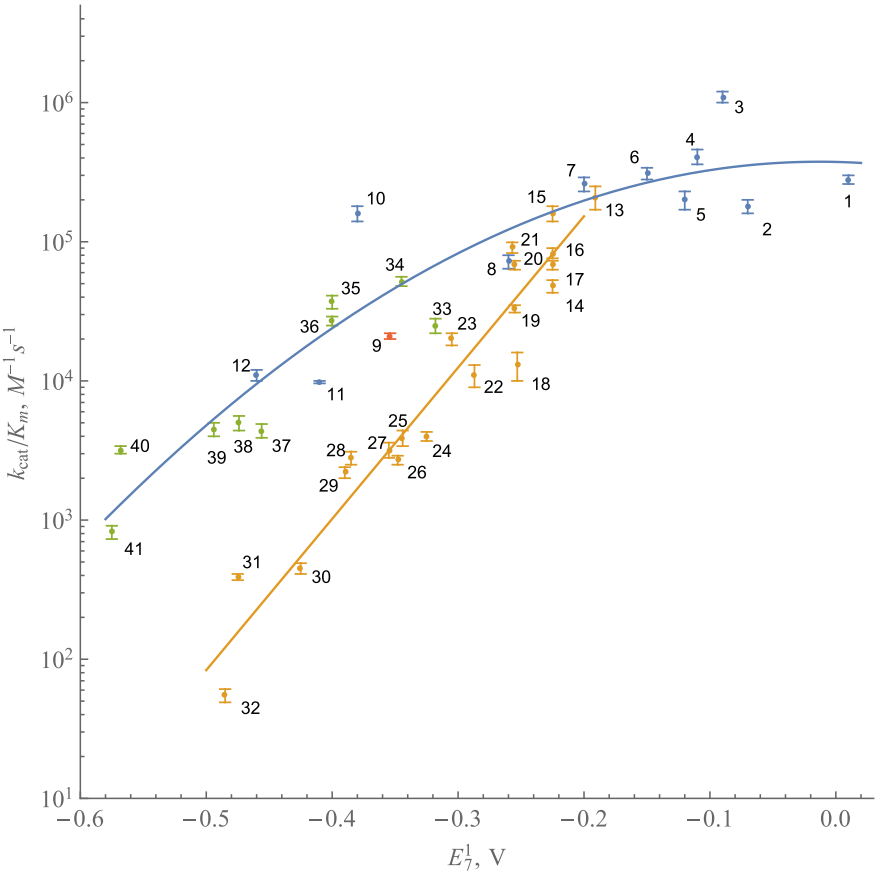

Figure 16. The dependence of the reactivity of quinones (blue disks), nitroaromatic compounds (orange disks) and aromatic N-oxides (green disks) on their single-electron reduction midpoint potentials at pH 7.0 (E_7^1) in log10 scale. The numbers of compounds and their reduction potentials are given in table 4.

In order to assess the substrate specificity of *Pf*FNR, the reduction of three series of electron acceptors, namely quinones (Q), nitroaromatic compounds and aromatic *N*-oxides whose single-electron reduction midpoint potentials (E_7^1) vary from 0.01 V to -0.575 V were examined (table 4). Additionally ferricyanide, $Fe(EDTA)^-$ and benzylviologen, all of them well known single-electron acceptors, were studied. The apparent reduction maximal rate constants $k_{cat(app.)}$ of electron acceptors at 100 μM NADPH and their respective k_{cat}/K_m values are given in table 4. The k_{cat} values for a number of less-active oxidants were not determined due to near linear dependence of the reaction rate on their concentrations. Tetryl (table 4, 13) exhibited the highest k_{cat} value overall under experimental conditions, equaling 40 s^{-1}, while it was around 33 s^{-1} for several quinones (table 4, compounds 1, 3, 8). The highest bimolecular rate constant, $k_{cat}/K_m = 1.1 \pm 0.1 \times 10^6$, was found in the case of juglone, as per earlier reports [91].

The log k_{cat}/K_m of $ArNO_2$ exhibits a linear dependence on the E_7^1, while quinones and aromatic *N*-oxides are characterized by a parabolic dependence on their E_7^1 values (table 4, Fig. 16). Moreover, their log k_{cat}/K_m values are higher in general, owing to the difference of two orders of magnitude between the electron self-exchange rate constants of $ArNO_2$ (~10^6 $M^{-1}s^{-1}$) and Q and ArN→O (~10^8 $M^{-1}s^{-1}$) [26]. One is also to note that the reactivity of a single-electron acceptor benzylviologen closely matches that of quinones (Fig. 16, compound 9).

3.1.1.2. Reactions of *Pf*FNR with plasmodione derivatives: possible substrate specificity

Plasmodione (3-[4-(trifluormethyl)benzyl]-menadione, PD) and its derivatives are promising novel antimalarial compounds [171]. However, their redox properties, including the reactions with redox enzymes of *P. falciparum*, have been studied to a limited extent [171–175]. In this context, *Pf*FNR is a potential candidate for their bioreductive activation-inducing redox cycling, which may be partly responsible for their antiplasmodial action. Thus, it is important to determine whether the plasmodione derivatives follow simple log (rate) constant *vs*. E_7^1 relationship, characteristic for model quinones, or may possess enhanced reactivity, i.e., specificity. For this reason, one has to assess the E_7^1 values of plasmodione derivatives, that, according to the best of authors' knowledge, are not available so far. Due to the instability of quinone radicals in an aqueous medium the values of their single-electron reduction potential are usually acquired by using pulse-radiolysis [17]. However low solubility of plasmodione and its derivatives make this approach

Table 4. Steady-state rate constants of reduction of nonphysiological electron acceptors by NADPH catalyzed by *Pf*FNR. [NADPH] = 100 μM, 0.1 M potassium phosphate + 1 mM EDTA, pH 7.0, t = 25 °C.

No.	Compound	E_7^1 (V)[a]	k_{cat} (s^{-1})	k_{cat}/K_m ($M^{-1}s^{-1}$)
	Quinones			
1	2-CH_3-1,4-benzoquinone	0.01	32.4 ± 4.1	$2.8 \pm 0.2 \times 10^5$
2	2,5-$(CH_3)_2$-1,4-benzoquinone	−0.07	26.0 ± 2.3	$1.8 \pm 0.2 \times 10^5$
3	5-OH-1,4-naphthoquinone	−0.09	35.7 ± 5.1	$1.1 \pm 0.1 \times 10^6$
4	5,8-$(OH)_2$-1,4-naphthoquinone	−0.11	25.0 ± 3.8	$4.1 \pm 0.5 \times 10^5$
5	9,10-Phenathrene quinone	−0.12	20.3 ± 3.3	$2.0 \pm 0.3 \times 10^5$
6	1,4-Naphthoquinone	−0.15	16.9 ± 2.1	$3.1 \pm 0.3 \times 10^5$
7	2-CH_3-1,4-naphthoquinone	−0.20	26.5 ± 3.2	$2.6 \pm 0.3 \times 10^5$
8	$(CH_3)_4$-1,4-benzoquinone	−0.26	33.1 ± 4.3	$7.2 \pm 0.8 \times 10^4$
9	Benzylviologen	−0.354	4.80 ± 0.6	$2.1 \pm 0.1 \times 10^4$
10	9,10-Anthraquinone-2-sulphonate	−0.38	27.0 ± 3.2	$1.6 \pm 0.2 \times 10^5$
11	2-OH-1,4-naphthoquinone	−0.41	2.60 ± 0.3	$9.8 \pm 0.2 \times 10^3$
12	2-CH_3-3-OH-1,4-naphthoquinone	−0.46	14.0 ± 1.2	$1.1 \pm 0.1 \times 10^4$
	Nitroaromatic compounds			
13	Tetryl	−0.191	40.0 ± 5.1	$2.1 \pm 0.4 \times 10^5$
14	Nitrofuran IIIa	−0.225		$4.8 \pm 0.5 \times 10^4$
15	Nitrofuran IIIb	−0.225		$1.6 \pm 0.2 \times 10^5$
16	Nitrofuran IIIh	−0.225		$8.3 \pm 0.7 \times 10^4$
17	*N*-methylpicramide	−0.225		$6.8 \pm 0.5 \times 10^4$
18	2,4,6-Trinitrotoluene	−0.253		$1.3 \pm 0.3 \times 10^4$
19	Nifuroxime	−0.255		$3.3 \pm 0.2 \times 10^4$
20	Nitrofurantoin	−0.255		$6.8 \pm 0.5 \times 10^4$
21	1,4-Dinitrobenzene	−0.257		$9.1 \pm 0.8 \times 10^4$
22	1,2-Dinitrobenzene	−0.287		$1.1 \pm 0.2 \times 10^4$
23	5-Nitrothiophene-2-carbonic acid morpholide	−0.305		$2.0 \pm 0.2 \times 10^4$
24	4-Nitrobenzaldehyde	−0.325		$4.0 \pm 0.3 \times 10^3$

Table 4. (*cont*.)

No.	Compound	E_7^1 (V)	k_{cat} (s^{-1})	k_{cat}/K_m ($M^{-1}s^{-1}$)
25	3,5-Dinitrobenzoic acid	−0.344		$3.9 \pm 0.5 \times 10^3$
26	1,3-Dinitrobenzene	−0.348		$2.7 \pm 0.2 \times 10^3$
27	4-Nitroacetophenone	−0.355		$3.2 \pm 0.4 \times 10^3$
28	CB-1954	−0.385		$2.8 \pm 0.3 \times 10^3$
29	2-Nitrothiophene	−0.390		$2.2 \pm 0.2 \times 10^3$
30	4-Nitrobenzoic acid	−0.425		$4.5 \pm 0.4 \times 10^2$
31	4-Nitrobenzyl alcohol	−0.475		$3.9 \pm 0.2 \times 10^2$
32	Nitrobenzene	−0.485		$5.5 \pm 0.6 \times 10^1$
	Aromatic *N*-oxides			
33	1,2,4-benzotriazine-1,4-dioxide	−0.318		$2.5 \pm 0.3 \times 10^4$
34	7-CF_3-tirapazamine	−0.345	11.5 ± 2.0	$5.2 \pm 0.4 \times 10^4$
35	7-Cl-tirapazamine	−0.400	14.8 ± 1.3	$3.7 \pm 0.4 \times 10^4$
36	7-F-tirapazamine	−0.400		$2.7 \pm 0.2 \times 10^4$
37	3-NH_2-1,2,4-benzotriazine-1,4-dioxide (tirapazamine)	−0.456		$4.4 \pm 0.5 \times 10^3$
38	7-CH_3-tirapazamine	−0.474		$5.0 \pm 0.6 \times 10^3$
39	7-C_2H_5O-tirapazamine	−0.494		$4.5 \pm 0.5 \times 10^3$
40	3-NH_2-1,2,4-benzotriazine-1-oxide	−0.568		$3.2 \pm 0.2 \times 10^3$
41	Quinoxaline-1,4-dioxide	−0.575		$8.2 \pm 0.9 \times 10^2$
	Inorganic complexes			
42	Ferricyanide	0.41	47.9 ± 4.0	$3.0 \pm 0.4 \times 10^6$
43	$Fe(EDTA)^-$	0.12		$4.3 \pm 0.2 \times 10^4$

[a] – taken from [17,158].

unfeasible. The problem can be overcome by using an alternative approach for a rough estimation of E_7^1 according to the rates of O_2 consumption during the quinone-mediated oxidation of ascorbate (Eq. 25) [167]. In the case of quinones with available values of $E_7^1 < -0.1$ V, the rate of O_2 consumption is characterized by a linear log *k vs*. E_7^1 relationship and the data obtained can be described by a linear correlation (Eq. 28)

$$\log k = (2.818 \pm 0.172) + (11.663 \pm 0.728)E_7^1 \qquad R^2 = 0.966 \qquad (28)$$

and it closely matches results obtained previously [167]. Thus, it was possible to calculate the unavailable E_7^1 values for the PD derivatives. These values are considered to be realistic since the differences between experimentally determined E_7^1 values and the calculated $E_{7(calc.)}^1$ values do not exceed 30 milivolts (table 5, compounds 12 – 21).

The data obtained shows that the $E_{7(calc.)}^1$ of plasmodione is more negative than that of menadione (2-CH_3-1,4-naphthtoquinone) due to the 3-benzyl substituent having an electron-donating character whereas the electron-accepting 3-benzoyl substituent of PDO increases its E_7^1 value so it becomes closer to that of 1,4-naphthoquinone. The E_7^1 value of PD-bzol lies between those of PD and PDO. Moreover, the $E_{7(calc.)}^1$ value sequence of 4′-substituted PDO derivatives closely matches the σ_p values of the substituents: 5 (−NO_2, $\sigma_p = 0.78$) ≥ PDO (−CF_3, $\sigma_p = 0.54$) > 6 (−C≡CH, $\sigma_p = 0.23$) ≥ 7 (−Br, $\sigma_p = 0.23$) and is in agreement with reported values [171,176].

The formation of hydrogen bonds between quinone carbonyl groups with 5(8)-OH substituents increases the E_7^1 value of 1,4-naphthoquinones [17]. This phenomenon is evidenced by an increase in $E_{7(calc.)}^1$ of 5-OH- substituted 3-benzoylmenadione 8 with respect to the unsubstituted analogue 7.

Table 5. Rate constants (*k*) of ascorbate oxidation by quinones and 3-benz(o)ylmenadione derivatives, their experimentally derived E_7^1 values taken from [17] and $E_{7(calc.)}^1$ values calculated according to Eq. 28.

No.	Quinone	k ($M^{-1}s^{-1}$)	E_7^1 (V)	$E_{7(calc.)}^1$ (V)
1	Plasmodione (PD)	0.30 ± 0.02		−0.286 ± 0.024
2	PD-bzol	1.17 ± 0.36		−0.236 ± 0.024
3	PDO	4.62 ± 0.99		−0.185 ± 0.019
4	I	1.12 ± 0.13		−0.238 ± 0.022
5	II	0.43 ± 0.07		−0.273 ± 0.023
6	III	2.89 ± 0.46		−0.202 ± 0.020
7	IV	4.75 ± 0.53		−0.183 ± 0.017
8	V	5.60 ± 0.53		−0.169 ± 0.018

Table 5 (cont.)

No.	Quinone	k ($M^{-1}s^{-1}$)	E_7^1 (V)	$E_{7(calc.)}^1$ (V)
9	VI	1.10 ± 0.2		−0.238 ± 0.022
10	VII	0.81 ± 0.14		−0.249 ± 0.022
11	VIII	13.9 ± 1.9		−0.144 ± 0.018
12	5-OH-1,4-naphthoquinone	53.5 ± 6.7	−0.09	−0.093 ± 0.017
13	5,8-$(OH)_2$-1,4-naphthoquinone	48.9 ± 5.2	−0.11	−0.097 ± 0.016
14	9,10-phenanthrenequinone	15.2 ± 0.9	−0.12	−0.140 ± 0.017
15	1,4-naphthoquinone	15.9 ± 1.4	−0.15	−0.139 ± 0.017
16	$(CH_3)_3$-1,4-benzoquinone	16.5 ± 1.8	−0.17	−0.137 ± 0.018
17	2-CH_3-1,4-naphthoquinone	2.38 ± 0.5	−0.20	−0.209 ± 0.021
18	$(CH_3)_4$-1,4-benzoquinone	0.3 ± 0.05	−0.26	−0.286 ± 0.024
19	1,8-$(OH)_2$-9,10-anthraquinone	0.136 ± 0.02	−0.30	−0.316 ± 0.025
20	1,4-$(OH)_2$-9,10-anthraquinone	0.091 ± 0.009	−0.33	−0.331 ± 0.026
21	2-OH-1,4-naphthoquinone	0.018 ± 0.003	−0.41	−0.391 ± 0.029

The steady-state kinetic parameters of the *Pf*FNR catalyzed reduction of PD derivatives with a constant concentration of NADPH are given in table 6. The quinone dependent enzymatic oxidation of NADPH is accompanied by a SOD-sensitive reduction of cyt *c*, i.e., a single-electron character of the quinone reduction accompanied by redox cycling and $O_2^{\bullet-}$ formation is evident.

The coupled cyt *c* reduction by high potential PDO derivatives is less sensitive to SOD in comparison to the low potential ones like PD. The high potential semiquinones, being engaged in a redox equilibrium with the $O_2/O_2^{\bullet-}$ couple, yield a lower amount of $O_2^{\bullet-}$ compared to the low potential semiquinones. It follows that the reduction of cyt *c* mediated by quinones characterized by a higher $E_{7(calc.)}^1$ should be less sensitive to the action of SOD [177].

The reactivity of *Pf*FNR towards model quinones with $E_7^1 = -0.15 - -0.41$ V exhibits a linear dependence on their E_7^1 values (Fig. 17). Importantly, the reactivity of most 3-benz(o)ylmenadione derivatives is much higher than that of model benzoquinones and naphthoquinones with similar $E_{7(calc.)}^1$ values. A possible explanation for the higher reactivity is the high lipophilicity, expressed as log*D*, in most cases exceeding that of model quinones significantly (table 6).

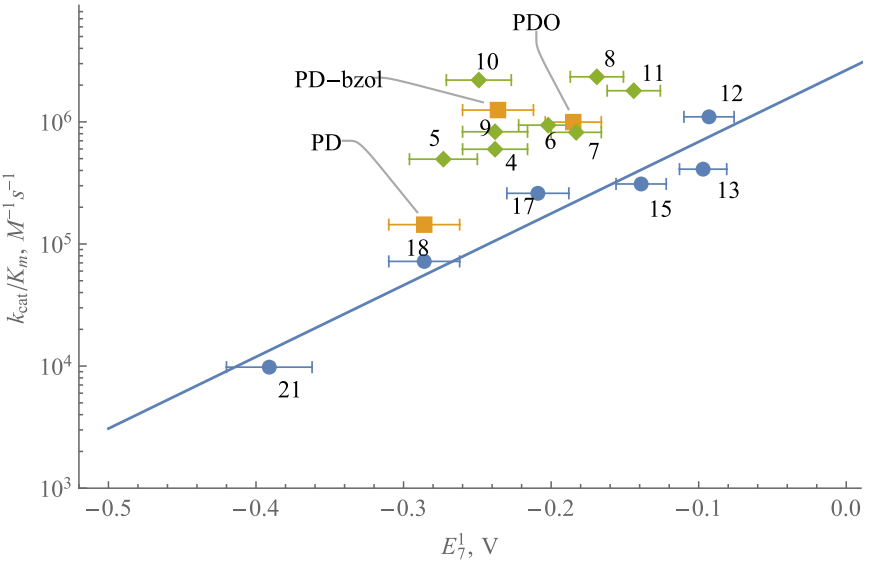

Figure 17. The relationship between the reactivity of *Pf*FNR toward PD, PD-bzol, PDO, PDO derivatives 4 – 11 and model quinones 12 – 18 and their $E_{7(calc.)}^{1}$ values. The numbers of compounds are taken from table 6. The straight line represents the best linear fit of the data related to model quinones 12 – 13, 15, 17 – 18 and 21.

Table 6. $E^1_{7(calc.)}$ values of PD derivatives and model quinones, their reduction rate constants in *Pf*FNR-catalyzed reactions, relative cytochrome *c* reduction rates v_i(cyt *c*)/v_i(NADPH) and their sensitivity to 100 U/mL superoxide dismutase (SOD), and calculated log*D* values

No.	Quinone	$E^1_{7(calc.)}$ (V)	Reactivity with *Pf*FNR		$\frac{v_i(\text{cyt } c)}{v_i(\text{NADPH})}$ (%)	Inhibition by SOD (%)	Log*D*
			k_{cat} (s^{-1})	k_{cat}/K_m ($M^{-1}s^{-1}$)			
1	Plasmodione (PD)	−0.286 ± 0.024	2.6	1.44×10^5	146	94	4.74
2	PD-bzol	−0.236 ± 0.024	5.8	1.25×10^6	195	48	3.67
3	PDO	−0.185 ± 0.019	4.3	9.96×10^5	195	46	4.11
4	I	−0.238 ± 0.022	3.1	5.97×10^5	169	52	4.25
5	II	−0.273 ± 0.023	12.3	4.95×10^5	180	19	2.92
6	III	−0.202 ± 0.020	12	9.40×10^5	193	30	2.92
7	IV	−0.183 ± 0.017	10.2	8.21×10^5	164	75	3.17
8	V	−0.169 ± 0.018	6.4	2.34×10^6	182	31	3.17
9	VI	−0.238 ± 0.022	13.3	8.30×10^5	186	28	3.38
10	VII	−0.249 ± 0.022	5.6	2.20×10^6	195	36	4.00
11	VIII	−0.144 ± 0.018	12.7	1.80×10^6	192	19	4.28
12	5-OH-1,4-naphthoquinone	−0.093 ± 0.017	35.7	1.10×10^6			1.82
13	5,8-$(OH)_2$-1,4-naphthoquinone	−0.097 ± 0.016	25.0	4.10×10^5			2.17
15	1,4-naphthoquinone	−0.139 ± 0.017	16.9	3.10×10^5			1.50
17	2-CH_3-1,4-naphthoquinone	−0.209 ± 0.021	26.5	2.60×10^5	190	50	1.89
18	$(CH_3)_4$-1,4-benzoquinone	−0.286 ± 0.024	33.1	7.20×10^4			2.61
21	2-OH-1,4-naphthoquinone	−0.391 ± 0.029	2.6	9.80×10^3			−0.7

3.1.2.The studies of inhibition of *Pf*FNR

During the transhydrogenase reaction of *Pf*FNR, 3-acetylpyridine adenine dinucleotide phosphate (3-AcADP$^+$) is reduced at the expense of NADPH (AcADP$^+$ → AcADPH), however the k_{cat} of the reaction did not depend on the concentration of NADPH (in the 25 – 200 μM range) and was equal to 3.2 ± 0.4 s^{-1} (Fig. 18). On the other hand, the k_{cat}/K_m for the oxidant did decrease with the increase in NADPH concentration, meaning that NADPH inhibits the reaction competitively in regards to AcADP$^+$ due to occupying the pyridine nucleotide binding site of the reduced enzyme. According to Eq. 20, the K_{is} of NADPH, which describes the effect of NADPH on the slopes in the Lineweaver-Burk plots, is equal to 140 ± 20 μM, and the k_{cat}/K_m for AcADP$^+$ at [NADPH] = 0 is equal to 9.3 ± 0.8 × 10^3 $M^{-1}s^{-1}$ (Fig. 18).

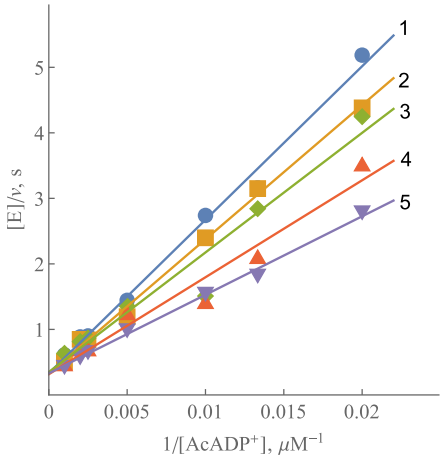

Figure 18. Steady-state kinetics of the reduction of 3-acetylpyridine adenine dinucleotide phosphate (AcADP$^+$) by *Pf*FNR. NADPH concentrations are 200 μM (1), 150 μM (2), 100 μM (3), 50 μM (4), 25 μM (5).

The inhibition of *Pf*FNR by the reaction product NADP$^+$ was examined next. It acts as a competitive inhibitor towards NADPH when there is a fixed concentration of juglone present (Fig. 19A) with K_i = 1.42 ± 0.13 mM according to Eq. 20. When the concentration of NADPH is held constant at 50 μM, NADP$^+$ inhibits juglone reduction uncompetitively (Fig. 19B) with K_i = 1.83 ± 0.19 mM according to Eq. 21. When compared to previous data obtained in 0.05 M Hepes, the use of 0.1 M phosphate buffer decreased the

k_{cat}/K_m for NADPH and increased the K_i of $NADP^+$ by close to an order of magnitude [178,179].

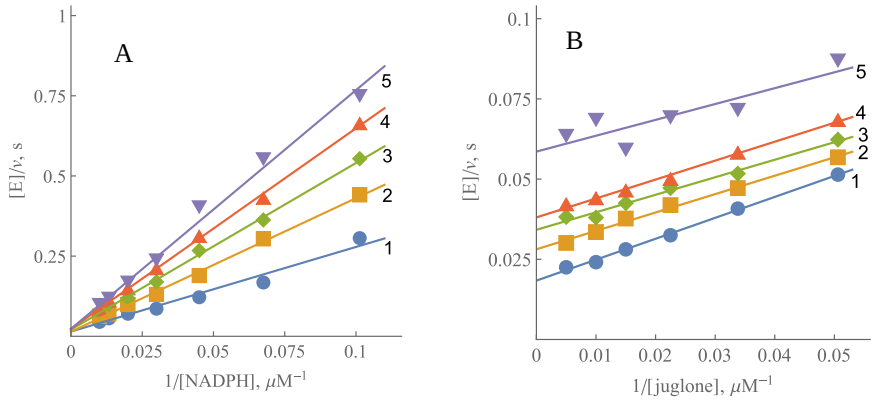

Figure 19. Inhibition of the juglone reductase reaction of *Pf*FNR by $NADP^+$. (A) Inhibition at varied NADPH concentrations in the presence of 100 μM juglone and (B) inhibition at varied juglone concentrations in the presence of 100 μM NADPH. $NADP^+$ concentrations are 0 (1), 1.0 mM (2), 2.0 mM (3), 3.0 mM (4) and 5.0 mM (5).

3.1.3. The effects of ionic strength and pH on the kinetics of *Pf*FNR with nonphysiological electron acceptors

P. falciparum ferredoxin (*Pf*Fd) is the physiological oxidant of *Pf*FNR. The affinity between the two proteins decreases with increasing ionic strength of the solution due to *Pf*Fd being charged negatively and *Pf*FNR containing positively charged amino acid residues [180,181]. The effects of ionic strength on the reduction rates of nonphysiological oxidants in the *Pf*FNR-catalyzed reactions allowed the assessment of the role of electrostatic interactions. It has been reported that high concentration of ferricyanide inhibits the NADPH-ferricyanide reductase reaction of *Pf*FNR with ferricyanide acting competitively towards NADPH with K_i = 230 μM [89]. However, when the medium is phosphate buffer (as in this case) and not 0.1 M Tris/HCl, substrate inhibition by ferricyanide is not evident. Hence it was possible to perform a more thorough analysis of reduction kinetics. There is a bell-shaped dependence of the log k_{cat}/K_m for ferricyanide, $Fe(EDTA)^-$ and benzylviologen on the ionic strength of the solution with the two later electron acceptors showing highly similar dependencies regardless of their opposite electrostatic charges (Fig. 20, 1 – 3). In contrast to the charged species, the k_{cat}/K_m of the neutral electron acceptor tetramethyl-1,4-benzoquinone (duroquinone) did not depend on the ionic strength (Fig. 20, 4).

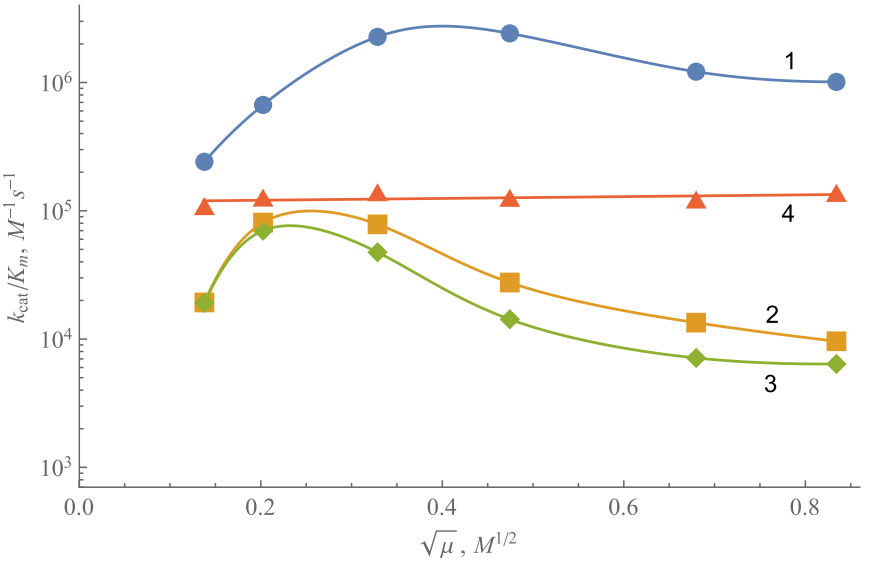

Figure 20. Effects of the ionic strength on the reactivity of *Pf*FNR towards the electron acceptors. The dependence of log k_{cat}/K_m for ferricyanide (1), $Fe(EDTA)^-$ (2), benzylviologen (3) and duroquinone (4) on the ionic strength of the potassium phosphate buffer at pH 7.0.

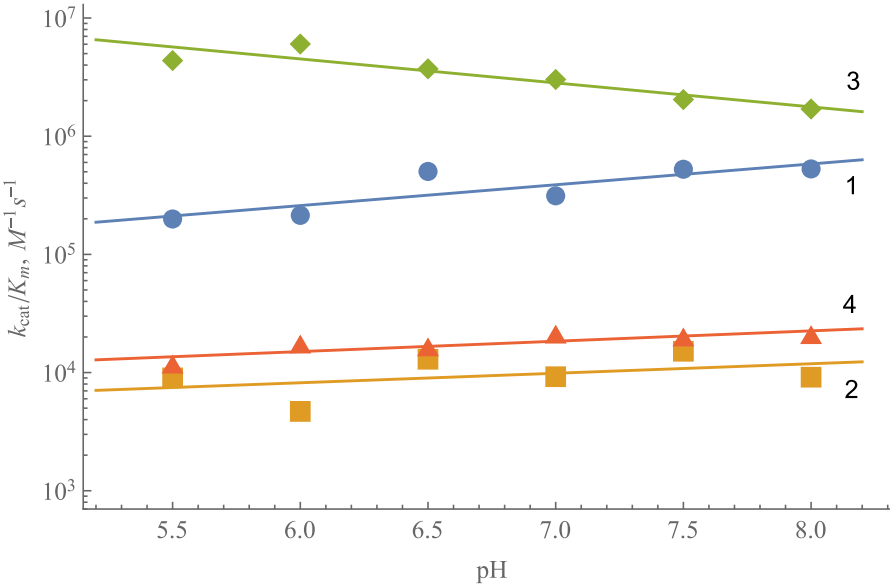

Figure 21. Effects of pH on the reactivity expressed in log k_{cat}/K_m of *Pf*FNR towards the electron acceptors. The oxidants are 1,4-naphthoquinone (1), trinitrotoluene (2), ferricyanide (3) and benzylviologen (4).

The effect of pH on the kinetics of *Pf*FNR catalyzed reaction was tested with four nonphysiological oxidants – uncharged 1,4-naphthoquinone and TNT (Fig. 21, 1 and 2), negatively charged ferricyanide and positively charged benzylviologen (Fig. 21, 3 and 4). There was a slight increase in reactivity upon increasing the pH of the medium with uncharged or positively charged oxidants, whereas ferricyanide exhibited a decreasing reactivity.

3.1.4. Stimulation of acceptor reductase activity of *Pf*FNR by *Pf*Fd

The complex formation between *Pf*FNR and *Pf*Fd at intermediate ionic strength is characterized by micromolar K_d values [90,181]. *Pf*Fd stimulated the reduction of quinones and nitroaromatics by *Pf*FNR and there appears a biphasicity in the corresponding Lineweaver-Burk plots (Fig. 22A, 3, 4).

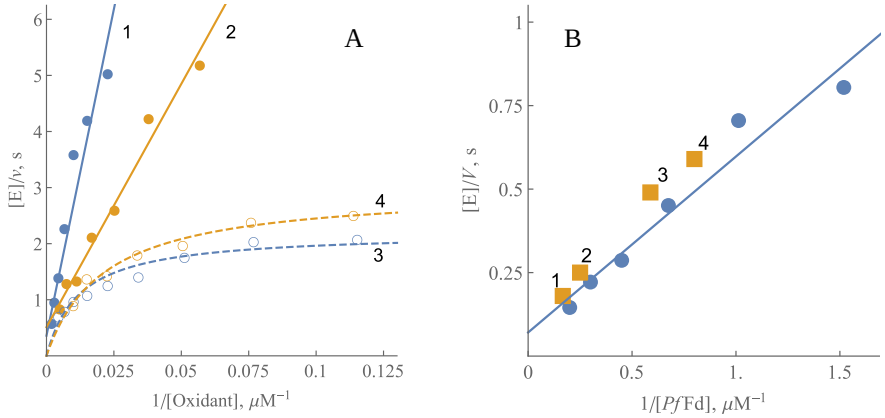

Figure 22. Stimulation of quinone- and nitroreductase reactions of *Pf*FNR by ferredoxin. (A) The dependence of the *Pf*FNR catalyzed NADPH oxidation rate on the concentration of *p*-nitroacetophenone (1, 4) or 2-OH-1,4-naphthoquinone (2, 3) in the absence of *Pf*Fd (1, 2) or in the presence of 1.7 μM (3) or 4.0 μM (4) *Pf*Fd; concentration of NADPH is 100 μM. (B) The dependence of the rate of cytochrome *c* reduction by *Pf*FNR on the concentration of *Pf*Fd (solid circles). [NADPH] = 100 μM, [cytochrome *c*] = 50 μM. Orange circles show the rates of the "slower" phase of NADPH oxidation in the presence of duroquinone (1), *p*-nitroacetophenone (2, 4) and 2-OH-1,4-naphthoquinone (3) at respective concentrations of *Pf*Fd on single-electron base. The maximal rates were obtained by fitting the kinetic data of the "slower" phase (5 – 6 lower concentrations of the oxidant) to the parabolic expression.

The maximal rates of their "slower" phase (low concentration of the oxidant, higher k_{cat}/K_m) were close to the rates of cytochrome *c* reduction at corresponding *Pf*Fd concentrations (Fig. 22B), which in turn are equal to the rate of *Pf*Fd reduction by *Pf*FNR. Under the given conditions (0.1 M potassium phosphate buffer, pH 7.0), the maximal rate of this reaction at saturating *Pf*Fd concentration was $16 \pm 2.5\ s^{-1}$ on the one-electron base, which was close to the values reported previously by Balconi and colleagues [90]. The higher ionic strength of the medium may be responsible for the increase in apparent Michaelis constants, $K_{m(app.)} = 5.2 \pm 1.3\ \mu M$, which is significantly higher than the one reported previously [90].

3.1.5. Presteady-state kinetics studies of *Pf*FNR

The spectral changes of *Pf*FNR bound FAD during the multiple turnover under aerobic conditions give insight into the reoxidation mechanism of the enzyme. Tetramethyl-1,4-benzoquinone was used as an electron acceptor because of it not absorbing light at ≥460 nm and having a semiquinone form that is rapidly reoxidized by oxygen [182]. In control experiments performed in the absence of quinone, the initial fast phase of FAD reduction by NADPH seen at 460 nm is followed by a slower reoxidation by oxygen. This is accompanied by a transient increase in absorbance at 600 nm at the same time scale (Fig. 23A). The addition of quinone accelerates the reoxidation of $FADH^{\bullet-}$ and the decay of the 600 nm absorbing species by up to two orders of magnitude (Fig. 23B). This shows that, under given experimental conditions, O_2 plays a negligible role in the kinetics of enzyme reoxidation. This process is also accompanied by a transient increase in absorbance at 600 nm.

It was assumed that complete FAD reduction corresponds to the maximum ΔA_{460} after the enzyme is mixed with NADPH in the absence of quinone (Fig. 23A). This 460 nm absorbance change was close to that expected using the value $\Delta\varepsilon_{460} = 7.8\ mM^{-1}cm^{-1}$ for the absorbance difference between the oxidized and two-electron reduced *Pf*FNR [90,178,179]. A $k_{ox} = 0.18 \pm 0.02\ s^{-1}$ was obtained for the reoxidation of *Pf*FNR with oxygen (Fig. 23A) and it was similar to the *Pf*FNR NADPH oxidase activity in the steady-state. An apparent bimolecular rate constant of $1.34 \pm 0.37 \times 10^5\ M^{-1}s^{-1}$ was obtained from the k_{ox} dependence on the duroquinone concentration (Fig. 23D) which was comparable to the k_{cat}/K_m in the steady state (Table 4), however, the obtained $k_{ox(max)} = 155 \pm 32\ s^{-1}$ should be regarded cautiously since the limited solubility of the oxidant might have made it impossible to obtain a saturating concentration, i.e., sufficiently high k_{ox} values.

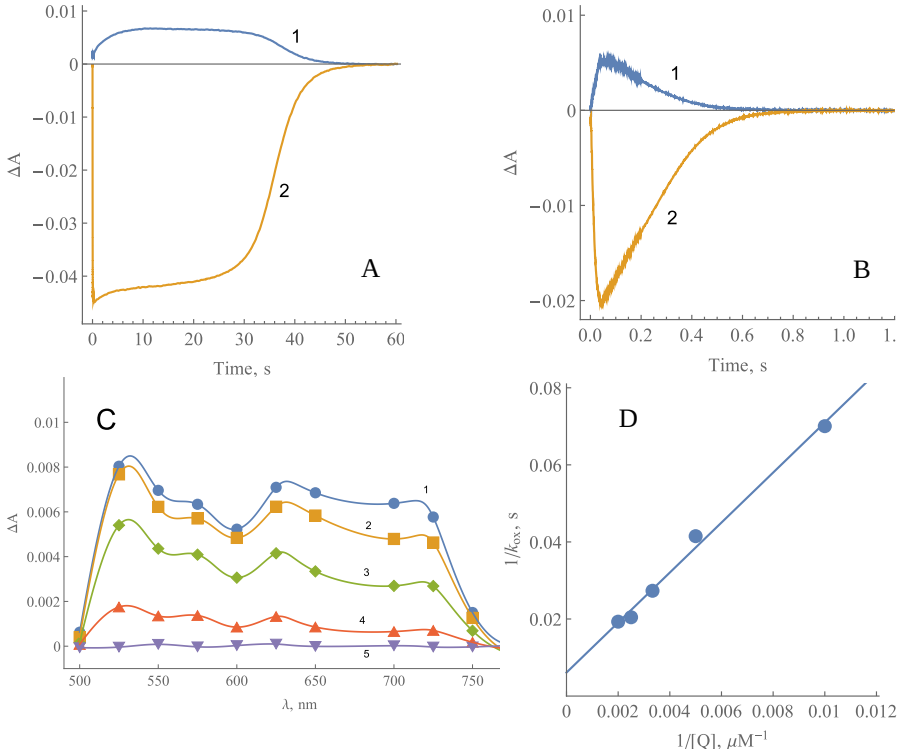

Figure 23. Turnover of *Pf*FNR in the presence of NADPH and oxidants. (A, B) The kinetics of the absorbance changes at 600 nm (1) and 460 nm (2) during the reduction of *Pf*FNR (6.0 μM) by 50 μM NADPH and its subsequent reoxidation by oxygen (A) or 250 μM duroquinone (B) (concentrations after mixing). (C) Transient spectra of reaction intermediates formed during the turnover of *Pf*FNR with duroquinone. Difference in absorbance after 50 ms (1), 100 ms (2), 200 ms (3), 400 ms (4) and 1 s (5). The reaction is considered complete at 1.2 s. (D) The dependence of the apparent first-order reoxidation rate constant on the concentration of duroquinone.

3.1.6. Characterization of the mechanism of reduction of nonphysiological electron acceptors by *Pf*FNR

Since *Pf*FNR follows a *ping-pong* mechanism, the reductive and oxidative half-reactions can proceed independently and k_{cat} can be expressed as Eq. 29:

$$\frac{1}{k_{cat}} = \frac{1}{k_{red(max)}} + \frac{1}{k_{ox(max)}} \qquad (29)$$

Where $k_{red(max)}$ and $k_{ox(max)}$ are the maximal rates of reductive and oxidative half-reactions, respectively. The overall catalytic process should be partly limited by both oxidative and reductive half-reactions in the case of tetramethyl-1,4-benzoquinone, since the maximal rates of *Pf*FNR reduction by NADPH at pH 7.0 is 125 – 148 s^{-1} [89,179], and a comparable value $k_{ox(max)}$ = 155 ± 32 s^{-1} was obtained for duroquinone under multiple turnover conditions. On the other hand, the rate of enzyme reduction with a fixed concentration of NADPH should be the same, regardless of the oxidant used, and the observed differences in $k_{cat(app.)}$ (Table 4) should be attributed to different maximal rates of reoxidation. Thus for oxidants whose $k_{cat(app.)}$ values are close to that of duroquinone (k_{cat} = 33.1 ± 4.3 s^{-1}), for example 2-CH_3-1,4-benzoquinone or 2-CH_3-1,4-naphthoquinone (k_{cat} = 32.4 ± 4.1 s^{-1} and k_{cat} = 26.5 ± 3.2 s^{-1}, respectively), the overall catalytic process should be partly limited by both oxidative and reductive reactions, as well. The lower values of $k_{cat(app.)}$ for other compounds imply that in these cases the process is limited by the oxidative half-reaction.

Reduced *Pf*FNR is reoxidized in a single-electron way and the oxidative half-reaction must proceed through two steps, namely $FADH^- \rightarrow FADH^\bullet$ and $FADH^\bullet \rightarrow FAD$. A possible rate-limiting step of the overall process is the oxidation of FAD semiquinone and this is supported by several facts. The 600 nm absorbing species is formed during the reoxidation of reduced *Pf*FNR by quinones (Fig. 23B), which may point to a transient $FADH^\bullet$ accumulation [21,75]. Absorption above 700 nm is not characteristic of FADH [169] and indicates a parallel formation of other reaction intermediates (Fig. 23C). For example, CTCs of two-electron reduced FAD absorb up to 1000 nm [81]. However, this possibility should be ruled out because the spectrum of the intermediates ends at 770 – 800 nm. Additionally, the $FADH^-$-$NADP^+$ complexes are characterized by ε ~ 1.0 $mM^{-1}cm^{-1}$ at 610 – 725 nm [183]. A more likely supposition is that the data in figure 23B reflect the formation of $FADH^\bullet$-NADP(H) complexes observed in adrenodoxin reductase, which absorb at λ > 700 nm, but are only partly characterized [184,185].

NADPH acts as a competitive inhibitor with respect to the oxidant in the reduction of $AcADP^+$ by *Pf*FNR whereas it does not inhibit quinone reduction (Fig. 19). It follows that quinones and $AcADP^+$ oxidize different redox forms of *Pf*FNR possessing different affinities for NADPH. Since $AcADP^+$ is an obligatory two-electron (hydride) acceptor, it can be reduced only by a two-electron reduced FAD and this argues against its involvement as a rate-limiting step in quinone reduction. $NADP^+$ acts as a competitive inhibitor with respect to NADPH and as an uncompetitive inhibitor with respect to quinones

which is attributable to a specific case of a *ping-pong* mechanism, where $NADP^+$ binds relatively tightly to the oxidized form of *Pf*FNR while binding weakly (or not binding at all) when *Pf*FNR is reduced by two electrons [186]. Thus it is tempting to state that *Pf*FNR has properties in common with FNRs from *Anabaena* and spinach, where it is the oxidation of $FADH^{\bullet}$ that is the rate-limiting step of reactions with various nonphysiological electron acceptors [21,75,76,187].

The studies of the effects of ionic strength in the reaction with charged oxidants gives some insight into the action of charged amino acid residues in the vicinity of the isoalloxazine ring of FAD (Fig. 20). The observed bell-shape-like dependences of the reactivity of oppositely charged oxidants on the ionic strength of the solution were unexpected but are similar to those observed in *Anabaena* FNR [75]. A possible explanation for the observed phenomenon is that the oxidants may interact with both negatively charged Glu314 and positively charged Lys287 (Glu308 – Arg274 pair in *Anabaena* [180,188] the latter participating in the binding of *Pf*Fd and situated close to the dimethylbenzene part of the isoalloxazine ring [89,181]. This is also in line with the fact that ferricyanide competes with the nicotinamide mononucleotide part of $NADP^+$ for binding close to the isoalloxazine ring [89]. Other positively charged residues participating in the binding of *Pf*Fd, such as Arg98, Arg290 or Lys308 are further away from the isoalloxazine thus unlikely to interact with low molecular weight oxidants [181]. The data obtained in the pH dependency studies cannot be adequately explained at this time and warrants further studies (Fig. 21).

The stimulation of the nonphysiological acceptor reductase reactions of *Pf*FNR by *Pf*Fd shows it providing an alternative pathway for the reduction to proceed via reduced *Pf*Fd (Fig. 22). Better accessibility of the active center of *Pf*Fd is a likely explanation given the similar redox potentials of both proteins [90,180]. Moreover, it could be considered a general feature of this group of redox proteins, since such stimulation had previously been observed in reactions of bovine adrenodoxin reductase and adrenodoxin and *Anabaena* FNR and Fd [45,75].

Given that there is no strict substrate specificity apart from an increase in the log k_{cat}/K_m with increasing E_7^1, an outer sphere electron transfer mechanism for the reduction of quinones, nitroaromatics and aromatic *N*-oxides appears to be likely. Indeed, it is well established that it is the case for FNR from *Anabaena*, P-450R and NOS [29,75,119]. According to Eqs. 12 – 14 stemming from the works of Marcus [24] and 100-fold difference in k_{22} values between nitroaromatics and quinones or aromatic *N*-oxides, the difference in reactivities of $ArNO_2$ are unsurprisingly 10 times lower than those of quinones

and ArN→O of similar E_7^1 values [26,34]. Redox cycling oxidants of particular interest include the promising novel antimalarial plasmodione and its metabolites or various functional derivatives, high energy nitroaromatic compounds like nitrobenzimidazolones and tumorocidal aromatic *N*-oxides. Moreover, when taken together with other flavoenzymes electrontransferases, the reactivity of *Pf*FNR-catalyzed one-electron reduction can be used to calculate the expected E_7^1 to within 30 mV thus providing an alternative means of E_7^1 estimation when it is hampered by low solubility of a compound of interest.

3.1.7. The estimation of unknown E_7^1 values of aromatic oxidants according to their single-electron reduction rate constants by *Pf*FNR

3.1.7.1. The estimation of unknown E_7^1 values of nitroaromatic compounds

A clearly defined linear relationship between E_7^1 and the logarithm of k_{cat}/K_m in the case of single-electron reduction reactions of nitroaromatic compounds catalyzed by dehydrogenases – electrontransferases, such as NADPH:cytochrome P-450 reductase (P-450R) [119], *Saccharomyces cerevisiae L*-lactate:cytochrome *c* reductase (flavocytochrome b_2, Fcb2) [189] or algal ferredoxin:$NADP^+$ reductase from *Anabaena* PCC7119 (*An*FNR) [75]. Reduction proceeds in the general form of $ArNO_2 \rightarrow ArNO_2^{\bullet-}$ and the apparent low selectivity towards the structure of the oxidant is consistent with the outer sphere electron transfer model [23,189]. However, possible specific interactions introduce data scattering when calculating the unavailable E_7^1 values and one can minimize that by calculating the means from several different enzymatic systems. According to the data presented in table 7, *Pf*FNR is similar to the enzymes mentioned earlier in this regard. The equation (30) in table 8 was derived according to the data in table 7 while Eqs. 31 – 33 are given for comparative purposes with data derived from earlier studies [189].

The mean values of calculated single-electron reduction potentials were obtained and the standard errors do not exceed 30 millivolts, while the experimental error in E_7^1 determination by pulse radiolysis is ± 8 – 15 mV [190]. The difference between E_7^1 and $E_{7(calc.)}^1$ does not exceed ±33 mV with the average difference being ±17 mV, except for 4-nitrobenzyl alcohol (table 9). While some of the $E_{7(calc.)}^1$ values are higher than −0.25 V (compounds

Table 7. The bimolecular rate constants (k_{cat}/K_m) of reduction of nitroaromatic compounds by electrontransferases. The rate constants of P-450R, *An*FNR and Fcb2 were taken from an earlier study for comparison [189].

No.	Compound	k_{cat}/K_m ($M^{-1}s^{-1}$)			
		PfFNR	**P-450R**	***An*FNR**	**Fcb2**
14	3,5-Dinitrobenzamide	4.9×10^3	3.0×10^5	1.2×10^4	8.5×10^2
15	*N*-methylpicramide	6.8×10^4	2.0×10^6	2.6×10^4	
16	Pentryl	2.9×10^5	1.3×10^7	5.5×10^5	
17	2,4-Dinitrophenyl-*N*-methylnitramine	7.1×10^4	3.8×10^6	2.5×10^5	
18	5-Nitrobenzimidazolone	8.9×10^3		6.0×10^2	2.0×10^2
19	5,6-Dinitrobenzimidazolone	1.8×10^4		1.9×10^4	3.2×10^3
20	4,5,6-Trinitrobenzimidazolone	7.5×10^4	2.6×10^6	1.0×10^5	1.5×10^4
21	4,5,6,7-Tetranitrobenzimidazolone	6.6×10^5	8.1×10^5	3.1×10^5	3.2×10^4
22	5-Amino-4,6-dinitrobenzimidazolone	2.8×10^4		2.7×10^4	5.3×10^3
23	NTO	1.7×10^2	9.0×10^2	5.5×10^1	

Table 8. The expressions of linear log k_{cat}/K_m *vs.* E_7^1 relationships and the respective R-squared values

Enzyme	**Log k_{cat}/K_m**	**R^2**	
*Pf*FNR	$(7.3054 \pm 0.3702) + (10.7971 \pm 1.0542)E_7^1$	0.9051	(30)
P-450R	$(8.5883 \pm 0.6261) + (10.3179 \pm 1.7980)E_7^1$	0.7671	(31)
*An*FNR	$(6.8590 \pm 0.5287) + (10.4984 \pm 1.5055)E_7^1$	0.8155	(32)
Fcb2	$(6.6157 \pm 0.1376) + (11.6152 \pm 0.3782)E_7^1$	0.9937	(33)

Table 9. The single-electron reduction potentials E_7^1 of nitroaromatic compounds, calculated according to Eqs. 30 – 33 from table 8.

No.	Compound	E_7^1 (V)[a]	$E_{7(calc.)}^1$ (V)				
			Eq. 30	Eq. 31	Eq. 32	Eq. 33	Mean
1	Nitrobenzene	−0.485	−0.499	−0.461	−0.515	−0.483	−0489 ± 0.012
2	4-Nitrobenzyl alcohol	−0.475	−0.427	−0.414	−0.429		−0.423 ± 0.005
3	4-Nitrobenzoic acid	−0.425	−0.423	−0.439	−0.410	−0.423	−0.423 ± 0.006
4	CB-1954	−0.385	−0.355		−0.316	−0.385	−0.352 ± 0.020
5	4-Nitroacetophenone	−0.355	−0.350	−0.348	−0.363	−0.363	−0.356 ± 0.004
6	1,3-Dinitrobenzene	−0.348	−0.357	−0.307	−0.332		−0.332 ± 0.014
7	3,5-Dinitrobenzoic acid	−0.344	−0.343	−0.306	−0.360		−0.336 ± 0.016
8	4-Nitrobenzaldehyde	−0.325	−0.343	−0.412	−0.292	−0.323	−0.342 ± 0.025
9	1,2-Dinitrobenzene	−0.287	−0.306	−0.291	−0.336		−0.311 ± 0.013
10	1,4-Dinitrobenzene	−0.257	−0.228	−0.244	−0.248		−0.240 ± 0.006
11	Nifuroxim	−0.255	−0.266	−0.294	−0.295	−0.263	−0.279 ± 0.009
12	Nitrofurantoin	−0.255	−0.240	−0.294	−0.272	−0.246	−0.263 ± 0.013
13	TNT	−0.253	−0.301	−0.254	−0.282		−0.279 ± 0.013
14	3,5-Dinitrobenzamide		−0.335	−0.310	−0.279	−0.318	−0.311 ± 0.012
15	*N*-methylpicramide		−0.240	−0.249	−0.253		−0.247 ± 0.004
16	Pentryl		−0.188	−0.188	−0.150		−0.175 ± 0.013
17	2,4-Dinitrophenyl-*N*-methylnitramine		−0.238	−0.228	−0.177		−0.214 ± 0.019
18	5-Nitrobenzimidazolone		−0.314		−0.380	−0.371	−0.355 ± 0.021
19	5,6-Dinitrobenzimidazolone		−0.289		−0.264	−0.268	−0.273 ± 0.008
20	4,5,6-Trinitrobenzimidazolone		−0.236	−0.240	−0.208	−0.211	−0.224 ± 0.009
21	4,5,6,7-Tetranitrobenzimidazolone		−0.157	−0.278	−0.169	−0.183	−0.197 ± 0.028
22	5-Amino-4,6-dinitrobenzimidazolone		−0.273		−0.252	−0.250	−0.258 ± 0.007

Table 9 (cont.)

No.	Compound	E_7^1 (V)	$E_{7(calc.)}^1$ (V)				
			Eq. 30	**Eq. 31**	**Eq. 32**	**Eq. 33**	**Mean**
23	NTO		−0.458	−0.498	−0.461		−0.472 ± 0.013

[a] – taken from [17].

15-17, 20, 21), the high electron-accepting potency of these compounds is in line with the data obtained in quantum mechanical calculations where these compounds are shown to possess enthalpies of single-electron reduction that are more negative than that of TNT [23].

3.1.7.2. Reactions of *Pf*FNR with aromatic *N*-oxides with uncharacterized E_7^1 values

It is somewhat interesting to examine the reactions of *Pf*FNR with ArN→O of unknown E_7^1 values, since this might be helpful in the estimation of these values. The k_{cat}/K_m values of these compounds are given in table 10. In most cases the reaction rates were proportional to the concentration of the compounds up to the limits of their solubility, 300 – 600 μM. Redox cycling of the synthesized ArN→O was demonstrated by the reduction of cytochrome *c*. The reaction rates were equal to 175 – 190% that of NADPH oxidation rate, whereas cyt *c* reduction was inhibited by 20 – 60% upon addition of 100 U/ml superoxide dismutase, pointing to the formation of a superoxide.

The reactivity of compounds 1 – 7 with available E_7^1 values (table 10) may be characterized by a linear dependence (Eq. 34):

$$\Delta\log\left(k_{cat}/K_m\right)/\Delta E_7^1 = 6.07 \pm 1.05\,\mathrm{V}^{-1} \qquad (34)$$

Alternatively, the reactivity of TPZ and its 7-substituted derivatives increases with the σ_p value of substituents, expressed as Eq. 35:

$$\Delta\log\left(k_{cat}/K_m\right)/\Delta\sigma_p = 1.53 \pm 0.35 \qquad (35)$$

σ is the substituent constant measuring the total polar effect exerted by a given substituent relative to there being no substituent on the reaction center and the indices *m* (*meta*) and *p* (*para*) denote the relative position. This shows that the reactivity of compounds is not structurally specific and is governed mainly by their electron-accepting properties. On the other hand, while the reactivity of BTRDO, TPZ and 3-substituted derivatives of TPZ increases with either σ_p or σ_m values of substituents, the dependence is less pronounced. (Table 10, Figure 24).

Table 10. Tirapazamine and its derivatives used in the calculation of substituents' effects on the reactivity of the compound

No.	Compound	k_{cat}/K_m, $M^{-1}s^{-1}$	E_7^1, V[a]	σ_{p1}[b]	σ_{p2}[b]	σ_m[b]
1	BTRDO	2.5×10^4	−0.318	–	0	0
2	7-CF_3-TPZ	5.2×10^4	−0.345	0.54	–	–
3	7-Cl-TPZ	3.7×10^4	−0.400	0.23	–	–
4	7-F-TPZ	2.7×10^4	−0.400	0.06	–	–

Table 10 (cont.)

No.	Compound	k_{cat}/K_m, $M^{-1}s^{-1}$	E_7^1, V	σ_{p1}	σ_{p2}	σ_m
5	TPZ	4.4×10^3	−0.456	0	−0.66	−0.16
6	7-CH_3-TPZ	5.0×10^3	−0.474	−0.17	–	–
7	7-C_2H_5O-TPZ	4.5×10^3	−0.494	−0.27	–	–
8	7-CF_3O-TPZ	3.8×10^4	–	0.35	–	–
9	3-$NHCOCH_3$-TPZ	6.3×10^4	–	–	0	0.21
10	3-$NHSO_2CF_3$-TPZ	2.6×10^4	–	–	0.39	0.44
11	3-$NHSO_2CH_3$-TPZ	7.9×10^3	–	–	0.03	0.2

[a] – taken from [158], [b] – taken from [176]

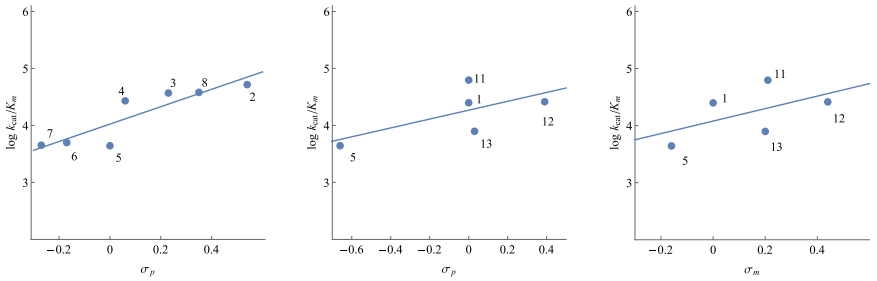

Figure 24. The relationship between a reactivity of a compound and the effect of a substituent as calculated according to Taft – Hammet equation. The compounds are given in table 10.

In parallel, the k_{cat}/K_m values of ArN→O with another single-electron transferring flavoenzyme, NADPH:cytochrome P-450 reductase (P-450R) were determined. These experiments were carried out by dr. Audronė Marozienė and dr. Lina Misevičienė. In this case, log k_{cat}/K_m for ArN→O also increased with increasing E_7^1 [26]. One may use the geometric average of k_{cat}/K_m obtained from several enzymatic systems, which improves the accuracy of the prediction [23,189]. The geometric averages of log k_{cat}/K_m in the table 11 were obtained according to Eq. 36:

$$\log\left(k_{cat}/K_m\right)_{avg} = 0.5\log\left(k_{cat}/K_m\right)_{P\text{-}450R} + \log\left(k_{cat}/K_m\right)_{PfFNR} \qquad (36)$$

The logarithms of reduction rate constants for compounds 10 – 18 (table 11) correlate well with their E_7^1 values (Eq. 37):

$$\log\left(k_{cat}/K_m\right)_{avg} = \left(7.23 \pm 0.29\right) + \left(6.96 \pm 0.65\right)E_7^1 \qquad R^2 = 0.9430 \qquad (37)$$

For compounds with unavailable E_7^1 values the introduction of electron-accepting substituents into 3-NH_2 group or into 7- and 2- positions of the aromatic system in most cases increased their log k_{cat}/K_m (avg) when compared

to the parent compound. Therefore, it appears to be a suitable parameter to describe the ease of single-electron reduction of ArN→O.

Table 11. The single-electron reduction midpoint potentials (E_7^1) of aromatic *N*-oxides, the steady-state bimolecular rate constants (k_{cat}/K_m) of their reduction by P-450R and *Pf*FNR and the logs of the geometric averages of their reactivity.

No.	Compound	E_7^1 (V)[a]	k_{cat}/K_m ($M^{-1}s^{-1}$)		Log k_{cat}/K_m (avg)
			P-450R[c]	*Pf*FNR	
1	7-CF_3O-tirapazamine		$4.6 \pm 0.4 \times 10^4$	$3.8 \pm 0.4 \times 10^4$	4.62
2	3-CH_3CONH-1,2,4-benzotriazine-1,4-dioxide		$7.0 \pm 0.5 \times 10^4$	$6.2 \pm 0.5 \times 10^4$	4.82
3	3-CH_3OCONH-1,2,4-benzotriazine-1,4-dioxide		$8.0 \pm 0.9 \times 10^4$	$4.8 \pm 0.4 \times 10^4$	4.78
4	3-CF_3SO_2NH-1,2,4-benzotriazine-1,4-dioxide		$2.5 \pm 0.3 \times 10^4$	$2.6 \pm 0.3 \times 10^4$	4.41
5	3-CH_3SO_2NH-1,2,4-benzotriazine-1,4-dioxide		$2.7 \pm 0.3 \times 10^3$	$7.9 \pm 0.5 \times 10^3$	3.67
6	2-CF_3-quinoxaline-1,4-dioxide	−0.465[b]	$2.7 \pm 0.3 \times 10^4$	$8.9 \pm 0.7 \times 10^3$	4.19
7	2-NH_2-3-CN-quinoxaline-1,4-dioxide		$4.7 \pm 0.4 \times 10^3$	$1.8 \pm 0.2 \times 10^4$	3.96
8	1,2,4-benzotriazine-1-oxide	−0.431[b]	$1.7 \pm 0.2 \times 10^4$	$4.3 \pm 0.3 \times 10^3$	3.94
9	3-CH_3CONH-1,2,4-benzotriazine-1-oxide		$8.7 \pm 0.9 \times 10^3$	$1.6 \pm 0.1 \times 10^3$	3.58
	ArN→O with available E_7^1 values				
10	1,2,4-benzotriazine-1,4-dioxide	−0.318	$4.3 \pm 0.4 \times 10^5$	$2.5 \pm 0.3 \times 10^4$	5.00
11	7-CF_3-tirapazamine	−0.345	$8.7 \pm 0.7 \times 10^4$	$5.2 \pm 0.4 \times 10^4$	4.83
12	7-Cl-tirapazamine	−0.400	$6.9 \pm 0.7 \times 10^4$	$3.7 \pm 0.4 \times 10^4$	4.71
13	7-F-tirapazamine	−0.400	$3.4 \pm 0.3 \times 10^4$	$2.7 \pm 0.2 \times 10^4$	4.48
14	3-NH_2-1,2,4-benzotriazine-1,4-dioxide	−0.455	$1.1 \pm 0.1 \times 10^4$	$4.4 \pm 0.5 \times 10^3$	3.84
15	7-CH_3-tirapazamine	−0.474	$8.6 \pm 0.7 \times 10^3$	$5.0 \pm 0.6 \times 10^3$	3.82
16	7-C_2H_5O-tirapazamine	−0.494	$4.5 \pm 0.5 \times 10^3$	$4.5 \pm 0.5 \times 10^3$	3.65
17	3-NH_2-1,2,4-benzotriazine-1-oxide	−0.568	$2.8 \pm 0.2 \times 10^3$	$3.2 \pm 0.2 \times 10^3$	3.48
18	Quinoxaline-1,4-dioxide	−0.575	$3.3 \pm 0.2 \times 10^3$	$8.2 \pm 0.9 \times 10^2$	3.22

[a] – [31,158,191]; [b] – calculated using the ΔE_7^1 between compounds 11 and 14 and 17 and 14, respectively; [c] – taken from [26].

3.2. *Rhodopseudomonas palustris* ferredoxin:NADP$^+$ reductase

3.2.1. Steady-state kinetics and oxidant substrate specificity of *Rp*FNR

Earlier kinetic studies of *Rp*FNR focused on the classical nonphysiological single-electron acceptor of FNRs, ferricyanide [105]. Here juglone was identified as an efficient nonphysiological oxidant of *Rp*FNR, similarly to other electrontransferases, like FNRs from *Anabaena* or *P. falciparum*. At varied concentrations of NADPH and fixed concentrations of juglone, a series of parallel lines was obtained in double reciprocal plots (Fig. 25).

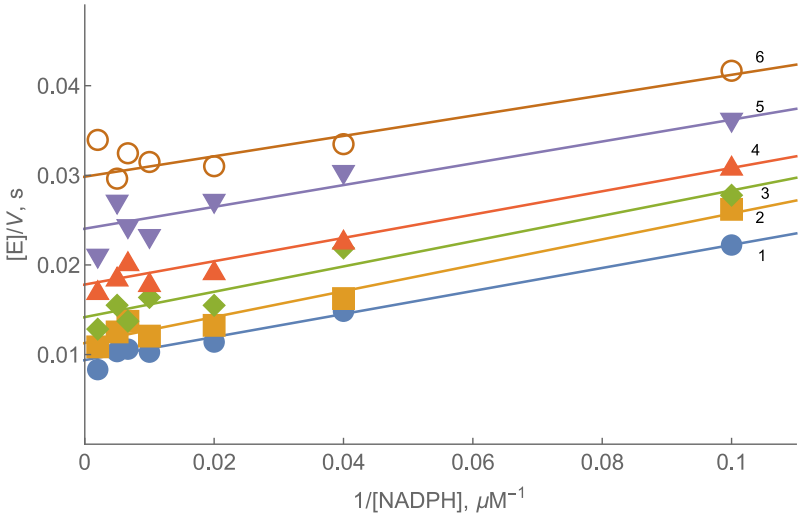

Figure 25. Lineweaver-Burk plot of the steady state kinetics of oxidation of NADPH catalyzed by *Rp*FNR in the presence of juglone. Juglone concentrations are 200 μM (1), 133 μM (2), 89 μM (3), 59 μM (4), 39 μM (5) and 26 μM (6).

This is indicative of the quinone reductase reaction of *Rp*FNR proceeding via a *ping-pong* mechanism. According to Eq. 19, the k_{cat} value for juglone reduction at infinite NADPH concentration is 157 ± 7.0 s^{-1}, and the values of the bimolecular rate constants k_{cat}/K_m for NADPH and juglone are equal to 8.7 ± 0.7 × 10^6 $M^{-1}s^{-1}$ and 1.62 ± 0.15 × 10^6 $M^{-1}s^{-1}$, respectively. The value of k_{cat}/K_m for NADPH is similar to that obtained using ferricianyde as an oxidant, 5.5 × 10^6 $M^{-1}s^{-1}$ [105].

The oxidant substrate specificity of *Rp*FNR was assessed similarly to *Pf*FNR, examining its reactions with quinones, nitroaromatics and aromatic

N-oxides with available E_7^1 values; additionally, several single-electron acceptors, namely ferricyanide, Fe(EDTA)$^-$ and benzylviologen, were also studied. The apparent maximal reduction rate constants $k_{cat(app.)}$ of the electron acceptors in the presence of 100 μM NADPH and their respective k_{cat}/K_m values are given in Table 12.

Table 12. Steady-state rate constants of the reduction of nonphysiological electron acceptors by 100 μM NADPH catalyzed by *Rp*FNR.

No.	Compound	E^1_7 (V)[a]	$k_{cat(app)}$ (s^{-1})	k_{cat}/K_m ($M^{-1}s^{-1}$)
	Quinones			
1	1,4-Benzoquinone	0.090	130 ± 16	$9.4 \pm 0.8 \times 10^5$
2	2-CH_3-1,4-benzoquinone	0.010	130 ± 12	$5.6 \pm 0.6 \times 10^5$
3	2,6-$(CH_3)_2$-1,4-benzoquinone	−0.070	52.1 ± 1.8	$2.1 \pm 0.13 \times 10^5$
4	5-OH-1,4-naphthoquinone	−0.090	138.5 ± 9.3	$1.5 \pm 0.23 \times 10^6$
5	5,8-$(OH)_2$-1,4-naphthoquinone	−0.110	45.4 ± 3.4	$3.5 \pm 0.2 \times 10^6$
6	9,10-Phenanthrene quinone	−0.120	34.6 ± 2.4	$2.0 \pm 0.4 \times 10^6$
7	1,4-Naphthoquinone	−0.150	110 ± 13	$2.3 \pm 0.4 \times 10^5$
8	2-CH_3-1,4-naphthoquinone	−0.200	21.6 ± 2.1	$6.0 \pm 0.8 \times 10^4$
9	$(CH_3)_4$-1,4-benzoquinone	−0.260	4.07 ± 0.53	$1.1 \pm 0.1 \times 10^4$
10	9,10-Anthraquinone-2-sulphonate	−0.380	3.56 ± 0.33	$1.0 \pm 0.16 \times 10^4$
11	2-OH-1,4-naphthoquinone	−0.410	0.26 ± 0.03	$3.1 \pm 0.2 \times 10^3$
12	2-CH_3-3-OH-1,4-naphthoquinone	−0.460	1.35 ± 0.13	$4.8 \pm 0.4 \times 10^3$
	Nitroaromatic compounds			
13	Tetryl	−0.191	5.69 ± 0.14	$4.35 \pm 0.30 \times 10^4$
14	*N*-methylpicramide	−0.225	1.93 ± 0.26	$4.8 \pm 0.6 \times 10^3$
15	2,4,6-Trinitrotoluene	−0.253	1.30 ± 0.13	$2.43 \pm 0.14 \times 10^3$
16	Nifuroxime	−0.255	4.40 ± 0.32	$6.9 \pm 0.4 \times 10^3$
17	Nitrofurantoin	−0.255	2.21 ± 0.12	$5.1 \pm 0.5 \times 10^3$
18	*p*-Dinitrobenzene	−0.257	2.21 ± 0.35	$3.1 \pm 0.2 \times 10^3$
19	*o*-Dinitrobenzene	−0.287	0.48 ± 0.07	$1.28 \pm 0.2 \times 10^3$
20	4-Nitrobenzaldehyde	−0.325	0.97 ± 0.13	$2.38 \pm 0.4 \times 10^3$
21	3,5-Dinitrobenzoic acid	−0.344	0.09 ± 0.01	$2.91 \pm 0.2 \times 10^3$
22	*m*-Dinitrobenzene	−0.348	0.42 ± 0.06	$9.6 \pm 0.7 \times 10^2$
23	4-Nitroacetophenone	−0.355	0.30 ± 0.05	$8.0 \pm 0.67 \times 10^2$
24	CB-1954	−0.385	0.52 ± 0.05	$1.75 \pm 0.14 \times 10^3$
25	4-Nitrobenzyl alcohol	−0.475	0.23 ± 0.03	$2.50 \pm 0.16 \times 10^2$
	Aromatic *N*-oxides			
26	7-F-tirapazamine	−0.400	1.20 ± 0.11	$1.80 \pm 0.31 \times 10^3$
27	Tirapazamine	−0.456	0.53 ± 0.04	$9.41 \pm 0.82 \times 10^2$
28	7-C_2H_5O-tirapazamine	−0.494	0.46 ± 0.03	$4.91 \pm 0.32 \times 10^3$
	Single-electron acceptors			
29	Ferricyanide[b]	0.410	394 ± 19	$8.8 \pm 1.0 \times 10^6$
30	Fe(EDTA)$^-$	0.120	1.2 ± 0.1	$2.4 \pm 0.2 \times 10^3$
31	Benzylviologen	−0.354	19.6 ± 2.3	$3.6 \pm 0.3 \times 10^4$

[a] – taken from [17,35,158]; [b] – calculated on single-electron basis.

The log k_{cat}/K_m values of nitroaromatics exhibit a linear although somewhat scattered dependence on their E_7^1 values (Fig. 26). In general, the log k_{cat}/K_m values of quinones, including the single-electron acceptor benzylviologen, and aromatic *N*-oxides are higher than those of $ArNO_2$ and are characterized by a parabolic dependence on their E_7^1 values, similarly to *Pf*FNR (this work) and spinach or *Anabaena* FNRs [75].

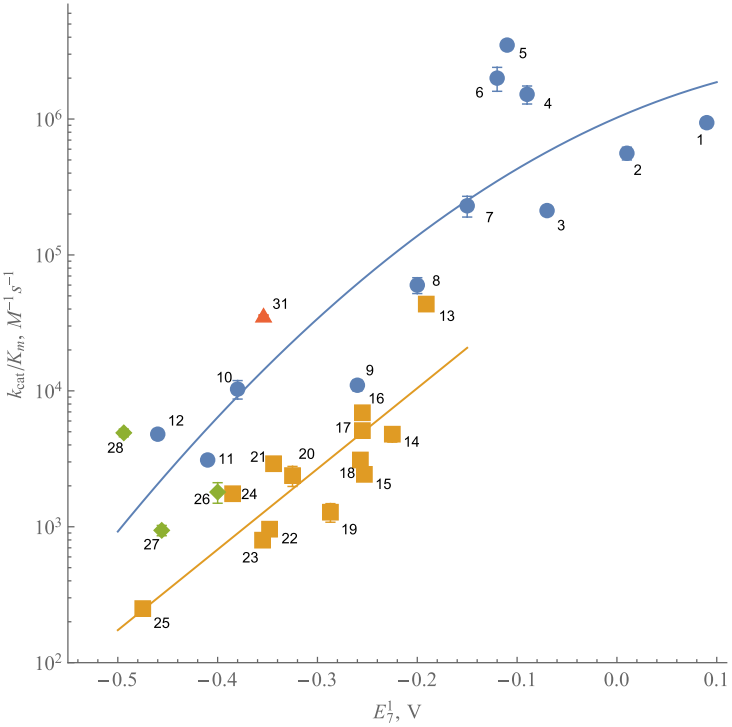

Figure 26. Dependence of the reactivity of quinones, nitroaromatic compounds, aromatic *N*-oxides and benzylviologen on their single-electron reduction midpoint potentials (E_7^1) in $\log_{10}$ scale. Numbers and reduction potentials of compounds are given in table 12.

It was found that the single-electron flux for enzymatic reduction of 50 – 100 μM 1,4-benzoquinone by 50 – 100 μM NADPH was equal to 54 ± 4 % of the total flux. The assessment of the single-electron flux in the reduction of nitroaromatic compounds was based on the $ArNO_2^{\bullet-}$ mediated reduction of the added cytochrome *c*. It was found that in the presence of 50 μM NADPH and 100 μM TNT or *p*-nitrobenzaldehyde the rate of *Rp*FNR-catalyzed reduction of 50 μM cytochrome *c* was equal to 91 ± 2% and 97 ± 3% of the doubled NADPH oxidation rate, respectively. The reactions were inhibited by 49% and

37% by the addition of 100 U/ml superoxide dismutase, which reflects the rapid reoxidation of $ArNO_2^{\bullet-}$ with O_2 and the participation of superoxide in the reduction of cytochrome *c*. Thus, it can be concluded that *Rp*FNR reduces $ArNO_2$ in a single-electron way.

Investigation of the inhibition of the quinone reductase reaction of *Rp*FNR by the reaction product $NADP^+$ showed that at fixed concentrations of juglone (200 μM), $NADP^+$ acts as a competitive inhibitor towards NADPH (Fig. 27A) with K_{is} = 150 ± 10 μM (Eq. 20). However, $NADP^+$ acts as an apparently noncompetitive inhibitor towards juglone (Fig. 27B) at fixed concentration of NADPH (100 μM) with K_{ii} = 1.7 ± 0.1 mM (Eq. 21)

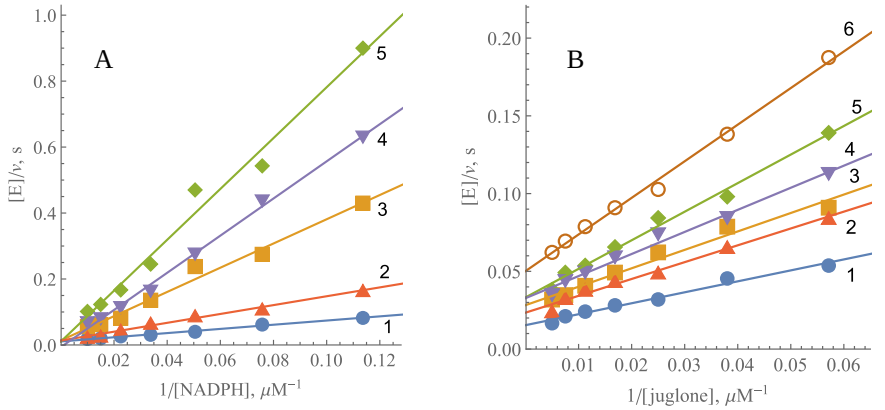

Figure 27. Inhibition of *Rp*FNR-catalyzed reactions by $NADP^+$. (A) Competitive inhibition of the juglone reductase reaction of *Rp*FNR by $NADP^+$ at varied concentrations of NADPH and in the presence of 200 μM juglone. $NADP^+$ concentrations are 0 (1), 0.25 mM (2), 0.5 mM (3), 0.75 mM (4) and 1.0 mM (5). (B) Noncompetitive inhibition at varied juglone concentration in the presence of 100 μM NADPH. $NADP^+$ concentrations are 0 (1), 0.5 mM (2), 1.0 mM (3), 1.5 mM (4), 2.0 mM (5) and 3.0 mM (6).

3.2.2.Presteady-state kinetic studies of *Rp*FNR

The spectral changes of *Rp*FNR-bound FAD during its multiple turnover under aerobic conditions in the presence of NADPH and $(CH_3)_4$-1,4-benzoquinone were investigated to get insight into the enzyme reoxidation mechanism. In control experiments (in the absence of quinone) the initial fast phase of FAD reduction by NADPH monitored at 460 nm is followed by a slow reoxidation by oxygen (Fig. 28A). This is accompanied by a transient increase in absorbance at 600 nm at the same time scale. The addition of

quinone accelerates the reoxidation of $FADH^-$ and the decay of the 600 nm-absorbing species by more than one order of magnitude (Fig. 28B).

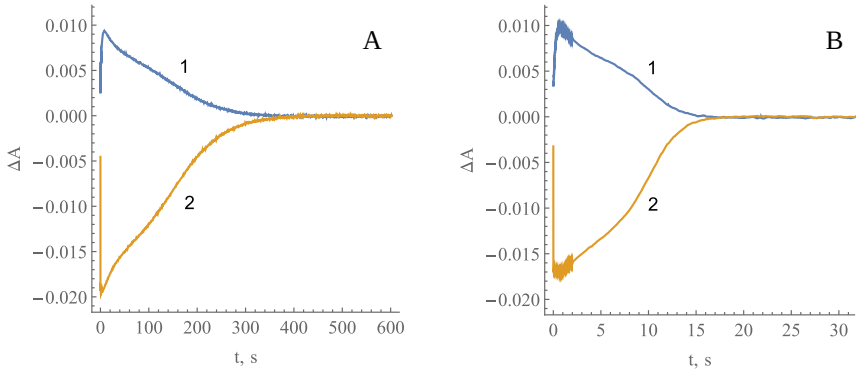

Figure 28. The absorbance changes at 600 nm (1) and 460 nm (2) during the reduction of *Rp*FNR (4.0 μM) by 50 μM NADPH and its subsequent reoxidation by oxygen (A) or 250 μM duroquinone (B). Concentrations reported after mixing.

The maximum ΔA_{460} after the enzyme is mixed with NADPH (Fig. 28A) corresponds to 90% of *Rp*FNR FAD absorbance decrease after the enzyme is mixed with an excess NADPH under anaerobic conditions [103,105]. Assuming that the maximum extent of enzyme reduction under aerobic conditions is 90%, $k_{ox} = 0.11 \pm 0.01\ s^{-1}$ according to Eq. 23 for the reoxidation of *Rp*FNR with oxygen, which was close to the enzymatic NADPH oxidase activity under steady state. In the presence of 250 μM duroquinone, $k_{ox} = 2.05 \pm 0.07\ s^{-1}$, which is close to the value obtained in the steady-state experiments (table 12).

The measurements of absorbance changes were performed at different wavelengths in order to characterize the reaction intermediates absorbing at 600 nm (Fig. 28). The results show that the absorbance initially increases in the range of 525 – 750 nm with $\lambda_{max} \approx 720$ nm (Fig. 29). Subsequently the formation and decay of a secondary flat absorbance band with a maximum at 600 – 700 nm can be seen. The formation of transient species is not caused by the interaction of isoalloxazine ring of the FAD and quinone, because analogous transient absorbance spectra were obtained during the reoxidation of *Rp*FNR with O_2 (data not shown).

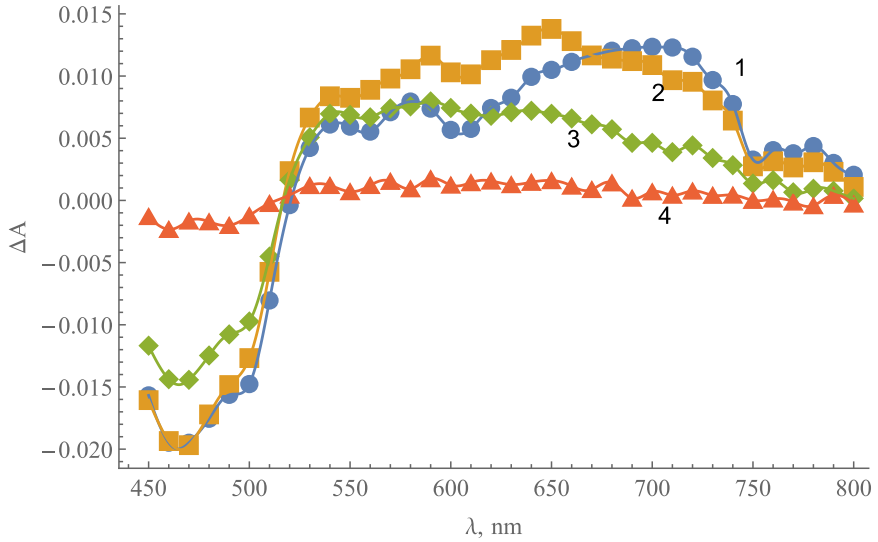

Figure 29. Transient spectra of reaction intermediates formed during the turnover of *Rp*FNR. Difference in absorbance is shown at several timepoints over the 450 – 800 nm wavelength range. Concentration of *Rp*FNR, 4.0 μM; NADPH, 50 μM; duroquinone, 250 μM. Spectra correspond to absorbance changes at 100 ms (1), 1 s (2), 5 s (3) and 20 s (4).

3.2.3.Redox potentials of *Rp*FNR

The standard reduction potential (E_7^0, the potential of E-FAD/E-FADH$^-$ redox couple) of *Rp*FNR was determined by examining its reactions with 3-AcADP(H). AcADP$^+$ is chosen instead of NADP$^+$ because the lack of a suitable electron donor renders reduction of NADP$^+$ by *Rp*FNR under steady-state conditions problematic [103]. The E_7^0 value for AcADP$^+$/AcADPH couple is equal to −0.258 V [164]. During the enzymatic reduction of AcADP$^+$ by NADPH, the maximum rate was reached at 200 μM NADPH. Under these conditions, k_{cat} = 53.3 ± 3.1 s^{-1} and k_{cat}/K_m for AcADP$^+$ was estimated to be 2.27 ± 0.35 x 10^6 M^{-1}s^{-1}.

In the reverse reaction using AcADPH generated *in situ* and 1.0 mM ferricyanide as an electron acceptor, k_{cat} = 18.6 ± 0.7 s^{-1}, and k_{cat}/K_m for AcADPH is calculated to be 6.0 ± 0.6 x 10^5 M^{-1}s^{-1} on the two-electron basis (Fig. 30C). According to the Haldane relationship, the equilibrium constant K of the redox reaction with AcADP$^+$/AcADPH couple corresponds to the ratio of k_{cat}/K_m for AcADPH and AcADP$^+$, respectively. According to the Nernst equation, the difference between the redox potentials of the reactants, ΔE^0, equals 0.0295 V × log$K$. Thus K = 0.264 ± 0.067 and E_7^0 for the enzyme is −0.276 ± 0.003 V.

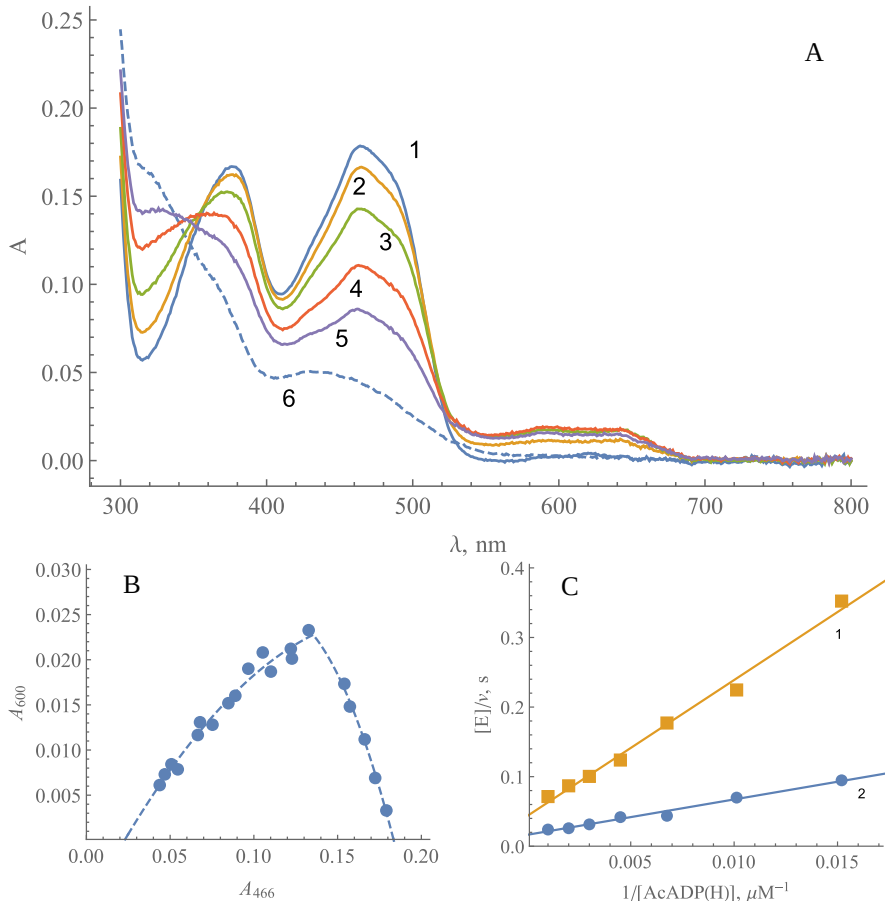

Figure 30. Determination of redox potentials of *Rp*FNR. (A) Spectra obtained during the photoreduction of 16.6 μM *Rp*FNR at different times of illumination: immediately after mixing (1), after 10 min (2), 25 min (3), 40 min (4), 50 min (5) and 70 min (6, fully reduced enzyme). (B) The interdependence of absorbance changes at 466 and 600 nm during photoreduction. (C) Rates of *Rp*FNR-catalyzed oxidation of AcADPH with 1 mM ferricyanide (1) and reduction of $AcADP^+$ with 200 μM NADPH (2).

During the photoreduction of *Rp*FNR in the presence of 5-deaza-FMN and EDTA, the neutral FAD semiquinone ($FADH^•$) exhibiting the characteristic absorbance at 550 – 650 nm is formed (Fig. 30A). The amount of E-$FADH^•$ was calculated using ε_{600} = 5.0 $mM^{-1}cm^{-1}$ [169] and the amount equals 26.5% (Fig. 30B). According to Eqs. 26 and 27, K_s = 0.520 and ΔE_7^1 = −0.017 V, which corresponds to E_7 (E-FAD/E-$FADH^•$) = −0.285 V and

E_7 (E-FADH$^{\bullet}$/E-FADH^{-}) = −0.268 V. However, one cannot rule out the possibility of some alterations in these values since ε_{600} of FADH of *Rp*FNR was not determined definitively.

3.2.4.Discussion

Some redox properties of a TrxR-type FNR from *R. palustris* were determined and compared to plastidic FNRs due to *Rp*FNR being able to react with redox active xenobiotics and in regards of *R. palustris* being a model microorganism for anaerobic metabolism of organic compounds where *Rp*FNR may possibly be involved.

The redox potentials of a representative of TrxR-type FNR were determined for the first time. E_7^0 of *Rp*FNR equals −0.276 V (Fig. 30) being similar to the redox potential of plant-type FNR from *P. falciparum*, −0.280 V [90] and more positive than that of spinach FNR, −0.342 V [187]. A relatively high FADH$^{\bullet}$ stability of 26.5% at equilibrium is comparable to that of spinach or *Anabaena* FNR, 27% at pH 7.0 and 22% at pH 8.0, respectively [187,192]. *Rp*FNR lacks the *Anabaena* FNR-specific Ser80-Glu301 ion pair [76] (corresponding to Ser96-Glu312 in *So*FNR [193]), which forms a hydrogen bond with the N5 of the FAD isoalloxazine ring and contributes to FADH$^{\bullet}$ stability. However, based on structural data of other FNRs and flavodoxins, the stability of FADH$^{\bullet}$ may be enhanced by the π-π interaction between the isoalloxazine and the terminal Tyr328 (Tyr98 in *Desulfovibrio vulgaris* flavodoxin [194], Tyr303 in *Anabaena* PCC7119 FNR [51]), formation of hydrogen bonds between N3 of the isoalloxazine ring and carboxy group of Asp56 (corresponding to Glu59 of *Clostridium beijerinckii* flavodoxin [195]) and between O2 and the amide group of Ile300 (corresponding to Ile356 of AdxR [196]). According to the data presented here, the likely direction of electron transfer catalyzed by *Rp*FNR is the reduction of Fd at the expense of NADPH.

Quinone reduction via a *ping-pong* mechanism points to separate reductive and oxidative half-reactions, which is a common theme for other FNRs. No strict oxidant specificity bar an increase in their log k_{cat}/K_m with increasing E_7^1 can be discerned which is in line with an outer sphere electron transfer model (Fig. 26) [24]. According to Eqs. 12 – 14, log k_{12} will exhibit a parabolic (square) dependence on ΔE^1 with a slope of 8.45 V^{-1} at $\Delta E^1 = \pm 0.15$ V in a reaction of an electron donor with a series of homologous oxidants displaying the same k_{22}. The reactivity of $ArNO_2$ is about 10 times lower when compared to quinones and ArN→O of similar E_7^1 values which is in line with the 100-fold difference in their k_{22} [26,34]. It can be noted that the reactivity

of *Rp*FNR in reactions with quinones and $ArNO_2$ is close to that observed with plant-type *Pf*FNR and *An*FNR [75]. On the other hand, $AcADP^+$ is 10 times better at oxidizing *Rp*FNR (Fig. 30C) than *Pf*FNR (Fig. 18). A plausible explanation for the considerable variation of k_{cat} values of the reactions (table 12) is the oxidative half-reaction being a rate limiting step of the catalytic cycle. The data in figure 27 show that the dominant mechanism of inhibition of the reaction product $NADP^+$ is its competition with NADPH for binding to the oxidized form of the enzyme. The noncompetitive inhibition with respect to the oxidant differs somewhat from the uncompetitive inhibition seen in analogous *Anabaena* or *P. falciparum* FNR-catalyzed reactions ([75], Fig. 19).

According to previous studies, photoreduced *Anabaena* FNR was reoxidized by quinones in two steps, $FADH^- \rightarrow FADH^\bullet$ and $FADH^\bullet \rightarrow FAD$, with $FADH^\bullet$ oxidation being the rate-limiting step [21,75]. This was evidenced by a transient formation of $FADH^\bullet$ with 600 nm absorption (Fig. 28). The reoxidation of *Rp*FNR should also involve single-electron transfer steps, since it reduces quinones in a predominantly single-electron way. Because the decay of the transient 600 nm absorption and the enzyme reoxidation monitored at 460 nm proceeds with a similar rate, the $FADH^\bullet$ oxidation can be a rate-limiting step in quinone reduction by *Rp*FNR. The absorption characteristics of *Rp*FNR multiple turnover intermediates are analogous to the ones seen in *Pf*FNR, with the absorption above 700 nm being uncharacteristic of FADH and pointing to the formation of some other intermediates. As discussed previously for *Pf*FNR regarding the extinction coefficient of $FADH^-$-$NADP^+$ complexes, the intermediates would exhibit approximately one third of the absorption increase that can be seen in figure 29, thus they can be ruled out.

3.3. Neuronal NO synthase

3.3.1. Steady-state kinetics and substrate specificity of nNOS

The aim of this part of work was the further characterization of acceptor-reductase activity of neuronal nitric oxide synthase (nNOS) with an emphasis on its conformational changes in the presence of calmodulin (CaM) and the possible participation of the heme moiety in the reactions. It had been previously established that quinones and nitroaromatic compounds form separate series of oxidants whose reactivity (log k_{cat}/K_m) increases with their E_7^1 in the absence of CaM in the nNOS catalyzed reaction [29]. Expanding on this, a number of oxidants possessing a broad range of E_7^1 values and different electrostatic charges were examined, including anticancer agents (derivatives of tirapazamine, dinitrobenzamide CB-1954) and toxic environment pollutants (tetryl, 2,4,6-trinitroluene) [29,130,131,147–149,197]. The measurements were performed at a single saturating concentration of NADPH, 50 μM, since K_m for NADPH in nNOS-catalyzed reactions is in the micromolar range [198].

The assessment of a previously unexplored group of oxidants ArN→O in the absence of CaM shows that the log k_{cat}/K_m values of tirapazamine derivatives, quinones and a quinoidal single-electron acceptor benzylviologen follow a common parabolic dependence on their E_7^1 values (Fig. 31A). As is the case with *Pf*FNR and *Rp*FNR, this may be attributed to their similar electron self-exchange rate constants, ~10^8 $M^{-1}s^{-1}$ [25,26]. As expected, the addition of CaM increases both the k_{cat} and k_{cat}/K_m values, although to a different extent; the latter values are increased up to two orders of magnitude. While the resulting dependence on E_7^1 values appears to be somewhat more scattered (Fig. 31B), the reactivity of ArN→O remains similar to that of quinones. $ArNO_2$ are less reactive than quinones in the presence of CaM, similarly to the trend seen in the absence of CaM [29]. The addition of H_4B decreased the rate constants of reduction of tetramethyl-1,4-benzoquinone (duroquinone) by 7 – 10%, and the addition of 1.0 mM dithiothreitol did not influence the reaction rate. The addition of 1.0 mM NO_2-Arg, an inhibitor of nNOS that binds to the heme moiety, decreased the k_{cat} of reaction by 25% (table 13).

Table 13. Steady-state rate constants of the reduction of nonphysiological electron acceptors by NADPH catalyzed by nNOS. [NADPH] = 50 μM, 0.1 M Tris/HCl + 1 mM EDTA + 100 mM NaCl, pH 7.0, 25 °C; 10 μg/mL calmodulin and 1.0 mM $CaCl_2$, where applicable.

No.	Compound	E_7^1, V[a]	-CaM		+CaM	
			k_{cat} (s^{-1})	k_{cat}/K_m ($M^{-1}s^{-1}$)	k_{cat} (s^{-1})	k_{cat}/K_m ($M^{-1}s^{-1}$)
	Aromatic *N*-oxides					
1	7-CF_3-tirapazamine	−0.345	3.98 ± 0.38	9.9 ± 1.2 x 10^3	16.3 ± 1.8	2.5 ± 0.2 x 10^4
2	7-Cl-tirapazamine	−0.400	0.84 ± 0.08	1.4 ± 0.1 x 10^3	14.8 ± 1.7	4.0 ± 0.6 x 10^5
3	7-F-tirapazamine	−0.400	2.84 ± 0.23	1.2 ± 0.1 x 10^4	11.1 ± 1.1	1.4 ± 0.1 x 10^5
4	Tirapazamine	−0.456	0.69 ± 0.09	1.1 ± 0.1 x 10^3	5.22 ± 0.66	3.9 ± 0.2 x 10^4
5	7-CH_3-tirapazamine	−0.474	0.60 ± 0.09	1.3 ± 0.2 x 10^3	n.d.	n.d.
6	7-C_2H_5O-tirapazamine	−0.494	0.67 ± 0.09	2.2 ± 0.2 x 10^3	2.94 ± 0.71	2.6 ± 0.2 x 10^4
	Quinones					
7	1,4-Benzoquinone	0.09	12.9 ± 1.5	5.1 ± 0.7 x 10^5	61.4 ± 7.2	1.3 ± 0.2 x 10^6
8	2,5-$(CH_3)_2$-1,4-benzoquinone	−0.07	6.84 ± 0.42	1.4 ± 0.2 x 10^5	55.8 ± 3.4	1.0 ± 0.1 x 10^6
9	5-OH-1,4-naphthoquinone	−0.09	23.3 ± 1.9	2.8 ± 0.4 x 10^6	42.2 ± 1.8	7.0 ± 0.6 x 10^6
10	5,8-$(OH)_2$-1,4-naphthoquinone	−0.11	11.5 ± 1.2	1.8 ± 0.2 x 10^6	24.7 ± 4.8	5.0 ± 0.5 x 10^7
11	1,4-Naphthoquinone	−0.15	7.98 ± 0.40	3.4 ± 0.7 x 10^5	38.2 ± 2.6	2.4 ± 0.3 x 10^6
12	2-CH_3-1,4-naphthoquinone	−0.20	8.50 ± 0.80	1.6 ± 0.3 x 10^5	37.9 ± 2.5	1.3 ± 0.2 x 10^6
13	$(CH_3)_4$-1,4-benzoquinone	−0.26	4.71 ± 0.34	8.0 ± 1.0 x 10^4	115.0 ± 7.0	2.1 ± 0.2 x 10^6
					112.2 ± 4.3[b]	1.2 ± 0.1 x 10^6[b]
					84.3 ± 5.1[c]	1.1 ± 0.1 x 10^6[c]
14	2-OH-1,4-naphthoquinone	−0.41	0.39 ± 0.05	4.4 ± 0.4 x 10^3	3.11 ± 0.35	4.0 ± 0.3 x 10^4
	Single electron acceptors					
15	Ferricyanide	0.41	30.4 ± 3.5	1.2 ± 0.2 x 10^5	102.4 ± 5.9	3.3 ± 0.3 x 10^6

Table 13 (cont.)

No.	Compound		-CaM		+CaM	
			k_{cat} (s^{-1})	k_{cat}/K_m ($M^{-1}s^{-1}$)	k_{cat} (s^{-1})	k_{cat}/K_m ($M^{-1}s^{-1}$)
16	Cytochrome *c*	0.25	9.66 ± 0.35	1.9 ± 0.2 x 10^5	104.1 ± 2.2	5.3 ± 0.3 x 10^6
17	$Fe(EDTA)^-$	0.12	7.30 ± 1.30	7.0 ± 1.0 x 10^3	11.0 ± 1.2	2.8 ± 0.2 x 10^4
18	Benzylviologen	−0.354	6.60 ± 0.40	3.4 ± 0.2 x 10^4	23.5 ± 1.4	1.7 ± 0.1 x 10^5
	Nitroaromatic compounds					
19	Tetryl	−0.191			52.0 ± 2.6	6.8 ± 0.5 x 10^6
20	2,4,6-Trinitrotoluene	−0.253			46.4 ± 5.2	1.5 ± 0.1 x 10^5
21	1,2-Dinitrobenzene	−0.287			18.9 ± 3.0	8.0 ± 0.7 x 10^4
22	1,3-Dinitrobenzene	−0.348			10.1 ± 0.9	8.9 ± 0.6 x 10^3
23	4-Nitroacetophenone	−0.355			4.67 ± 1.40	2.7 ± 0.3 x 10^4
24	CB-1954	−0.385			8.83 ± 0.80	2.7 ± 0.2 x 10^4

[a] – taken from [17,158]

[b] – the reaction medium contains H_4B and Arg

[c] – the reaction medium contains H_4B, Arg and 1.0 mM NO_2-Arg

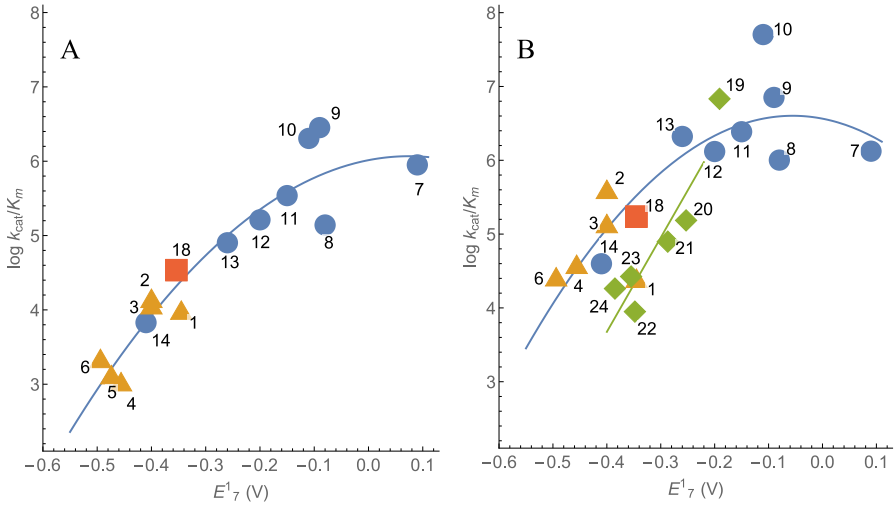

Figure 31. The dependence of the reactivity of quinones (blue disks), aromatic *N*-oxides (orange triangles), nitroaromatic compounds (green diamonds) and benzylviologen (red square) on their single-electron reduction midpoint potentials E_7^1 in the absence (A) and presence (B) of CaM and Ca^{2+}. The numbers correspond to compounds given in table 13.

Electrostatic interactions play an important role in the electron transfer reactions of FMN, first in the association of the FMN-binding domain with the FAD-binding domain, and next in the complex formation with the heme domain, which also involves conformational changes [123,199–203]. Most studies on the effects of ionic strength on the reactivity of nonphysiological oxidants, however, were performed with a single concentration thus providing limited information on the mode of their interaction with the FMN domain [199,201,202]. By using varied concentrations of a neutral oxidant duroquinone, it was found that its k_{cat} attains the maximum value at high ionic strength (Fig. 32A). Similar dependence was also seen for k_{cat} of cytochrome *c*, benzylviologen and ferricyanide (data not shown). On the other hand, the presence of CaM affects the relationship between k_{cat} of duroquinone and ionic strength of the medium with a clearly defined bell shape appearing under these conditions and the maximum value of k_{cat} is attained at lower ionic strength. The ionic strength, while increasing the k_{cat}/K_m of duroquinone, attenuates the activating effect of calmodulin (Fig. 32B). As shown in Fig. 32C, the log k_{cat}/K_m of negatively charged oxidants ferricyanide and $Fe(EDTA)^-$ increases with increasing ionic strength of the solution while the decrease of the reactivity of positively charged cytochrome *c* and benzylviologen is less

pronounced. In general, this points to the interaction of charged oxidants with a negatively charged FMN-binding domain.

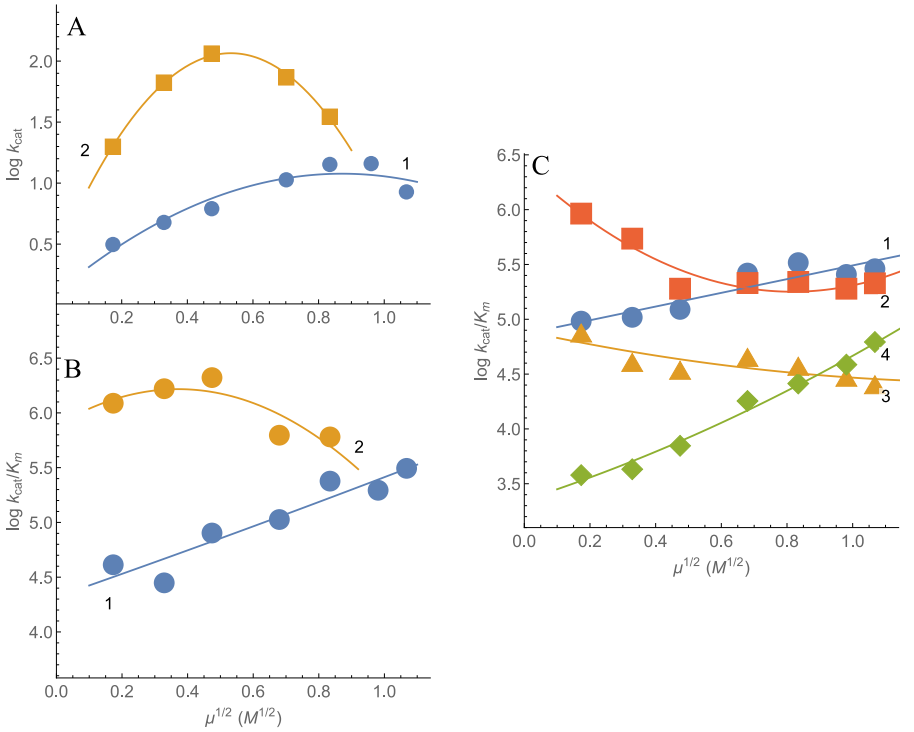

Figure 32. The effects of ionic strength on the reactivity of nNOS towards electron acceptors. (A) The dependence of k_{cat} of duroquinone on the ionic strength in the absence of CaM (1, blue disks) and its presence (2, orange rectangles). (B) The dependence of k_{cat}/K_m of duroquinone on the ionic strength in the absence of CaM (1, blue disks) and its presence (2, orange rectangles). (C) The dependence of k_{cat}/K_m for ferricyanide (1, blue disks), cytochrome *c* (2, red squares), $Fe(EDTA)^-$ (3, green diamonds) and benzylviologen (4, orange triangles) on their ionic strength. [NADPH] = 50 μM, ionic strength varied by the addition of NaCl to 0.03 M Tris/HCl.

The character of inhibition by the reaction product $NADP^+$ and its relationship with NADP(H)-induced conformational transitions had not been sufficiently assessed [198,204]. Typical inhibition patterns were obtained at several concentrations of $NADP^+$ and its redox inactive derivative 2′,5′-ADP (Fig. 33). At a fixed concentration of duroquinone, both compounds act as competitive inhibitors towards NADPH decreasing the k_{cat}/K_m of NADPH without affecting the k_{cat} value of the reaction, meaning they bind at the NADPH-binding site in the oxidized enzyme form. However, with a fixed

concentration of NADPH, both compounds act noncompetitively towards duroquinone, decreasing its k_{cat}/K_m and the k_{cat} of the reaction.

The noncompetetive inhibition constants (K_i) were calculated according to Eq. 22. They were equal to 2.5 ± 0.2 mM for $NADP^+$ and 0.25 ± 0.04 mM for 2′,5′-ADP. The decrease of $k_{cat(app.)}$ in the presence of high concentrations of $NADP^+$ and 2′,5′-ADP (Fig. 33B) is probably related to an increased K_m of NADPH (Fig. 33A), meaning that in this case 50 μM of NADPH is no longer a saturating concentration and does not ensure the maximum reaction rate.

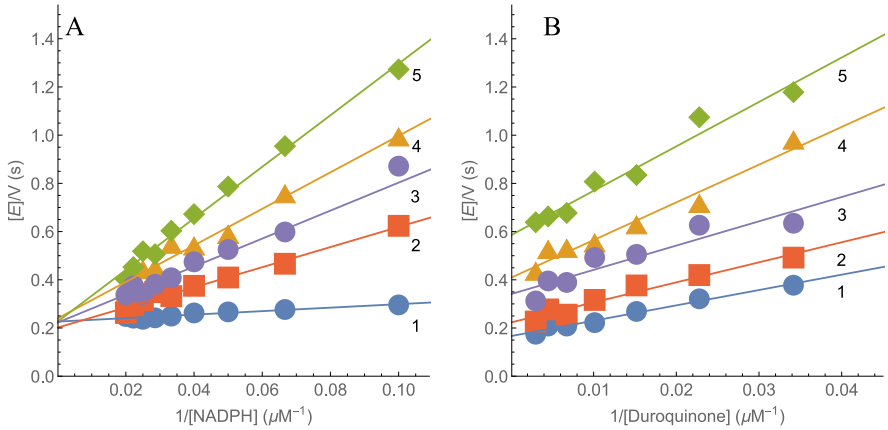

Figure 33. Inhibition of the duroquinone reductase reaction of nNOS by $NADP^+$ and 2′,5′-ADP. (A) Inhibition at varied NADPH concentrations in the presence of 250 μM duroquinone: 1 – no inhibitor, 2 – 200 μM $NADP^+$, 3 – 400 μM $NADP^+$, 4 – 50 μM 2′,5′-ADP, 5 – 100 μM 2′,5′-ADP. (B) Inhibition at varied concentrations of duroquinone in the presence of 50 μM NADPH: 1 – no inhibitor, 2 – 1.0 mM $NADP^+$, 3- 2.0 mM $NADP^+$, 4 – 250 μM 2′,5′-ADP, 5 – 500 μM 2′,5′-ADP.

3.3.2. Presteady-state kinetic studies of nNOS

The investigation of the changes of flavin and heme absorbance during enzyme multiple turnover under aerobic conditions gives insights into the mechanism of nNOS reoxidation by quinones. The reduction of flavins and heme was monitored following their absorbance decrease at 485 nm (heme isosbestic point) and 397 nm, respectively, whereas the formation of Fe^{2+}-NO complex was monitored following the absorbance increase at 436 nm [133,134,205]. The oxidation of NADPH was monitored according to the absorbance decrease at 340 nm. As seen in Fig. 34, nNOS was rapidly reduced by NADPH and slowly reoxidized by O_2. The amplitude of absorbance

changes at 397 nm (Fig. 34C) was comparable to those at 485 nm (Fig. 34B), pointing to a strong contribution of flavin spectral changes. The 436 nm absorbance changes (Fig. 34D) are contrary to those expected for Fe^{2+}-NO formation [133,205] and are attributable to FAD-FMN reduction. The 485, 397 and 436 nm absorbance not returning to initial levels after oxidation by O_2 is indicative of a stable single-electron reduced FAD-FMN as a reduction product (Fig. 34B-D) [129–131,146,205]. The final drop of absorbance at 397 nm may also be partly caused by the oxidation of NADPH which absorbs light at this wavelength, albeit weakly. The addition of duroquinone increased the enzyme reoxidation rate by more than an order of magnitude and it also decreased the amplitude of absorbance changes (Fig. 34).

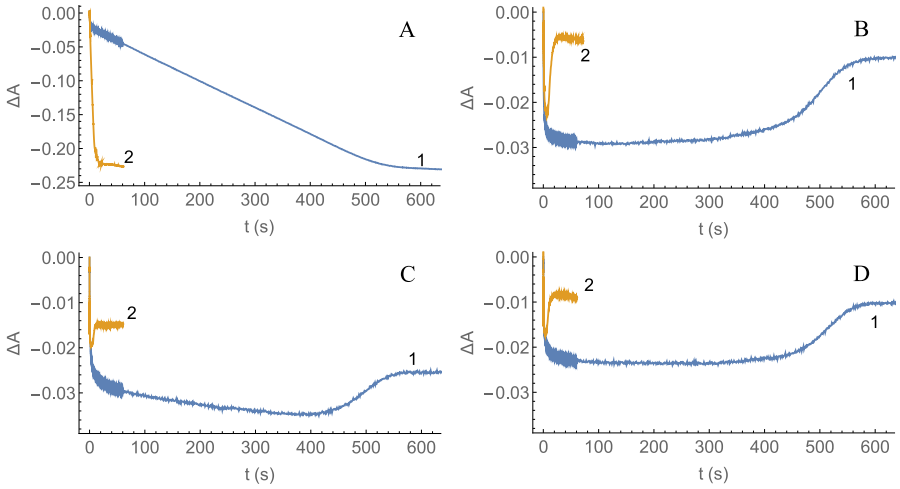

Figure 34. Multiple turnover kinetics of nNOS reduction and reoxidation and NADPH oxidation by O_2 (1) or 100 μM duroquinone (2) in the absence of CaM. The absorbance changes were followed at 340 nm (A), 485 nm (B), 397 nm (C) and 436 nm (D). Concentrations of nNOS and NADPH after mixing, 2.0 μM and 30 μM.

The presence of CaM and H_4B enhanced the turnover of nNOS (Fig. 35A). Like in the control experiments (Fig. 34), the addition of duroquinone accelerates the reoxidation of nNOS by an order of magnitude (data not shown). The presence of NOS substrate arginine enabled studying the full turnover of the enzyme and the assessment of flavins and heme in the reduction of xenobiotics. An increase in absorbance at 436 nm after the addition of *L*-arginine to the reaction mixture indicates the formation of Fe^{2+}-NO complex (Fig. 35B).

The analysis of initial absorbance changes of nNOS at 485 nm shows that NADPH reduced flavins biphasically, with k_{red} of 144.7 ± 1.5 s^{-1} and 3.4 ± 0.2 s^{-1} for the fast and slow phases with 70% and 30% amplitudes, respectively. The heme absorbance changes at 397 nm are characterized by k_{red} of 67.6 ± 2.8 s^{-1} and 1.05 ± 0.1 s^{-1}, respectively, with amplitudes being 50%. The kinetics of Fe^{2+}-NO formation at 436 nm followed after the initial 15 ms absorbance drop due to flavin reduction are characterized by k_{red} of 35.3 ± 2.4 s^{-1} and 1.1 ± 0.1 s^{-1} with amplitudes being 62% and 38%, respectively. The obtained rate constants are comparable with the ones obtained during reduction of nNOS by excess NADPH under aerobic conditions [205] and with the data obtained in further studies [206]. A second slow phase may be attributed to subsequent processes, e.g., the start of enzyme multiple turnover. The maximum absorbance change at 485 nm was close to that expected using $\Delta\varepsilon_{485}$ = 12.4 $mM^{-1}cm^{-1}$ for the absorbance difference between the oxidized and three-electron reduced FAD-FMN domain of nNOS [207], i.e., to almost complete formation of three-electron reduced form. For the estimation of the maximum concentration of Fe^{2+}-NO complex, the absorbance difference between Fe^{2+}-NO and Fe^{3+} forms of flavin-free nNOS heme domain, $\Delta\varepsilon_{436}$ = 34.1 $mM^{-1}cm^{-1}$ [133] was corrected for the absorbance difference between oxidized and three-electron reduced flavin reductase domain, $\Delta\varepsilon_{436}$ = 11.2 $mM^{-1}cm^{-1}$ [207]. Applying the obtained value $\Delta\varepsilon_{436}$ = 22.9 $mM^{-1}cm^{-1}$ one may conclude that during the turnover, 67% of heme exist in Fe^{2+}-NO form, which is close to values previously reported [134].

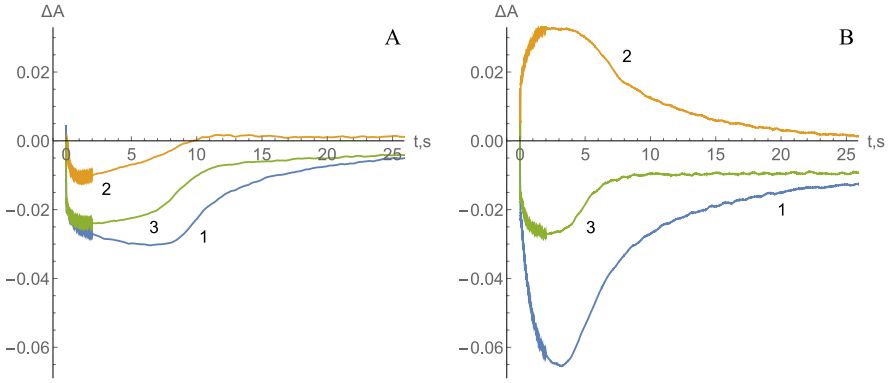

Figure 35. Multiple turnover kinetics of nNOS reduction and reoxidation by O_2 in the presence of NADPH, Cam, H_4B (A) and NADPH, Cam, H_4B and Arg (B). The absorbance changes were followed at 397 nm (1), 436 nm (2) and 485 nm (3). Concentrations of nNOS and NADPH after mixing, 2.0 μM and 30 μM.

The addition of duroquinone enhances the flavin reoxidation rate and decreases the amplitude of absorbance changes at 485 nm (Fig. 36A). The kinetics of reoxidation were analyzed by the method of Chance [166] using Eq. 23.

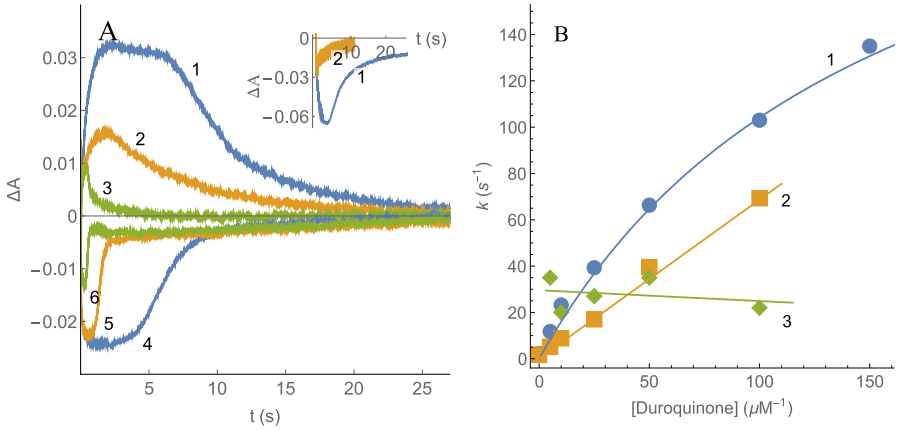

Figure 36. The kinetics of nNOS reduction and reoxidation under multiple turnover conditions in the presence of CaM, H_4B and Arg. The concentrations of enzyme and compounds ar given after mixing. (A) The spectral changes of 2.0 μM nNOS monitored at 436 nm (1 – 3) and at 485 nm (4 – 6) during the reduction of 30 μM NADPH and subsequent reoxidation by O_2 (1, 4) and by 5.0 μM (2, 5) or 50 μM (3, 6) duroquinone. The inset shows the kinetics of spectral changes at 397 nm in the absence (1) and in the presence of 100 μM duroquinone (2). (B) Dependence of the apparent first order rate constants of reoxidation of reduced FAD-FMN (1), reoxidation of Fe^{2+}-NO complex (2) and formation of Fe^{2+}-NO complex (3) on duroquinone concentration.

The dependence of k_{ox} on duroquinone concentration (Fig. 36B) corrected for k_{ox} for reaction with O_2, 2.24 s^{-1}, gives an apparent bimolecular rate constant of $1.7 \pm 0.1 \times 10^6$ $M^{-1}s^{-1}$, which is comparable with the stead-state k_{cat}/K_m value for this oxidant (Table 12), and $k_{ox(max)} = 267 \pm 30$ s^{-1}. Thus using duroquinone as an oxidant, the k_{cat} of the steady-state reaction is limited mainly by the reductive half-reaction. Although duroquinone accelerates nNOS oxidation followed at 397 nm with a similar rate, a further assessment of the reoxidation of Fe^{2+}-NO complex was made since it is the predominant form of heme during the enzyme turnover [134] and its absorbance changes are opposite to those of flavin cofactors. One may note the analysis of this

reaction according to Eq. 23 is complicated by the branched catalytic cycle of nNOS with the parallel electron flux through several Fe^{2+} complexes (Fig. 11). After the conditional assumption that the maximum concentration of Fe^{2+}-NO during turnover in the presence of O_2 is equal to enzyme concentration and after the correction for k_{ox} of oxygen, 1.8 s^{-1}, an apparent bimolecular rate constant of its reoxidation equaling $7.4 \pm 0.85 \times 10^5$ $M^{-1}s^{-1}$ is obtained. The addition of 100 U/mL SOD did not affect the rate of Fe^{2+}-NO reoxidation by duroquinone.

Analogously the rate constants of Fe^{2+}-NO formation during the enzyme reduction by NADPH (k_{red}) were calculated according to Eq. 24 [166]. Although scattered (Fig. 36B), the obtained values of k_{red} were comparable with k_{red} = 35.3 s^{-1} obtained in the analysis of absorbance increase in the absence of duroquinone. Finally, an increase in duroquinone concentration has little effect on the value of k_{red}.

3.3.3.Discussion

Several specific properties of nNOS relevant to the reduction of quinones, nitroaromatics and aromatic *N*-oxides can be disclosed. The absence of a well-defined oxidant specificity except for the reactivity increase with increasing E_7^1 and the difference between two series of compounds show that that outer sphere electron transfer model is applicable for nNOS catalyzed reactions. nNOS activity in the presence of CaM, i.e., under conditions that closely resemble physiological conditions, increases and approaches that of rat P-450R [26], thus it is possible that there are similarities in oxidative stress-type cytotoxicity of redox cycling xenobiotics in particular types of cells.

Ionic strength effects point to conformational changes of the FMN-binding domain having a role in the reduction of external oxidants. A negatively charged Glu762 of the FMN-binding domain interacts with Arg1229 of the FAD domain, and there is an interaction of Glu762, Glu816 and Glu819 with Lys423, Lys620 and Lys660 in an alternative conformation [123,203]. High ionic strength was also reported to enhance the reduction of FAD by NADPH and the interflavin electron transfer [202]. A likely explanation is that the enzyme adopts a conformation with a better FMN accessibility; moreover, ionic strength then mimics the effects of CaM. Using k_{cat}/K_m as a value for the measurement of reactivity, it was possible to show the existence of an ionic strength-induced conformational change which increases the reactivity of an uncharged oxidant duroquinone. Moreover, the expected dependence on ionic strength is distorted for the reactions of negatively charged FMN-binding domain with charged oxidants. Contrary to

P-450R where the limiting reactivity is attained at $\mu^{1/2} = 0.5 – 0.6\ M^{1/2}$ [119], the reactivity of negatively charged oxidants in the nNOS-catalyzed reaction does not reach the limiting value even at $\mu^{1/2} = 1.0\ M^{1/2}$, presumably because of the general increase in the FMN accessibility.

Previous presteady-state studies of nNOS show that the binding of NADP(H) to the reduced flavin domain inhibits the reduction of external oxidants, possibly via induced conformational changes restricting the accessibility of FMN [204] and a nicotinamide ring-lacking 2′,5′-ADP does not inhibit the reaction. However, the data presented here and corroborating an earlier study show that $NADP^+$ and 2′,5′-ADP act as competitive inhibitors towards NADPH [198]. Moreover, these inhibitors act noncompetitively towards duroquinone and the decreased $k_{cat(app.)}$ can be attributed to an increased K_m of NADPH at high concentration of an inhibitor, in which case 50 μM NADPH falls short of a saturating concentration. Another possible explanation is the involvement of a four-electron reduced flavin domain in the presteady-state experiments [204], while in our case, i.e. under the steady-state conditions, the enzyme cycles between a one- and three-electron reduced states in the steady state [129–131]. The reductive half-reaction plays the main role in limiting the k_{cat} of duroquinone in steady-state reaction. However, the k_{cat} for most other oxidants is limited by the oxidative half-reaction (Fig. 36B, table 13).

According to previous studies, N^{ω}-nitroarginine binding to the heme moiety and preventing its reduction by $FMNH_2$ [144] does not inhibit the reduction of nilutamide or CB1954 by nNOS [148,149], leading to a conclusion that heme does not participate in the reduction of these compounds. One may note, however, that these experiments were performed in the absence of arginine, i.e., under the conditions where Fe^{2+}-NO is not formed. The multiple turnover experiments, however, show that duroquinone oxidizes both the reduced FAD-FMN and heme, particularly its Fe^{2+}-NO form (Fig. 36). The decrease of amplitude and lifetime of absorbance transient at 436 nm is not caused by the interception of electron flux from $FMNH_2$ to heme because the rate constant of Fe^{2+}-NO formation (k_{red}) decreases insignificantly with increasing duroquinone concentration (Fig. 36B). Dissociation of $NO^{\bullet}$ driven by high rate of formation of peroxynitrite under the action of $O_2^{\bullet-}$ formed during redox cycling of duroquinone is another potential mechanism for Fe^{2+}-NO decay [199]. However, this decomposition happens only after addition of complex destabilizing chaotropic agents. Moreover, Fe^{2+}-NO depletion by duroquinone is SOD-insensitive and this argues against the involvement of superoxide in Fe^{2+}-NO decomposition. Fe^{2+}-NO being less

reactive than the reduced FAD-FMN (rate of formation 35.3 s^{-1} whereas rate of reduction of FAD-FMN is 144.7 s^{-1} and k_{cat} of the steady state reaction is 112.2 s^{-1}) points to heme having a minor role in electron flux for the reduction of external electron acceptors. Therefore, $FMNH_2$ remains the preferential electron donor. This is similar to reactions of flavohemoglobin where heme is oxidized much slower by quinones than the reduced FAD during turnover [208].

The involvement of heme moiety in the reduction of drugs and xenobiotics by NOS had been demonstrated only in the case of iNOS-catalyzed reduction of the anticancer prodrug 1,4-bis(aminoalkyl-*N*-oxide)-anthracene-9,10-dione (AQ4N), which is converted into its bis(aminoalkyl) derivative [209]. The data presented here (Fig. 36) expand the knowledge of the variety of structures that may be activated this way, thus opening a perspective for the design of heme-targeted bioreductively activated agents. Moreover, there may be implications for more detailed studies of cytochrome P-450 catalyzed single-electron reduction of quinones, aromatic *N*-oxides and nitroaromatics [120,210,211]. Even though these reactions are relevant to the cytotoxicity of the abovementioned compounds, their mechanisms are not disclosed at the molecular level because proteoliposomal preparations rather than isolated enzymes are used in these studies.

3.4. Electron transfer distances in the reactions of different electrontransferases with prooxidant xenobiotics

The outer sphere electron transfer model can be employed in calculating the electron transfer distances in *Pf*FNR catalyzed reactions. The k_{11} values of metalloproteins for the reactions with inorganic complexes are related to the distance of electron transfer R_p when electrostatic interactions are absent, i.e. at infinite ionic strength [212]:

$$R_p\,(\text{Å}) = 6.3 - 0.35 \ln k_{11} \qquad (30)$$

This treatment to estimate the distances of electron transfer has been used when analysing single-electron oxidation of P-450R, FNR from *Anabaena* and NOS by quinones, nitroaromatics and inorganic complexes [29,75,119]. R_p values for organic oxidants were calculated to be between 3.4 and 5.0 Å, whereas hydrophilic ferricyanide and $Fe(EDTA)^-$ are incapable of entering the protein globule and R_p values for the latter were up to two times higher. An overestimation of distances is plausible in the case of flavoproteins due to the dimethylbenzene part of the isoalloxazine ring being partly exposed to the solvent [124,213,214] so the values should be regarded cautiously in approximately assessing the "intrinsic" reactivity of a flavoenzyme. A further complication for the estimation of k_{11} and R_p in *Pf*FNR catalysis derives from the unknown E_7^1 of the FAD/FADH$^\bullet$ couple. It was noted that during the reductive titration of *Pf*FNR, the extent of FAD semiquinone stabilization is low, however its quantitative characterization was not provided [90]. Thus, the values of k_{11} were calculated assuming a 5% and 15% FADH$^\bullet$ formation at equilibrium.

Inorganic electron acceptors ferricyanide and $Fe(EDTA)^-$ are characterized by $k_{22} = 4.6 \times 10^5$ $M^{-1}s^{-1}$ and 6.9×10^4 $M^{-1}s^{-1}$ respectively at infinite ionic strength [212]. At $\mu = 1.1$ M, their respective k_{12} values are equal to 1.0×10^6 $M^{-1}s^{-1}$ and 1.0×10^4 $M^{-1}s^{-1}$ (Fig. 20). According to the Nernst equation and assuming $E_7^{\text{FAD/FADH}^-} = -0.28$ V [90], $E_7^{\text{FAD/FADH}^\bullet} = -0.308$ V (15% FADH$^\bullet$ stabilization) and $E_7^{\text{FAD/FADH}^\bullet} = -0.337$ V (5% FADH$^\bullet$ stabilization). The k_{11} values of *Pf*FNR can be obtained from the following expression [215]:

$$\log k_{11} = \log k_{12} - \log k_{22} - 0.5\log K + \log Z - \\ -\sqrt{(\log Z - \log k_{12})^2 + \log K\,(\log Z - \log k_{12})} \qquad (31)$$

For the reactions with ferricyanide $\log k_{11} = -4$ and $\log k_{11} = -4.39$, for 15% and 5% FADH$^\bullet$ stabilization, respectively; for $Fe(EDTA)^-$ the respective

values are log k_{11} = −3.46 and log k_{11} = −3.89. In the case of Q and $ArNO_2$ one can infer the approximate k_{11} values from the data in Fig. 16 at $\Delta E_7^1 = 0$, where $k_{12} = \sqrt{k_{11} \times k_{22}}$. When stabilization is at 15%, the log k_{11} values are equal to 1.90 ± 0.08 for Q and 1.80 ± 0.12 for $ArNO_2$ and fall to 1.60 ± 0.09 and 0.80 ± 0.09 respectively at 5% $FADH^{\bullet}$ stabilization.

Application of the Mauk model is possible for the reactions of *Rp*FNR with Q and $ArNO_2$, the approximate k_{11} values may be obtained from the data of Fig. 26 at $\Delta E_7^1 = 0$, where $k_{12} = (k_{11} \times k_{22})^{1/2}$. At E_7^1 of the oxidant being equal to −0.285 V, the log k_{11} values are equal to 1.36 ± 0.46 (quinones) and 1.04 ± 0.22 (nitroaromatics), which then gives R_p = 5.2 ± 0.4 Å and R_p = 5.4 ± 0.2 Å, respectively, according to Eq. 30. It can be noted that the possible uncertainty of the E-$FADH^{\bullet}$ potential in the range of 10–15 mV has almost no effect on the R_p value, changing it by only 0.1 Å. Thus, these R_ps are close to the R_p values for plant-type FNRs given previously, indicating that possible steric interferences in the structure of *Rp*FNR may not affect the low M_r oxidant reduction rate.

Calmodulin is known to accelerate the transitions between various conformational states of nNOS flavin reductase domain while favoring the conformational states with better FMN accessibility to the solvent [216,217], however it is also suggested that CaM acts in decreasing the E_7^1 of FMNH $FADH^{\bullet}/FMNH_2$ couple and increasing its reactivity [207]. The k_{11} values for nNOS are estimated from the data in Fig. 31 at $\Delta E_7^1 = 0$, where the one-electron reduction potentials of the oxidant and $FMNH^{\bullet}/FMNH_2$ couple should be equal. There are some doubts in the reported values of E_7^1 for $FMNH^{\bullet}/FMNH_2$ couple even after adjustment to pH 7.0 (table 14).

Table 14. Redox potentials of $FMNH^{\bullet}/FMNH_2$ couple from nNOS. Values in parentheses after adjustment to pH 7.0 assuming that the reduced FMN is doubly protonated [218].

Conditions	E^1 **(V)**	
	−CaM	**+CaM**
Holoenzyme, pH 7.0 [218]	−0.220	−0.220
Flavin reductase domain, pH 7.1 [139]	−0.274 (−0.268)	−0.267 (−0.261)
Flavin reductase domain, pH 7.4 [207]	−0.199 (−0.175)	−0.284 (−0.260)
Flavin reductase domain, pH 7.5 [136]		−0.300 (−0.270)
Flavin reductase domain, pH 7.6 [203]	−0.276 (−0.240)	

The highest and lowest pH-adjusted values of E_7^1 in the absence and presence of CaM were used in the calculations. Based on the data in fig. 31A

and Eq. 30 the obtained values are R_p = 3.9 ± 0.3 Å (log k_{11} = 3.0 ± 0.4) for E_7^1 = −0.175 V and R_p = 4.7 ± 0.5 Å (log k_{11} = 2.0 ± 0.3) for E_7^1 = −0.268 V. Alternatively, in the presence of CaM and based on the data in Fig. 31B, R_p = 2.8 ± 0.2 Å (log k_{11} = 4.4 ± 0.7) for E_7^1 = −0.220 V and R_p = 3.1 ± 0.2 Å (log k_{11} = 4.0 ± 0.6) for E_7^1 = −0.270 V. Therefore, the enhancement of nNOS reactivity by CaM can be attributed to an increased FMN accessibility regardless of a possible role in decreasing the redox potential of $FMNH^{\bullet}/FMNH_2$ [205].

The data presented in table 15 show the values of electron transfer distance, determined in this work and compared with results obtained in previous studies. In the case of *Pf*FNR and *Rp*FNR, the electron transfer distances appear to be larger than those of P-450R and close to those of FNR from *Anabaena* which in turn means that the FAD isoalloxazine ring of both of these plastidic FNRs is accessible to low M_r oxidants regardless of the differences in the isoalloxazine vicinity [89,181,214].

Table 15. Distances of the electron transfer in reactions of flavin-dependent electrontransferases with nonphysiological electron acceptors

Flavoprotein	Reaction	R_p (Å)			
		Q	$ArNO_2$	$Fe(CN)_6^{3-}$	$Fe(EDTA)^-$
P-450 [119]	$FMNH^- - e^- \rightarrow FMNH^{\bullet}$ E_7^1 = −0.270 V	3.4	4.2	8.1	7.3
nNOS [29]	$FMNH^- - e^- \rightarrow FMNH^{\bullet}$ E_7^1 = −0.274 V	4.7	3.9		
*An*FNR [75]	$FADH^{\bullet} - e^- - H^+ \rightarrow FAD$ E_7^1 = −0.280 V	5.0	4.4	9.2	10.4 – 11.4
*Pf*FNR	$FADH^{\bullet} - e^- - H^+ \rightarrow FAD$ E_7^1 = −0.308 V $FADH^{\bullet} - e^- - H^+ \rightarrow FAD$ E_7^1 = −0.337 V	4.8 5.0	4.9 5.6	9.5 9.8	9.1 9.4
*Rp*FNR	$FADH^{\bullet} - e^- - H^+ \rightarrow FAD$ E_7^1 = −0.285 V	5.2	5.4		
nNOS (−CaM)	$FMNH^- - e^- \rightarrow FMNH^{\bullet}$ E_7^1 = −0.175 V $FMNH^- - e^- \rightarrow FMNH^{\bullet}$ E_7^1 = −0.268 V	3.9 4.7			
nNOS (+CaM)	$FMNH^- - e^- \rightarrow FMNH^{\bullet}$ E_7^1 = −0.220 V $FMNH^- - e^- \rightarrow FMNH^{\bullet}$ E_7^1 = −0.270 V	2.8 3.1			

CONCLUSIONS

1. *P. falciparum* ferredoxin:$NADP^+$ oxidoreductase and *R. palustris* ferredoxin:$NADP^+$ oxidoreductase-catalyzed reduction of xenobiotics is similar to that of plastidic FNR from *Anabaena* in quantitative terms and the rate-limiting step is the oxidation of a FAD semiquinone.
2. *P. falciparum* ferredoxin enhances the reduction of xenobiotics by FNR by providing an alternative pathway for their reduction with higher reduction rate constant but a lower maximal turnover.
3. The redox potential analysis of a novel thioredoxin reductase-type *Rp*FNR was performed for the first time, giving the redox potential value $E_7^0 = -0.276$ V and demonstrating a relatively high stability of the semiquinone, 26.5% at equilibrium. These data are consistent with that of other FNRs.
4. The role of heme Fe^{2+}-NO complex of nNOS in the reduction of xenobiotics was shown for the first time with the complex taking up a minor portion of the electron flux for the reduction of external electron acceptors.
5. The studies of ionic strength effects on the kinetics of neuronal NO synthase demonstrate the interaction of electron acceptors with the negatively charged domain at the vicinity of FMN, and the occurrence of conformational changes of the enzyme that facilitate the access of electron acceptors to the active site at high ionic strength
6. It was shown that dehydrogenases – electrontransferases can be employed in the approximate determination of single-electron reduction potentials of nitroaromatic compounds and aromatic *N*-oxides.
7. The calculated electron transfer distances in *Pf*FNR and *Rp*FNR are similar to those calculated for *An*FNR and are around 5 Å for quinones and nitroaromatics. The electron transfer distances in nNOS in the presence of calmodulin, around 3.0 Å, are similar to those in cytochrome P-450 reductase.

REFERENCES

1. Leys, D.; Scrutton, N.S. Sweating the assets of flavin cofactors: new insight of chemical versatility from knowledge of structure and mechanism. *Curr. Opin. Struct. Biol.* **2016**, *41*, 19–26, doi:10.1016/j.sbi.2016.05.014.
2. Sobrado, P. Noncanonical reactions of flavoenzymes. *Int. J. Mol. Sci.* **2012**, *13*, 14219–14242, doi:10.3390/ijms131114219.
3. Piano, V.; Palfey, B.A.; Mattevi, A. Flavins as covalent catalysts: new mechanisms emerge. *Trends Biochem. Sci.* **2017**, *42*, 457–469, doi:10.1016/j.tibs.2017.02.005.
4. Hall, M. Flavoenzymes for biocatalysis. In *Enzymes*; 2020; Vol. 47, pp. 37–62 ISBN 9780128201374.
5. Fagan, R.L.; Palfey, B.A. Flavin-dependent enzymes. In *Comprehensive Natural Products II*; Elsevier, 2010; Vol. 7, pp. 37–113 ISBN 9780080453828.
6. Mewies, M.; McIntire, W.S.; Scrutton, N.S. Covalent attachment of flavin adenine dinucleotide (FAD) and flavin mononucleotide (FMN) to enzymes: The current state of affairs. *Protein Sci.* **1998**, *7*, 7–20, doi:10.1002/pro.5560070102.
7. Miura, R. Versatility and specificity in flavoenzymes: Control mechanisms of flavin reactivity. *Chem. Rec.* **2001**, *1*, 183–194, doi:10.1002/tcr.1007.
8. Lu, Y.; Marshall, N.M. Redox Potential. In *Encyclopedia of Biophysics*; Roberts, G.C.K., Ed.; Springer Berlin Heidelberg: Berlin, Heidelberg, 2013; pp. 2207–2211 ISBN 978-3-642-16712-6.
9. Ghisla, S.; Massey, V.; Lhoste, J.-M.; Mayhew, S.G. Fluorescence and optical characteristics of reduced flavines and flavoproteins. *Biochemistry* **1974**, *13*, 589–597, doi:10.1021/bi00700a029.
10. Muller, F.; Brustlein, M.; Hemmerich, P.; Massey, V.; Walker, W.H. Light-Absorption Studies on Neutral Flavin Radicals. *Eur. J. Biochem.* **1972**, *25*, 573–580, doi:10.1111/j.1432-1033.1972.tb01730.x.
11. Massey, V.; Hemmerich, P. Active-site probes of flavoproteins. *Biochem. Soc. Trans.* **1980**, *8*, 246–257, doi:10.1042/bst0080246.
12. Hemmerich, P.; Massey, V. The Role of the Apoprotein in Directing Pathways of Flavin Catalysis. In *Oxidases and Related Redox Systems*; Elsevier, 1982; pp. 379–405.
13. Massey, V. The Chemical and Biological Versatility of Riboflavin. *Biochem. Soc. Trans.* **2000**, *28*, 283, doi:10.1042/0300-5127:0280283.
14. Valiauga, B. Studies of reduction mechanisms of quinones and nitroaromatic compounds by flavoenzymes dehydrogenases-transhydrogenases, Vilnius University: Lithuania, 2020.
15. Čėnas, N.; Anusevičius, Ž.; Nivinskas, H.; Misevičienė, L.; Šarlauskas, J. Structure-Activity Relationships in Two-Electron Reduction of Quinones. In *Methods in Enzymology*; 2004; Vol. 382,

pp. 258–277.
16. Huynh, M.T.; Anson, C.W.; Cavell, A.C.; Stahl, S.S.; Hammes-Schiffer, S. Quinone 1 e – and 2 e – /2 H + Reduction Potentials: Identification and Analysis of Deviations from Systematic Scaling Relationships. *J. Am. Chem. Soc.* **2016**, *138*, 15903–15910, doi:10.1021/jacs.6b05797.
17. Wardman, P. Reduction Potentials of One-Electron Couples Involving Free Radicals in Aqueous Solution. *J. Phys. Chem. Ref. Data* **1989**, *18*, 1637–1755, doi:10.1063/1.555843.
18. Pal, H.; Mukherjee, T.; Mittal, J.P. One-electron reduction of 9, 10-anthraquinone, 1-amino-9, 10-anthraquinone and 1-hydroxy-9, 10-anthraquinone in aqueous-isopropanol-acetone mixed solvent: A pulse radiolysis study. *Radiat. Phys. Chem.* **1994**, *44*, 603–609, doi:10.1016/0969-806X(94)90219-4.
19. Čėnas, N.K.; Kanapienienė, J.J.; Kulys, J.J. NADH oxidation by quinone electron acceptors. *Biochim. Biophys. Acta - Bioenerg.* **1984**, *767*, 108–112, doi:10.1016/0005-2728(84)90084-7.
20. Kulys, J.J.; Čėnas, N.K. Oxidation of glucose oxidase from Penicillium vitale by one- and two-electron acceptors. *Biochim. Biophys. Acta - Protein Struct. Mol. Enzymol.* **1983**, *744*, 57–63, doi:10.1016/0167-4838(83)90340-0.
21. Anusevičius, Ž.; Misevičienė, L.; Medina, M.; Martinez-Julvez, M.; Gomez-Moreno, C.; Čėnas, N. FAD semiquinone stability regulates single- and two-electron reduction of quinones by Anabaena PCC7119 ferredoxin:NADP+ reductase and its Glu301Ala mutant. *Arch. Biochem. Biophys.* **2005**, *437*, 144–150, doi:10.1016/j.abb.2005.03.015.
22. Guo, S. tai; Liu, J.; Qian, W.; Zhu, W. hua; Zhang, C. yang A review of quantum chemical methods for treating energetic molecules. *Energ. Mater. Front.* **2021**, *2*, 292–305, doi:10.1016/j.enmf.2021.10.004.
23. Čėnas, N.; Nemeikaitė-Čėnienė, A.; Sergedienė, E.; Nivinskas, H.; Anusevičius, Ž.; Šarlauskas, J. Quantitative structure–activity relationships in enzymatic single-electron reduction of nitroaromatic explosives: implications for their cytotoxicity. *Biochim. Biophys. Acta - Gen. Subj.* **2001**, *1528*, 31–38, doi:10.1016/S0304-4165(01)00169-6.
24. Marcus, R.A.; Sutin, N. Electron transfers in chemistry and biology. *Biochim. Biophys. Acta - Rev. Bioenerg.* **1985**, *811*, 265–322, doi:10.1016/0304-4173(85)90014-X.
25. Grampp, G.; Jaenicke, W. ESR-spectroscopic investigation of the parallel electron and proton exchange between quinones and their radicals. *J. Electroanal. Chem. Interfacial Electrochem.* **1987**, *229*, 297–303, doi:10.1016/0022-0728(87)85147-1.
26. Nemeikaitė-Čėnienė, A.; Šarlauskas, J.; Jonušienė, V.; Marozienė, A.; Misevičienė, L.; Yantsevich, A. V.; Čėnas, N. Kinetics of Flavoenzyme-Catalyzed Reduction of Tirapazamine Derivatives:

Implications for Their Prooxidant Cytotoxicity. *Int. J. Mol. Sci.* **2019**, *20*, 4602, doi:10.3390/ijms20184602.
27. Meot-Ner, M.; Neta, P. Kinetics of electron transfer from nitroaromatic radical anions in aqueous solutions. Effects of temperature and steric configuration. *J. Phys. Chem.* **1986**, *90*, 4648–4650, doi:10.1021/j100410a036.
28. Nemeikaitė-Čėnienė, A.; Šarlauskas, J.; Anusevičius, Ž.; Nivinskas, H.; Čėnas, N. Cytotoxicity of RH1 and related aziridinylbenzoquinones: involvement of activation by NAD(P)H:quinone oxidoreductase (NQO1) and oxidative stress. *Arch. Biochem. Biophys.* **2003**, *416*, 110–118, doi:10.1016/S0003-9861(03)00281-9.
29. Anusevičius, Ž.; Nivinskas, H.; Šarlauskas, J.; Sari, M.-A.; Boucher, J.-L.; Čėnas, N. Single-electron reduction of quinone and nitroaromatic xenobiotics by recombinant rat neuronal nitric oxide synthase. *Acta Biochim. Pol.* **2013**, *60*, 217–222, doi:10.18388/abp.2013_1974.
30. Shen, X.; Gates, K.S. Enzyme-Activated Generation of Reactive Oxygen Species from Heterocyclic N-Oxides under Aerobic and Anaerobic Conditions and Its Relevance to Hypoxia-Selective Prodrugs. *Chem. Res. Toxicol.* **2019**, *32*, 348–361, doi:10.1021/acs.chemrestox.9b00036.
31. Shen, X.; Rajapakse, A.; Gallazzi, F.; Junnotula, V.; Fuchs-Knotts, T.; Glaser, R.; Gates, K.S. Isotopic labeling experiments that elucidate the mechanism of DNA strand cleavage by the hypoxia-selective antitumor agent 1,2,4-benzotriazine 1,4-Di- N -oxide. *Chem. Res. Toxicol.* **2014**, *27*, 111–118, doi:10.1021/tx400356y.
32. Yadav, P.; Marshall, A.J.; Reynisson, J.; Denny, W.A.; Hay, M.P.; Anderson, R.F. Fragmentation of the quinoxaline N-oxide bond to the OH radical upon one-electron bioreduction. *Chem. Commun.* **2014**, *50*, 13729–13731, doi:10.1039/c4cc05657d.
33. Fuchs, T.; Chowdhury, G.; Barnes, C.L.; Gates, K.S. 3-amino-1,2,4-benzotriazine 4-oxide: Characterization of a new metabolite arising from bioreductive processing of the antitumor agent 3-amino-1,2,4-benzotriazine 1,4-dioxide (tirapazamine). *J. Org. Chem.* **2001**, *66*, 107–114, doi:10.1021/jo001232j.
34. Wardman, P.; Dennis, M.F.; Everett, S.A.; Patel, K.B.; Stratford, M.R.L.; Tracy, M. Radicals from one-electron reduction of nitro compounds, aromatic N-oxides and quinones: the kinetic basis for hypoxia-selective, bioreductive drugs. *Biochem. Soc. Symp.* **1995**, *61*, 171–194, doi:10.1042/bss0610171.
35. Čėnas, N.; Nemeikaitė-Čėnienė, A.; Kosychova, L. Single- and Two-Electron Reduction of Nitroaromatic Compounds by Flavoenzymes: Mechanisms and Implications for Cytotoxicity. *Int. J. Mol. Sci.* **2021**, *22*, 8534, doi:10.3390/ijms22168534.

36. Nemeikaitė-Čėnienė, A.; Marozienė, A.; Misevičienė, L.; Tamulienė, J.; Yantsevich, A. V.; Čėnas, N. Flavoenzyme-catalyzed single-electron reduction of nitroaromatic antiandrogens: implications for their cytotoxicity. *Free Radic. Res.* **2021**, *55*, 246–254, doi:10.1080/10715762.2021.1919304.
37. Šarlauskas, J.; Dičkancaitė, E.; Nemeikaitė, A.; Anusevičius, Ž.; Nivinskas, H.; Segura-Aguilar, J.; Čėnas, N. Nitrobenzimidazoles as Substrates for DT-Diaphorase and Redox Cycling Compounds: Their Enzymatic Reactions and Cytotoxicity. *Arch. Biochem. Biophys.* **1997**, *346*, 219–229, doi:10.1006/abbi.1997.0285.
38. Adams, G.E.; Flockhart, I.R.; Smithen, C.E.; Stratford, I.J.; Wardman, P.; Watts, M.E. Electron-affinic sensitization. VII. A correlation between structures, one-electron reduction potentials, and efficiencies of nitroimidazoles as hypoxic cell radiosensitizers. *Radiat. Res.* **1976**, *67*, 9–20, doi:10.2307/3574491.
39. Adams, G.E.; Clarke, E.D.; Gray, P.; Jacobs, R.S.; Stratford, I.J.; Wardman, P.; Watts, M.E.; Parrick, J.; Wallace, R.G.; Smithen, C.E. Structure-activity relationships in the development of hypoxic cell radiosensitizers: II. Cytotoxicity and therapeutic ratio. *Int. J. Radiat. Biol.* **1979**, *35*, 151–160, doi:10.1080/09553007914550161.
40. Miškinienė, V.; Sergedienė, E.; Nemeikaitė, A.; Segura-Aguilar, J.; Čėnas, N. Role of redox cycling and activation by DT-diaphorase in the cytotoxicity of 5-(aziridin-1-yl)-2,4-dinitrobenzamide (CB-1954) and its analogs. *Cancer Lett.* **1999**, *146*, 217–222, doi:10.1016/S0304-3835(99)00271-2.
41. Miliukienė, V.; Čėnas, N. Cytotoxicity of Nitroaromatic Explosives and their Biodegradation Products in Mice Splenocytes: Implications for their Immunotoxicity. *Zeitschrift für Naturforsch. C* **2008**, *63*, 519–525, doi:10.1515/znc-2008-7-809.
42. Mulo, P.; Medina, M. Interaction and electron transfer between ferredoxin–NADP+ oxidoreductase and its partners: structural, functional, and physiological implications. *Photosynth. Res.* **2017**, *134*, 265–280, doi:10.1007/s11120-017-0372-0.
43. Grinberg, A. V.; Hannemann, F.; Schiffler, B.; Müller, J.; Heinemann, U.; Bernhardt, R. Adrenodoxin: Structure, stability, and electron transfer properties. *Proteins Struct. Funct. Genet.* **2000**, *40*, 590–612, doi:10.1002/1097-0134(20000901)40:4<590::AID-PROT50>3.0.CO;2-P.
44. Lambeth, J.D.; Kamin, H. Adrenodoxin reductase. Properties of the complexes of reduced enzyme with NADP+ and NADPH. *J. Biol. Chem.* **1976**, *251*, 4299–4306, doi:10.1016/S0021-9258(17)33296-9.
45. Čénas, N.K.; Marcinkevičiene, J.A.; Kulys, J.J.; Usanov, S.A. A negative cooperativity between NADPH and adrenodoxin on binding to NADPH:adrenodoxin reductase. *FEBS Lett.* **1990**, *259*, 338–340, doi:10.1016/0014-5793(90)80042-H.

46. Marcinkeviciene, J.; Cenas, N.; Kulys, J.; Usanov, S.A.; Sukhova, N.M.; Selezneva, I.S.; Gryazev, V.F. Nitroreductase reactions of the NADPH: adrenodoxin reductase and the adrenodoxin complex. *Biomed. Biochim. Acta* **1990**, *49*, 167–172.
47. Shin, M.; Arnon, D.I. Enzymic Mechanisms of Pyridine Nucleotide Reduction in Chloroplasts. *J. Biol. Chem.* **1965**, *240*, 1405–1411, doi:10.1016/s0021-9258(18)97591-5.
48. Ceccarelli, E.A.; Arakaki, A.K.; Cortez, N.; Carrillo, N. Functional plasticity and catalytic efficiency in plant and bacterial ferredoxin-NADP(H) reductases. *Biochim. Biophys. Acta - Proteins Proteomics* **2004**, *1698*, 155–165, doi:10.1016/j.bbapap.2003.12.005.
49. Ingelman, M.; Bianchi, V.; Eklund, H. The three-dimensional structure of flavodoxin reductase from Escherichia coli at 1.7 Å resolution. *J. Mol. Biol.* **1997**, *268*, 147–157, doi:10.1006/jmbi.1997.0957.
50. Tejero, J.; Pérez-Dorado, I.; Maya, C.; Martínez-Júlvez, M.; Sanz-Aparicio, J.; Gómez-Moreno, C.; Hermoso, J.A.; Medina, M. C-Terminal Tyrosine of Ferredoxin−NADP + Reductase in Hydride Transfer Processes with NAD(P) + /H. *Biochemistry* **2005**, *44*, 13477–13490, doi:10.1021/bi051278c.
51. Nogués, I.; Tejero, J.; Hurley, J.K.; Paladini, D.; Frago, S.; Tollin, G.; Mayhew, S.G.; Gómez-Moreno, C.; Ceccarelli, E.A.; Carrillo, N.; et al. Role of the C-Terminal Tyrosine of Ferredoxin-Nicotinamide Adenine Dinucleotide Phosphate Reductase in the Electron Transfer Processes with Its Protein Partners Ferredoxin and Flavodoxin. *Biochemistry* **2004**, *43*, 6127–6137, doi:10.1021/bi049858h.
52. Piubelli, L.; Aliverti, A.; Arakaki, A.K.; Carrillo, N.; Ceccarelli, E.A.; Karplus, P.A.; Zanetti, G. Competition between C-terminal Tyrosine and Nicotinamide Modulates Pyridine Nucleotide Affinity and Specificity in Plant Ferredoxin-NADP+ Reductase. *J. Biol. Chem.* **2000**, *275*, 10472–10476, doi:10.1074/jbc.275.14.10472.
53. Calcaterra, N.B.; Picó, G.A.; Orellano, E.G.; Ottado, J.; Carrillo, N.; Ceccarelli, E.A. Contribution of the FAD Binding Site Residue Tyrosine 308 to the Stability of Pea Ferredoxin-NADP+ Oxidoreductase. *Biochemistry* **1995**, *34*, 12842–12848, doi:10.1021/bi00039a045.
54. Deng, Z.; Aliverti, A.; Zanetti, G.; Arakaki, A.K.; Ottado, J.; Orellano, E.G.; Calcaterra, N.B.; Ceccarelli, E.A.; Carrillo, N.; Karplus, P.A. A productive NADP+ binding mode of ferredoxin-NADP+ reductase revealed by protein engineering and crystallographic studies. *Nat. Struct. Biol.* **1999**, *6*, 847–853, doi:https://doi.org/10.1038/12307.
55. Palatnik, J.F.; Valle, E.M.; Carrillo, N. Oxidative stress causes ferredoxin-NADP+ reductase solubilization from the thylakoid membranes in methyl viologen-treated plants. *Plant Physiol.* **1997**, *115*, 1721–1727, doi:10.1104/pp.115.4.1721.
56. Hajirezaei, M.-R.; Peisker, M.; Tschiersch, H.; Palatnik, J.F.; Valle,

E.M.; Carrillo, N.; Sonnewald, U. Small changes in the activity of chloroplastic NADP + -dependent ferredoxin oxidoreductase lead to impaired plant growth and restrict photosynthetic activity of transgenic tobacco plants. *Plant J.* **2002**, *29*, 281–293, doi:10.1046/j.0960-7412.2001.01209.x.

57. Krawetz, S.A.; Israelstam, G.F. Kinetics of pyridine nucleotide transhydrogenase from Chlorella. *Plant Sci. Lett.* **1978**, *12*, 323–326, doi:10.1016/0304-4211(78)90085-8.
58. Carrillo, N.; Ceccarelli, E.A. Open questions in ferredoxin-NADP+ reductase catalytic mechanism. *Eur. J. Biochem.* **2003**, *270*, 1900–1915, doi:10.1046/j.1432-1033.2003.03566.x.
59. Batie, C.J.; Kamin, H. Ferredoxin:NADP+ oxidoreductase. Equilibria in binary and ternary complexes with NADP+ and ferredoxin. *J. Biol. Chem.* **1984**, *259*, 8832–8839, doi:10.1016/S0021-9258(17)47229-2.
60. Nakamura, S.; Kimura, T. Studies on Spinach Ferredoxin-Nicotinamide Adenine Dinucleotide Phosphate Reductase. *J. Biol. Chem.* **1971**, *246*, 6235–6241, doi:10.1016/S0021-9258(18)61780-6.
61. Shin, M.; San Pietro, A. Complex formation of ferredoxin-NADP reductase with ferredoxin and with NADP. *Biochem. Biophys. Res. Commun.* **1968**, *33*, 38–42, doi:10.1016/0006-291X(68)90251-9.
62. Zanetti, G.; Curti, B. [22] Ferredoxin-NADP+ oxidoreductase. In *Methods in Enzymology*; Academic Press, 1980; Vol. 69, pp. 250–255.
63. Melamed-Harel, H.; Tel-Or, E.; Pietro, A.S. Effect of Ferredoxin on the Diaphorase Activity of Cyanobacterial Ferredoxin-NADP Reductase. *Plant Physiol.* **1985**, *77*, 229–231, doi:10.1104/pp.77.1.229.
64. Masaki, R.; Yoshikawa, S.; Matsubara, H. Steady-state kinetics of oxidation of reduced ferredoxin with ferredoxin-nadp+ reductase. *Biochim. Biophys. Acta - Protein Struct. Mol. Enzymol.* **1982**, *700*, 101–109, doi:10.1016/0167-4838(82)90297-7.
65. Grzyb, J.; Gagoś, M.; Gruszecki, W.I.; Bojko, M.; Strzałka, K. Interaction of ferredoxin:NADP+ oxidoreductase with model membranes. *Biochim. Biophys. Acta - Biomembr.* **2008**, *1778*, 133–142, doi:10.1016/j.bbamem.2007.09.028.
66. Shin, M.; Tagawa, K.; Arnon, D.I. Crystallization of ferredoxin-TPN reductase and its role in the photosynthetic apparatus of chloroplasts. *Biochem. Z.* **1963**, *338*, 84–96.
67. Karplus, P.A.; Daniels, M.J.; Herriott, J.R. Atomic Structure of Ferredoxin-NADP + Reductase: Prototype for a Structurally Novel Flavoenzyme Family. *Science (80-.).* **1991**, *251*, 60–66, doi:10.1126/science.1986412.
68. Bruns, C.M.; Karplus, A.P. Refined Crystal Structure of Spinach Ferredoxin Reductase at 1.7 Å Resolution: Oxidized, Reduced and 2′-Phospho-5′-AMP Bound States. *J. Mol. Biol.* **1995**, *247*, 125–145, doi:10.1006/jmbi.1994.0127.

69. Correll, C.C.; Ludwig, M.L.; Bruns, C.M.; Karplus, P.A. Structural prototypes for an extended family of flavoprotein reductases: Comparison of phthalate dioxygenase reductase with ferredoxin reductase and ferredoxin. *Protein Sci.* **1993**, *2*, 2112–2133, doi:10.1002/pro.5560021212.
70. Aliverti, A.; Piubelli, L.; Zanetti, G.; Curti, B.; Lübberstedt, T.; Herrmann, R.G. The Role of Cysteine Residues of Spinach Ferredoxin-NADP+ Reductase As Assessed by Site-Directed Mutagenesis. *Biochemistry* **1993**, *32*, 6374–6380, doi:10.1021/bi00076a010.
71. Zanetti, G.; Morelli, D.; Ronchi, S.; Negri, A.; Aliverti, A.; Curti, B. Structural studies on the interaction between ferredoxin and ferredoxin-NADP+ reductase. *Biochemistry* **1988**, *27*, 3753–3759, doi:10.1021/bi00410a035.
72. Shah, M.M.; Spain, J.C. Elimination of Nitrite from the Explosive 2,4,6-Trinitrophenylmethylnitramine (Tetryl) Catalyzed by Ferredoxin NADP Oxidoreductase from Spinach. *Biochem. Biophys. Res. Commun.* **1996**, *220*, 563–568, doi:10.1006/bbrc.1996.0443.
73. Fisher, J.; Abdella, B.R.J.; McLane, K.E. Anthracycline antibiotic reduction by spinach ferredoxin-NADP+ reductase and ferredoxin. *Biochemistry* **1985**, *24*, 3562–3571, doi:10.1021/bi00335a026.
74. Morales, R.; Kachalova, G.; Vellieux, F.; Charon, M.H.; Frey, M. Crystallographic studies of the interaction between the ferredoxin-NADP+ reductase and ferredoxin from the cyanobacterium Anabaena: Looking for the elusive ferredoxin molecule. *Acta Crystallogr. Sect. D Biol. Crystallogr.* **2000**, *56*, 1408–1412, doi:10.1107/S0907444900010052.
75. Anusevičius, Ž.; Martínez-Júlvez, M.; Genzor, C.G.; Nivinskas, H.; Gómez-Moreno, C.; Čėnas, N. Electron transfer reactions of Anabaena PCC 7119 ferredoxin:NADP+ reductase with nonphysiological oxidants. *Biochim. Biophys. Acta - Bioenerg.* **1997**, *1320*, 247–255, doi:10.1016/S0005-2728(97)00028-5.
76. Medina, M.; Martínez-Júlvez, M.; Hurley, J.K.; Tollin, G.; Gómez-Moreno, C. Involvement of Glutamic Acid 301 in the Catalytic Mechanism of Ferredoxin-NADP + Reductase from Anabaena PCC 7119. *Biochemistry* **1998**, *37*, 2715–2728, doi:10.1021/bi971795y.
77. Mayoral, T.; Medina, M.; Sanz-Aparicio, J.; Gómez-Moreno, C.; Hermoso, J.A. Structural basis of the catalytic role of Glu301 inAnabaena PCC 7119 ferredoxin-NADP+ reductase revealed by x-ray crystallography. *Proteins Struct. Funct. Genet.* **2000**, *38*, 60–69, doi:10.1002/(SICI)1097-0134(20000101)38:1<60::AID-PROT7>3.0.CO;2-B.
78. Sánchez-Azqueta, A.; Herguedas, B.; Hurtado-Guerrero, R.; Hervás, M.; Navarro, J.A.; Martínez-Júlvez, M.; Medina, M. A hydrogen bond network in the active site of Anabaena ferredoxin-NADP+ reductase

modulates its catalytic efficiency. *Biochim. Biophys. Acta - Bioenerg.* **2014**, *1837*, 251–263, doi:10.1016/j.bbabio.2013.10.010.
79. Aliverti, A.; Pandini, V.; Pennati, A.; de Rosa, M.; Zanetti, G. Structural and functional diversity of ferredoxin-NADP+ reductases. *Arch. Biochem. Biophys.* **2008**, *474*, 283–291, doi:10.1016/j.abb.2008.02.014.
80. Dumit, V.I.; Essigke, T.; Cortez, N.; Ullmann, G.M. Mechanistic Insights into Ferredoxin–NADP(H) Reductase Catalysis Involving the Conserved Glutamate in the Active Site. *J. Mol. Biol.* **2010**, *397*, 814–825, doi:10.1016/j.jmb.2010.01.063.
81. Sánchez-Azqueta, A.; Musumeci, M.A.; Martínez-Júlvez, M.; Ceccarelli, E.A.; Medina, M. Structural backgrounds for the formation of a catalytically competent complex with NADP(H) during hydride transfer in ferredoxin–NADP+ reductases. *Biochim. Biophys. Acta - Bioenerg.* **2012**, *1817*, 1063–1071, doi:10.1016/j.bbabio.2012.04.009.
82. Serre, L.; Vellieux, F.M.D.; Medina, M.; Gomez-Moreno, C.; Fontecilla-Camps, J.C.; Frey, M. X-ray Structure of the Ferredoxin:NADP+Reductase from the CyanobacteriumAnabaenaPCC 7119 at 1.8 Å Resolution, and Crystallographic Studies of NADP+Binding at 2.25 Å Resolution. *J. Mol. Biol.* **1996**, *263*, 20–39, doi:10.1006/jmbi.1996.0553.
83. Gardner, M.J.; Hall, N.; Fung, E.; White, O.; Berriman, M.; Hyman, R.W.; Carlton, J.M.; Pain, A.; Nelson, K.E.; Bowman, S.; et al. Genome sequence of the human malaria parasite Plasmodium falciparum. *Nature* **2002**, *419*, 498–511, doi:10.1038/nature01097.
84. Foth, B.J.; McFadden, G.I. The apicoplast: A plastid in Plasmodium falciparum and other apicomplexan parasites. In *International Review of Cytology*; 2003; Vol. 224, pp. 57–110.
85. Wicht, K.J.; Mok, S.; Fidock, D.A. Molecular Mechanisms of Drug Resistance in Plasmodium falciparum Malaria. *Annu. Rev. Microbiol.* **2020**, *74*, 431–454, doi:10.1146/annurev-micro-020518-115546.
86. Miotto, O.; Amato, R.; Ashley, E.A.; MacInnis, B.; Almagro-Garcia, J.; Amaratunga, C.; Lim, P.; Mead, D.; Oyola, S.O.; Dhorda, M.; et al. Genetic architecture of artemisinin-resistant Plasmodium falciparum. *Nat. Genet.* **2015**, *47*, 226–234, doi:10.1038/ng.3189.
87. Fairhurst, R.M.; Dondorp, A.M. Artemisinin-Resistant Plasmodium falciparum Malaria. *Microbiol. Spectr.* **2016**, *4*, 409–429, doi:10.1128/microbiolspec.EI10-0013-2016.
88. Stokes, B.H.; Dhingra, S.K.; Rubiano, K.; Mok, S.; Straimer, J.; Gnädig, N.F.; Deni, I.; Schindler, K.A.; Bath, J.R.; Ward, K.E.; et al. Plasmodium falciparum K13 mutations in Africa and Asia impact artemisinin resistance and parasite fitness. *Elife* **2021**, *10*, 1–29, doi:10.7554/eLife.66277.
89. Milani, M.; Balconi, E.; Aliverti, A.; Mastrangelo, E.; Seeber, F.; Bolognesi, M.; Zanetti, G. Ferredoxin-NADP+ Reductase from

Plasmodium falciparum Undergoes NADP+-dependent Dimerization and Inactivation: Functional and Crystallographic Analysis. *J. Mol. Biol.* **2007**, *367*, 501–513, doi:10.1016/j.jmb.2007.01.005.
90. Balconi, E.; Pennati, A.; Crobu, D.; Pandini, V.; Cerutti, R.; Zanetti, G.; Aliverti, A. The ferredoxin-NADP + reductase/ferredoxin electron transfer system of Plasmodium falciparum. *FEBS J.* **2009**, *276*, 3825–3836, doi:10.1111/j.1742-4658.2009.07100.x.
91. Grellier, P.; Marozienė, A.; Nivinskas, H.; Šarlauskas, J.; Aliverti, A.; Čėnas, N. Antiplasmodial activity of quinones: Roles of aziridinyl substituents and the inhibition of Plasmodium falciparum glutathione reductase. *Arch. Biochem. Biophys.* **2010**, *494*, 32–39, doi:10.1016/j.abb.2009.11.012.
92. de Rosa, M.; Nonnis, S.; Aliverti, A. Covalent inhibition of P. falciparum ferredoxin-NADP+ reductase: Exploring alternative strategies for the development of new antimalarial drugs. *Biochem. Biophys. Res. Commun.* **2021**, *577*, 89–94, doi:10.1016/j.bbrc.2021.09.008.
93. Kimata-Ariga, Y.; Morihisa, R. Effect of Artemisinin on the Redox System of NADPH/FNR/Ferredoxin from Malaria Parasites. *Antioxidants* **2022**, *11*, 273, doi:10.3390/antiox11020273.
94. Kimata-Ariga, Y.; Morihisa, R. Functional analyses of plasmodium ferredoxin Asp97Tyr mutant related to artemisinin resistance of human malaria parasites. *J. Biochem.* **2021**, *170*, 521–529, doi:10.1093/jb/mvab070.
95. Suwito, H.; Jumina; Mustofa; Pudjiastuti, P.; Fanani, M.; Kimata-Ariga, Y.; Katahira, R.; Kawakami, T.; Fujiwara, T.; Hase, T.; et al. Design and Synthesis of Chalcone Derivatives as Inhibitors of the Ferredoxin — Ferredoxin-NADP+ Reductase Interaction of Plasmodium falciparum: Pursuing New Antimalarial Agents. *Molecules* **2014**, *19*, 21473–21488, doi:10.3390/molecules191221473.
96. Larimer, F.W.; Chain, P.; Hauser, L.; Lamerdin, J.; Malfatti, S.; Do, L.; Land, M.L.; Pelletier, D.A.; Beatty, J.T.; Lang, A.S.; et al. Complete genome sequence of the metabolically versatile photosynthetic bacterium Rhodopseudomonas palustris. *Nat. Biotechnol.* **2004**, *22*, 55–61, doi:10.1038/nbt923.
97. Lu, J.; Holmgren, A. The thioredoxin antioxidant system. *Free Radic. Biol. Med.* **2014**, *66*, 75–87, doi:10.1016/j.freeradbiomed.2013.07.036.
98. Komori, H.; Seo, D.; Sakurai, T.; Higuchi, Y. Crystal structure analysis of Bacillus subtilis ferredoxin-NADP+ oxidoreductase and the structural basis for its substrate selectivity. *Protein Sci.* **2010**, *19*, 2279–2290, doi:10.1002/pro.508.
99. Muraki, N.; Seo, D.; Shiba, T.; Sakurai, T.; Kurisu, G. Asymmetric Dimeric Structure of Ferredoxin-NAD(P)+ Oxidoreductase from the Green Sulfur Bacterium Chlorobaculum tepidum: Implications for

Binding Ferredoxin and NADP+. *J. Mol. Biol.* **2010**, *401*, 403–414, doi:10.1016/j.jmb.2010.06.024.
100. Gudim, I.; Hammerstad, M.; Lofstad, M.; Hersleth, H.P. The Characterization of Different Flavodoxin Reductase-Flavodoxin (FNR-Fld) Interactions Reveals an Efficient FNR-Fld Redox Pair and Identifies a Novel FNR Subclass. *Biochemistry* **2018**, *57*, 5427–5436, doi:10.1021/acs.biochem.8b00674.
101. Seo, D.; Asano, T.; Komori, H.; Sakurai, T. Role of the C-terminal extension stacked on the re-face of the isoalloxazine ring moiety of the flavin adenine dinucleotide prosthetic group in ferredoxin-NADP+ oxidoreductase from Bacillus subtilis. *Plant Physiol. Biochem.* **2014**, *81*, 143–148, doi:10.1016/j.plaphy.2014.01.011.
102. Seo, D.; Asano, T. C-terminal residues of ferredoxin-NAD(P)+ reductase from Chlorobaculum tepidum are responsible for reaction dynamics in the hydride transfer and redox equilibria with NADP+/NADPH. *Photosynth. Res.* **2018**, *136*, 275–290, doi:10.1007/s11120-017-0462-z.
103. Seo, D.; Okabe, S.; Yanase, M.; Kataoka, K.; Sakurai, T. Studies of interaction of homo-dimeric ferredoxin-NAD(P)+ oxidoreductases of Bacillus subtilis and Rhodopseudomonas palustris, that are closely related to thioredoxin reductases in amino acid sequence, with ferredoxins and pyridine nucleotide coenzymes. *Biochim. Biophys. Acta - Proteins Proteomics* **2009**, *1794*, 594–601, doi:10.1016/j.bbapap.2008.12.014.
104. Hammerstad, M.; Hersleth, H.-P. Overview of structurally homologous flavoprotein oxidoreductases containing the low Mr thioredoxin reductase-like fold – A functionally diverse group. *Arch. Biochem. Biophys.* **2021**, *702*, 108826, doi:10.1016/j.abb.2021.108826.
105. Seo, D.; Muraki, N.; Kurisu, G. Kinetic and structural insight into a role of the re-face Tyr328 residue of the homodimer type ferredoxin-NADP+ oxidoreductase from Rhodopseudomonas palustris in the reaction with NADP+/NADPH. *Biochim. Biophys. Acta - Bioenerg.* **2020**, *1861*, 148140, doi:10.1016/j.bbabio.2019.148140.
106. Seo, D.; Soeta, T.; Sakurai, H.; Sétif, P.; Sakurai, T. Pre-steady-state kinetic studies of redox reactions catalysed by Bacillus subtilis ferredoxin-NADP + oxidoreductase with NADP + /NADPH and ferredoxin. *Biochim. Biophys. Acta - Bioenerg.* **2016**, *1857*, 678–687, doi:10.1016/j.bbabio.2016.03.005.
107. Seo, D.; Kitashima, M.; Sakurai, T.; Inoue, K. Kinetics of NADP+/NADPH reduction–oxidation catalyzed by the ferredoxin-NAD(P)+ reductase from the green sulfur bacterium Chlorobaculum tepidum. *Photosynth. Res.* **2016**, *130*, 479–489, doi:10.1007/s11120-016-0285-3.
108. Iyanagi, T.; Mason, H.S. Some Properties of Hepatic Reduced

Nicotinamide Adenine Dinucleotide Phosphate-Cytochrome c Reductase. *Biochemistry* **1973**, *12*, 2297–2308, doi:10.1021/bi00736a018.
109. Vermilion, J.L.; Coon, M.J. Highly purified detergent-solubilized NADPH-cytochrome P-450 reductase from phenobarbital-induced rat liver microsomes. *Biochem. Biophys. Res. Commun.* **1974**, *60*, 1315–1322, doi:10.1016/0006-291X(74)90341-6.
110. Vermilion, J.L.; Coon, M.J. Purified liver microsomal NADPH-cytochrome P-450 reductase. Spectral characterization of oxidation-reduction states. *J. Biol. Chem.* **1978**, *253*, 2694–2704, doi:10.1016/s0021-9258(17)40876-3.
111. Pandey, A. V.; Flück, C.E. NADPH P450 oxidoreductase: Structure, function, and pathology of diseases. *Pharmacol. Ther.* **2013**, *138*, 229–254, doi:10.1016/j.pharmthera.2013.01.010.
112. Hanukoglu, I.; Gutfinger, T. cDNA sequence of adrenodoxin reductase: Identification of NADP-binding sites in oxidoreductases. *Eur. J. Biochem.* **1989**, *180*, 479–484, doi:10.1111/j.1432-1033.1989.tb14671.x.
113. Bredt, D.S.; Glatt, C.E.; Hwang, P.M.; Fotuhi, M.; Dawson, T.M.; Snyder, S.H. Nitric oxide synthase protein and mRNA are discretely localized in neuronal populations of the mammalian CNS together with NADPH diaphorase. *Neuron* **1991**, *7*, 615–624, doi:10.1016/0896-6273(91)90374-9.
114. Murataliev, M.B.; Feyereisen, R.; Walker, F.A. Electron transfer by diflavin reductases. *Biochim. Biophys. Acta - Proteins Proteomics* **2004**, *1698*, 1–26, doi:10.1016/j.bbapap.2003.10.003.
115. Hubbard, P.A.; Shen, A.L.; Paschke, R.; Kasper, C.B.; Kim, J.J.P. NADPH-cytochrome P450 oxidoreductase. Structural basis for hydride and electron transfer. *J. Biol. Chem.* **2001**, *276*, 29163–29170, doi:10.1074/jbc.M101731200.
116. Das, A.; Sligar, S.G. Modulation of the cytochrome P450 reductase redox potential by the phospholipid bilayer. *Biochemistry* **2009**, *48*, 12104–12112, doi:10.1021/bi9011435.
117. Oprian, D.D.; Coon, M.J. Oxidation-reduction states of FMN and FAD in NADPH-cytochrome P-450 reductase during reduction by NADPH. *J. Biol. Chem.* **1982**, *257*, 8935–8944, doi:10.1016/S0021-9258(18)34223-6.
118. Orna, M. V.; Mason, R.P. Correlation of Kinetic Parameters of Nitroreductase Enzymes with Redox Properties of Nitroaromatic Compounds. *J. Biol. Chem.* **1989**, *264*, 12379–12384, doi:10.1016/S0021-9258(18)63869-4.
119. Čėnas, N.; Anusevičius, Ž.; Bironaitė, D.; Bachmanova, G.I.; Archakov, A.I.; Öllinger, K. The Electron-Transfer Reactions of NADPH-Cytochrome P450 Reductase with Nonphysiological Oxidants. *Arch. Biochem. Biophys.* **1994**, *315*, 400–406,

doi:10.1006/abbi.1994.1517.
120. Goeptar, A.R.; Scheerens, H.; Vermeulen, N.P.E. Oxygen and Xenobiotic Reductase Activities of Cytochrome P450. *Crit. Rev. Toxicol.* **1995**, *25*, 25–65, doi:10.3109/10408449509089886.
121. Alderton, W.K.; Cooper, C.E.; Knowles, R.G. Nitric oxide synthases: structure, function and inhibition. *Biochem. J.* **2001**, *357*, 593, doi:10.1042/0264-6021:3570593.
122. Daff, S. NO synthase: Structures and mechanisms. *Nitric Oxide* **2010**, *23*, 1–11, doi:10.1016/j.niox.2010.03.001.
123. Garcin, E.D.; Bruns, C.M.; Lloyd, S.J.; Hosfield, D.J.; Tiso, M.; Gachhui, R.; Stuehr, D.J.; Tainer, J.A.; Getzoff, E.D. Structural Basis for Isozyme-specific Regulation of Electron Transfer in Nitric-oxide Synthase. *J. Biol. Chem.* **2004**, *279*, 37918–37927, doi:10.1074/jbc.M406204200.
124. Wang, M.; Roberts, D.L.; Paschke, R.; Shea, T.M.; Masters, B.S.S.; Kim, J.-J.P. Three-dimensional structure of NADPH-cytochrome P450 reductase: Prototype for FMN- and FAD-containing enzymes. *Proc. Natl. Acad. Sci.* **1997**, *94*, 8411–8416, doi:10.1073/pnas.94.16.8411.
125. Stuehr, D.J.; Haque, M.M. Nitric oxide synthase enzymology in the 20 years after the Nobel Prize. *Br. J. Pharmacol.* **2019**, *176*, 177–188, doi:10.1111/bph.14533.
126. Panda, K.; Ghosh, S.; Stuehr, D.J. Calmodulin Activates Intersubunit Electron Transfer in the Neuronal Nitric-oxide Synthase Dimer. *J. Biol. Chem.* **2001**, *276*, 23349–23356, doi:10.1074/jbc.M100687200.
127. Sagami, I.; Daff, S.; Shimizu, T. Intra-subunit and inter-subunit electron transfer in neuronal nitric-oxide synthase. Effect of calmodulin on heterodimer catalysis. *J. Biol. Chem.* **2001**, *276*, 30036–30042, doi:10.1074/jbc.M104123200.
128. Siddhanta, U.; Presta, A.; Fan, B.; Wolan, D.; Rousseau, D.L.; Stuehr, D.J. Domain swapping in inducible nitric-oxide synthase: Electron transfer occurs between flavin and heme groups located on adjacent subunits in the dimer. *J. Biol. Chem.* **1998**, *273*, 18950–18958, doi:10.1074/jbc.273.30.18950.
129. Matsuda, H.; Iyanagi, T. Calmodulin activates intramolecular electron transfer between the two flavins of neuronal nitric oxide synthase flavin domain. *Biochim. Biophys. Acta - Gen. Subj.* **1999**, *1473*, 345–355, doi:10.1016/S0304-4165(99)00193-2.
130. Matsuda, H.; Kimura, S.; Iyanagi, T. One-electron reduction of quinones by the neuronal nitric-oxide synthase reductase domain. *Biochim. Biophys. Acta - Bioenerg.* **2000**, *1459*, 106–116, doi:10.1016/S0005-2728(00)00117-1.
131. Guan, Z.-W.; Kamatani, D.; Kimura, S.; Iyanagi, T. Mechanistic Studies on the Intramolecular One-electron Transfer between the Two Flavins in the Human Neuronal Nitric-oxide Synthase and Inducible Nitric-oxide Synthase Flavin Domains. *J. Biol. Chem.* **2003**, *278*,

30859–30868, doi:10.1074/jbc.M301929200.
132. Wei, C.-C.; Wang, Z.-Q.; Tejero, J.; Yang, Y.-P.; Hemann, C.; Hille, R.; Stuehr, D.J. Catalytic Reduction of a Tetrahydrobiopterin Radical within Nitric-oxide Synthase. *J. Biol. Chem.* **2008**, *283*, 11734–11742, doi:10.1074/jbc.M709250200.
133. Tejero, J.; Santolini, J.; Stuehr, D.J. Fast ferrous heme-NO oxidation in nitric oxide synthases. *FEBS J.* **2009**, *276*, 4505–4514, doi:10.1111/j.1742-4658.2009.07157.x.
134. Haque, M.M.; Tejero, J.; Bayachou, M.; Wang, Z.-Q.; Fadlalla, M.; Stuehr, D.J. Thermodynamic characterization of five key kinetic parameters that define neuronal nitric oxide synthase catalysis. *FEBS J.* **2013**, *280*, 4439–4453, doi:10.1111/febs.12404.
135. Aoyagi, M.; Arvai, A.S.; Tainer, J.A.; Getzoff, E.D. Structural basis for endothelial nitric oxide synthase binding to calmodulin. *EMBO J.* **2003**, *22*, 766–775, doi:10.1093/emboj/cdg078.
136. Garnaud, P.E.; Koetsier, M.; Ost, T.W.B.; Daff, S. Redox Properties of the Isolated Flavin Mononucleotide- and Flavin Adenine Dinucleotide-Binding Domains of Neuronal Nitric Oxide Synthase. *Biochemistry* **2004**, *43*, 11035–11044, doi:10.1021/bi049312v.
137. Adak, S.; Sharma, M.; Meade, A.L.; Stuehr, D.J. A conserved flavin-shielding residue regulates NO synthase electron transfer and nicotinamide coenzyme specificity. *Proc. Natl. Acad. Sci. U. S. A.* **2002**, *99*, 13516–13521, doi:10.1073/pnas.192283399.
138. Li, H.; Das, A.; Sibhatu, H.; Jamal, J.; Sligar, S.G.; Poulos, T.L. Exploring the electron transfer properties of neuronal nitric-oxide synthase by reversal of the FMN redox potential. *J. Biol. Chem.* **2008**, *283*, 34762–34772, doi:10.1074/jbc.M806949200.
139. Noble, M.A.; Munro, A.W.; Rivers, S.L.; Robledo, L.; Daff, S.N.; Yellowlees, L.J.; Shimizu, T.; Sagami, I.; Guillemette, J.G.; Chapman, S.K. Potentiometric Analysis of the Flavin Cofactors of Neuronal Nitric Oxide Synthase. *Biochemistry* **1999**, *38*, 16413–16418, doi:10.1021/bi992150w.
140. Stuehr, D.J. Mammalian nitric oxide synthases. *Biochim. Biophys. Acta - Bioenerg.* **1999**, *1411*, 217–230, doi:10.1016/S0005-2728(99)00016-X.
141. Shirran, S.; Garnaud, P.; Daff, S.; McMillan, D.; Barran, P. The formation of a complex between calmodulin and neuronal nitric oxide synthase is determined by ESI-MS. *J. R. Soc. Interface* **2005**, *2*, 465–476, doi:10.1098/rsif.2005.0055.
142. Spratt, D.E.; Taiakina, V.; Guillemette, J.G. FRET analysis of Calmodulin Binding to Nitric Oxide Synthase Peptides and Enzymes. *FASEB J.* **2007**, *21*, A645–A645, doi:https://doi.org/10.1096/fasebj.21.5.A645-b.
143. Abu-Soud, H.M.; Stuehr, D.J. Nitric oxide synthases reveal a role for calmodulin in controlling electron transfer. *Proc. Natl. Acad. Sci.*

1993, *90*, 10769–10772, doi:10.1073/pnas.90.22.10769.
144. Abu-Soud, H.M.; Feldman, P.L.; Clark, P.; Stuehr, D.J. Electron transfer in the nitric-oxide synthases. Characterization of L-arginine analogs that block heme iron reduction. *J. Biol. Chem.* **1994**, *269*, 32318–32326, doi:10.1016/S0021-9258(18)31638-7.
145. Schmidt, H.H.H.W.; Smith, R.M.; Nakane, M.; Murad, F. Ca2+/Calmodulin-Dependent NO Synthase Type I: A Biopteroflavoprotein with Ca2+/Calmodulin-Independent Diaphorase and Reductase Activities. *Biochemistry* **1992**, *31*, 3243–3249, doi:10.1021/bi00127a028.
146. Fu, J.; Yamamoto, K.; Guan, Z.-W.; Kimura, S.; Iyanagi, T. Human neuronal nitric oxide synthase can catalyze one-electron reduction of adriamycin: role of flavin domain. *Arch. Biochem. Biophys.* **2004**, *427*, 180–187, doi:10.1016/j.abb.2004.04.030.
147. Garner, A.P.; Paine, M.J.I.; Rodriguez-Crespo, I.; Chinje, E.C.; Ortiz De Montellano, P.; Stratford, I.J.; Tew, D.G.; Wolf, C.R. Nitric oxide synthases catalyze the activation of redox cycling and bioreductive anticancer agents. *Cancer Res.* **1999**, *59*, 1929–34.
148. Ask, K.; Dijols, S.; Giroud, C.; Casse, L.; Frapart, Y.-M.; Sari, M.-A.; Kim, K.-S.; Stuehr, D.J.; Mansuy, D.; Camus, P.; et al. Reduction of Nilutamide by NO Synthases: Implications for the Adverse Effects of This Nitroaromatic Antiandrogen Drug. *Chem. Res. Toxicol.* **2003**, *16*, 1547–1554, doi:10.1021/tx0340910.
149. Chandor, A.; Dijols, S.; Ramassamy, B.; Frapart, Y.; Mansuy, D.; Stuehr, D.; Helsby, N.; Boucher, J.-L. Metabolic Activation of the Antitumor Drug 5-(Aziridin-1-yl)-2,4-Dinitrobenzamide (CB1954) by NO Synthases. *Chem. Res. Toxicol.* **2008**, *21*, 836–843, doi:10.1021/tx7004234.
150. Lopes, M.Â.; Meisel, A.; Carvalho, F.D.; de Lourdes Bastos, M. Neuronal Nitric Oxide Synthase is a Key Factor in Doxorubicin-Induced Toxicity to Rat-Isolated Cortical Neurons. *Neurotox. Res.* **2011**, *19*, 14–22, doi:10.1007/s12640-009-9135-9.
151. Miller, R.T. Dinitrobenzene-Mediated Production of Peroxynitrite by Neuronal Nitric Oxide Synthase. *Chem. Res. Toxicol.* **2002**, *15*, 927–934, doi:10.1021/tx020016y.
152. Resende, F.F.B.; Titze-De-Almeida, S.S.; Titze-De-Almeida, R. Function of neuronal nitric oxide synthase enzyme in temozolomide-induced damage of astrocytic tumor cells. *Oncol. Lett.* **2018**, *15*, 4891–4899, doi:10.3892/ol.2018.7917.
153. Wang, J.; Guise, C.P.; Dachs, G.U.; Phung, Y.; Hsu, A. (Huai-L.; Lambie, N.K.; Patterson, A. V.; Wilson, W.R. Identification of one-electron reductases that activate both the hypoxia prodrug SN30000 and diagnostic probe EF5. *Biochem. Pharmacol.* **2014**, *91*, 436–446, doi:10.1016/j.bcp.2014.08.003.
154. Kumagai, Y.; Nakajima, H.; Midorikawa, K.; Homma-Takeda, S.;

Shimojo, N. Inhibition of Nitric Oxide Formation by Neuronal Nitric Oxide Synthase by Quinones: Nitric Oxide Synthase as a Quinone Reductase. *Chem. Res. Toxicol.* **1998**, *11*, 608–613, doi:10.1021/tx970119u.

155. Voegtle, H.L.; Sono, M.; Adak, S.; Pond, A.E.; Tomita, T.; Perera, R.; Goodin, D.B.; Ikeda-Saito, M.; Stuehr, D.J.; Dawson, J.H. Spectroscopic Characterization of Five- and Six-Coordinate Ferrous−NO Heme Complexes. Evidence for Heme Fe−Proximal Cysteinate Bond Cleavage in the Ferrous−NO Adducts of the Trp-409Tyr/Phe Proximal Environment Mutants of Neuronal Nitric Oxide Synthase. *Biochemistry* **2003**, *42*, 2475–2484, doi:10.1021/bi0271502.
156. Sievers, F.; Wilm, A.; Dineen, D.; Gibson, T.J.; Karplus, K.; Li, W.; Lopez, R.; McWilliam, H.; Remmert, M.; Söding, J.; et al. Fast, scalable generation of high-quality protein multiple sequence alignments using Clustal Omega. *Mol. Syst. Biol.* **2011**, *7*, 539, doi:10.1038/msb.2011.75.
157. Madeira, F.; Pearce, M.; Tivey, A.R.N.; Basutkar, P.; Lee, J.; Edbali, O.; Madhusoodanan, N.; Kolesnikov, A.; Lopez, R. Search and sequence analysis tools services from EMBL-EBI in 2022. *Nucleic Acids Res.* **2022**, 1–4, doi:10.1093/nar/gkac240.
158. Hay, M.P.; Gamage, S.A.; Kovacs, M.S.; Pruijn, F.B.; Anderson, R.F.; Patterson, A. V.; Wilson, W.R.; Brown, J.M.; Denny, W.A. Structure-activity relationships of 1,2,4-benzotriazine 1,4-dioxides as hypoxia-selective analogues of tirapazamine. *J. Med. Chem.* **2003**, *46*, 169–82, doi:10.1021/jm020367+.
159. Breccia, A.; Busi, F.; Gattavecchia, E.; Tamba, M. Reactivity of nitro-thiophene derivatives with electron and oxygen radicals studied by pulse radiolysis and polarographic techniques. *Radiat. Environ. Biophys.* **1990**, *29*, 153–160, doi:10.1007/BF01210519.
160. Monge, A.; Martinez-Crespo, F.J.; Lopez de Cerain, A.; Palop, J.A.; Narro, S.; Senador, V.; Marin, A.; Sainz, Y.; Gonzalez, M. Hypoxia-Selective Agents Derived from 2-Quinoxalinecarbonitrile 1,4-Di-N-oxides. 2. *J. Med. Chem.* **1995**, *38*, 4488–4494, doi:10.1021/jm00022a014.
161. Boyd, M.; Hay, M.P.; Boyd, P.D.W. Complete 1H,13C and15N NMR assignment of tirapazamine and related 1,2,4-benzotriazineN-oxides. *Magn. Reson. Chem.* **2006**, *44*, 948–954, doi:10.1002/mrc.1886.
162. Cichocki, B.A.; Donzel, M.; Heimsch, K.C.; Lesanavičius, M.; Feng, L.; Montagut, E.J.; Becker, K.; Aliverti, A.; Elhabiri, M.; Čėnas, N.; et al. Plasmodium falciparum Ferredoxin-NADP + Reductase-Catalyzed Redox Cycling of Plasmodione Generates Both Predicted Key Drug Metabolites: Implication for Antimalarial Drug Development. *ACS Infect. Dis.* **2021**, *7*, 1996–2012, doi:10.1021/acsinfecdis.1c00054.
163. Anusevičius, Ž.; Šarlauskas, J.; Nivinskas, H.; Segura-Aguilar, J.; Čėnas, N. DT-diaphorase catalyzes N-denitration and redox cycling of

tetryl. *FEBS Lett.* **1998**, *436*, 144–148, doi:10.1016/S0014-5793(98)01115-6.
164. Kaplan, N.O.; Ciotti, M.M. Chemistry and properties of the 3-acetylpyridine analogue of diphosphopyridine nucleotide. *J. Biol. Chem.* **1956**, *221*, 823–832, doi:10.1016/S0021-9258(18)65196-8.
165. Iyanagi, T.; Yamazaki, I. One-electron-transfer reactions in biochemical systems V. Difference in the mechanism of quinone reduction by the NADH dehydrogenase and the NAD(P)H dehydrogenase (DT-diaphorase). *Biochim. Biophys. Acta - Bioenerg.* **1970**, *216*, 282–294, doi:10.1016/0005-2728(70)90220-3.
166. Chance, B. A simple relationship for a calculation of the "on" velocity constant in enzyme reactions. *Arch. Biochem. Biophys.* **1957**, *71*, 130–136, doi:10.1016/0003-9861(57)90015-2.
167. Marozienė, A.; Nemeikaitė-Čėnienė, A.; Čėnas, N. Studies of quinone cytotoxicity mechanisms: determination of quinone/semiquinone redox couple potential according to quinone-mediated ascorbate oxidation kinetics. *Chemija* **2011**, *22*, 162–166.
168. Massey, V.; Hemmerich, P. A photochemical procedure for reduction of oxidation-reduction proteins employing deazariboflavin as catalyst. *J. Biol. Chem.* **1977**, *252*, 5612–5614, doi:10.1016/S0021-9258(17)40065-2.
169. Edmondson, D.E.; Tollin, G. Semiquinone formation in flavo- and metalloflavoproteins. In *Topics in current chemistry*; Springer: Berlin, Heidelberg, 1983; Vol. 108, pp. 109–138.
170. Mayhew, S.G. The effects of pH and semiquinone formation on the oxidation-reduction potentials of flavin mononucleotide. A reappraisal. *Eur. J. Biochem.* **1999**, *265*, 698–702, doi:10.1046/j.1432-1327.1999.00767.x.
171. Sidorov, P.; Desta, I.; Chessé, M.; Horvath, D.; Marcou, G.; Varnek, A.; Davioud-Charvet, E.; Elhabiri, M. Redox Polypharmacology as an Emerging Strategy to Combat Malarial Parasites. *ChemMedChem* **2016**, *11*, 1339–1351, doi:10.1002/cmdc.201600009.
172. Laure, J.; Lanfranchi, D.A.; Davioud-Charvet, E.; Elhabiri, M. A Physico-Biochemical Study on Potential Redox-Cyclers as Antimalarial and Antischistosomal Drugs. *Curr. Pharm. Des.* **2012**, 3539–3566, doi:10.2174/138161212801327284.
173. Salmon-Chemin, L.; Buisine, E.; Yardley, V.; Kohler, S.; Debreu, M.-A.; Landry, V.; Sergheraert, C.; Croft, S.L.; Krauth-Siegel, R.L.; Davioud-Charvet, E. 2- and 3-Substituted 1,4-Naphthoquinone Derivatives as Subversive Substrates of Trypanothione Reductase and Lipoamide Dehydrogenase from Trypanosoma c ruzi : Synthesis and Correlation between Redox Cycling Activities and in Vitro Cytotoxicity. *J. Med. Chem.* **2001**, *44*, 548–565, doi:10.1021/jm001079l.
174. Bauer, H.; Fritz-Wolf, K.; Winzer, A.; Kühner, S.; Little, S.; Yardley,

V.; Vezin, H.; Palfey, B.; Schirmer, R.H.; Davioud-Charvet, E. A Fluoro Analogue of the Menadione Derivative 6-[2‘-(3‘-Methyl)-1‘,4‘-naphthoquinolyl]hexanoic Acid Is a Suicide Substrate of Glutathione Reductase. Crystal Structure of the Alkylated Human Enzyme. *J. Am. Chem. Soc.* **2006**, *128*, 10784–10794, doi:10.1021/ja061155v.

175. Bielitza, M.; Belorgey, D.; Ehrhardt, K.; Johann, L.; Lanfranchi, D.A.; Gallo, V.; Schwarzer, E.; Mohring, F.; Jortzik, E.; Williams, D.L.; et al. Antimalarial NADPH-Consuming Redox-Cyclers As Superior Glucose-6-Phosphate Dehydrogenase Deficiency Copycats. *Antioxid. Redox Signal.* **2015**, *22*, 1337–1351, doi:10.1089/ars.2014.6047.
176. Hansch, C.; Leo, A.; Taft, R.W. A survey of Hammett substituent constants and resonance and field parameters. *Chem. Rev.* **1991**, *91*, 165–195, doi:10.1021/cr00002a004.
177. Butler, J.; Hoey, B.M. The apparent inhibition of superoxide dismutase activity by quinones. *J. Free Radic. Biol. Med.* **1986**, *2*, 77–81, doi:10.1016/0748-5514(86)90127-3.
178. Crobu, D.; Canevari, G.; Milani, M.; Pandini, V.; Vanoni, M.A.; Bolognesi, M.; Zanetti, G.; Aliverti, A. Plasmodium falciparum Ferredoxin-NADP + Reductase His286 Plays a Dual Role in NADP(H) Binding and Catalysis. *Biochemistry* **2009**, *48*, 9525–9533, doi:10.1021/bi9013209.
179. Baroni, S.; Pandini, V.; Vanoni, M.A.; Aliverti, A. A Single Tyrosine Hydroxyl Group Almost Entirely Controls the NADPH Specificity of Plasmodium falciparum Ferredoxin-NADP + Reductase. *Biochemistry* **2012**, *51*, 3819–3826, doi:10.1021/bi300078p.
180. Kimata-Ariga, Y.; Saitoh, T.; Ikegami, T.; Horii, T.; Hase, T. Molecular Interaction of Ferredoxin and Ferredoxin-NADP+ Reductase from Human Malaria Parasite. *J. Biochem.* **2007**, *142*, 715–720, doi:10.1093/jb/mvm184.
181. Kimata-Ariga, Y.; Yuasa, S.; Saitoh, T.; Fukuyama, H.; Hase, T. Plasmodium-specific basic amino acid residues important for the interaction with ferredoxin on the surface of ferredoxin-NADP+ reductase. *J. Biochem.* **2018**, *164*, 231–237, doi:10.1093/jb/mvy045.
182. O’Brien, P.J. Molecular mechanisms of quinone cytotoxicity. *Chem. Biol. Interact.* **1991**, *80*, 1–41, doi:10.1016/0009-2797(91)90029-7.
183. Tejero, J.; Peregrina, J.R.; Martínez-Júlvez, M.; Gutiérrez, A.; Gómez-Moreno, C.; Scrutton, N.S.; Medina, M. Catalytic mechanism of hydride transfer between NADP+/H and ferredoxin-NADP+ reductase from Anabaena PCC 7119. *Arch. Biochem. Biophys.* **2007**, *459*, 79–90, doi:10.1016/j.abb.2006.10.023.
184. Kitagawa, T.; Sakamoto, H.; Sugiyama, T.; Yamano, T. Formation of the semiquinone form in the anaerobic reduction of adrenodoxin reductase by NADPH. Resonance Raman, EPR, and optical spectroscopic evidence. *J. Biol. Chem.* **1982**, *257*, 12075–12080,

doi:10.1016/S0021-9258(18)33680-9.
185. Sakamoto, H.; Ohta, M.; Miura, R.; Sugiyama, T.; Yamano, T.; Miyake, Y. Studies on the Reaction Mechanism of NADPH-Adrenodoxin Reductase with NADPH1. *J. Biochem.* **1982**, *92*, 1941–1950, doi:10.1093/oxfordjournals.jbchem.a134125.
186. Valiauga, B.; Williams, E.M.; Ackerley, D.F.; Čėnas, N. Reduction of quinones and nitroaromatic compounds by Escherichia coli nitroreductase A (NfsA): Characterization of kinetics and substrate specificity. *Arch. Biochem. Biophys.* **2017**, *614*, 14–22, doi:10.1016/j.abb.2016.12.005.
187. Corrado, M.E.; Aliverti, A.; Zanetti, G.; Mayhew, S.G. Analysis of the Oxidation-Reduction Potentials of Recombinant Ferredoxin-NADP+ Reductase from Spinach Chloroplasts. *Eur. J. Biochem.* **1996**, *239*, 662–667, doi:10.1111/j.1432-1033.1996.0662u.x.
188. Kimata-Ariga, Y.; Kurisu, G.; Kusunoki, M.; Aoki, S.; Sato, D.; Kobayashi, T.; Kita, K.; Horii, T.; Hase, T. Cloning and Characterization of Ferredoxin and Ferredoxin-NADP+ Reductase from Human Malaria Parasite. *J. Biochem.* **2007**, *141*, 421–428, doi:10.1093/jb/mvm046.
189. Šarlauskas, J.; Nivinskas, H.; Anusevičius, Ž.; Misevičienė, L.; Marozienė, A.; Čėnas, N. Estimation of single-electron reduction potentials (E17) of nitroaromatic compounds according to the kinetics of their single-electron reduction by flavoenzymes. *Chemija* **2006**, *17*, 31–37.
190. Guissani, A.; Henry, Y.; Lougmani, N.; Hickel, B. Kinetic studies of four types of nitroheterocyclic radicals by pulse radiolysis. *Free Radic. Biol. Med.* **1990**, *8*, 173–189, doi:10.1016/0891-5849(90)90090-6.
191. Anderson, R.F.; Yadav, P.; Shinde, S.S.; Hong, C.R.; Pullen, S.M.; Reynisson, J.; Wilson, W.R.; Hay, M.P. Radical Chemistry and Cytotoxicity of Bioreductive 3-Substituted Quinoxaline Di- N - Oxides. *Chem. Res. Toxicol.* **2016**, *29*, 1310–1324, doi:10.1021/acs.chemrestox.6b00133.
192. Faro, M.; Gómez-Moreno, C.; Stankovich, M.; Medina, M. Role of critical charged residues in reduction potential modulation of ferredoxin-NADP + reductase. *Eur. J. Biochem.* **2002**, *269*, 2656–2661, doi:10.1046/j.1432-1033.2002.02925.x.
193. Aliverti, A.; Deng, Z.; Ravasi, D.; Piubelli, L.; Karplus, P.A.; Zanetti, G. Probing the Function of the Invariant Glutamyl Residue 312 in Spinach Ferredoxin-NADP+ Reductase. *J. Biol. Chem.* **1998**, *273*, 34008–34015, doi:10.1074/jbc.273.51.34008.
194. Swenson, R.P.; Krey, G.D. Site-Directed Mutagenesis of Tyrosine-98 in the Flavodoxin from Desulfovibrio vulgaris (Hildenborough): Regulation of Oxidation-Reduction Properties of the Bound FMN Cofactor by Aromatic, Solvent, and Electrostatic Interactions. *Biochemistry* **1994**, *33*, 8505–8514, doi:10.1021/bi00194a015.

195. Bradley, L.H.; Swenson, R.P. Role of hydrogen bonding interactions to N(3)H of the flavin mononucleotide cofactor in the modulation of the redox potentials of the Clostridium beijerinckii flavodoxin. *Biochemistry* **2001**, *40*, 8686–8695, doi:10.1021/bi010571j.
196. Ziegler, G.A.; Vonrhein, C.; Hanukoglu, I.; Schulz, G.E. The Structure of Adrenodoxin Reductase of Mitochondrial P 450 Systems: Electron Transfer for Steroid Biosynthesis. *J. Mol. Biol.* **1999**, *289*, 981–990, doi:10.1006/jmbi.1999.2807.
197. Kumagai, Y.; Kikushima, M.; Nakai, Y.; Shimojo, N.; Kunimoto, M. Neuronal nitric oxide synthase (NNOS) catalyzes one-electron reduction of 2,4,6-trinitrotoluene, resulting in decreased nitric oxide production and increased nNOS gene expression: implication for oxidative stress. *Free Radic. Biol. Med.* **2004**, *37*, 350–357, doi:10.1016/j.freeradbiomed.2004.04.023.
198. Wolthers, K.R.; Schimerlik, M.I. Reaction of Neuronal Nitric-Oxide Synthase with 2,6-Dichloroindolphenol and Cytochrome c 3+ : Influence of the Electron Acceptor and Binding of Ca 2+ -Activated Calmodulin on the Kinetic Mechanism. *Biochemistry* **2001**, *40*, 4722–4737, doi:10.1021/bi0023495.
199. Nishimura, J.S.; Narayanasami, R.; Miller, R.T.; Roman, L.J.; Panda, S.; Masters, B.S.S. The Stimulatory Effects of Hofmeister Ions on the Activities of Neuronal Nitric-oxide Synthase. *J. Biol. Chem.* **1999**, *274*, 5399–5406, doi:10.1074/jbc.274.9.5399.
200. Panda, K.; Haque, M.M.; Garcin-Hosfield, E.D.; Durra, D.; Getzoff, E.D.; Stuehr, D.J. Surface Charge Interactions of the FMN Module Govern Catalysis by Nitric-oxide Synthase. *J. Biol. Chem.* **2006**, *281*, 36819–36827, doi:10.1074/jbc.M606129200.
201. Welland, A.; Garnaud, P.E.; Kitamura, M.; Miles, C.S.; Daff, S. Importance of the Domain−Domain Interface to the Catalytic Action of the NO Synthase Reductase Domain. *Biochemistry* **2008**, *47*, 9771–9780, doi:10.1021/bi800787m.
202. Welland, A.; Daff, S. Conformation-dependent hydride transfer in neuronal nitric oxide synthase reductase domain. *FEBS J.* **2010**, *277*, 3833–3834, doi:10.1111/j.1742-4658.2010.07787.x.
203. Haque, M.M.; Tejero, J.; Bayachou, M.; Kenney, C.T.; Stuehr, D.J. A cross-domain charge interaction governs the activity of NO synthase. *J. Biol. Chem.* **2018**, *293*, 4545–4554, doi:10.1074/jbc.RA117.000635.
204. Craig, D.H.; Chapman, S.K.; Daff, S. Calmodulin Activates Electron Transfer through Neuronal Nitric-oxide Synthase Reductase Domain by Releasing an NADPH-dependent Conformational Lock. *J. Biol. Chem.* **2002**, *277*, 33987–33994, doi:10.1074/jbc.M203118200.
205. Miller, R.T.; Martásek, P.; Omura, T.; Siler Masters, B.S. Rapid Kinetic Studies of Electron Transfer in the Three Isoforms of Nitric Oxide Synthase. *Biochem. Biophys. Res. Commun.* **1999**, *265*, 184–188, doi:10.1006/bbrc.1999.1643.

206. Leferink, N.G.H.; Hay, S.; Rigby, S.E.J.; Scrutton, N.S. Towards the free energy landscape for catalysis in mammalian nitric oxide synthases. *FEBS J.* **2015**, *282*, 3016–3029, doi:10.1111/febs.13171.
207. Dunford, A.J.; Rigby, S.E.J.; Hay, S.; Munro, A.W.; Scrutton, N.S. Conformational and Thermodynamic Control of Electron Transfer in Neuronal Nitric Oxide Synthase. *Biochemistry* **2007**, *46*, 5018–5029, doi:10.1021/bi7001339.
208. Moussaoui, M.; Misevičienė, L.; Anusevičius, Ž.; Marozienė, A.; Lederer, F.; Baciou, L.; Čėnas, N. Quinones and nitroaromatic compounds as subversive substrates of Staphylococcus aureus flavohemoglobin. *Free Radic. Biol. Med.* **2018**, *123*, 107–115, doi:10.1016/j.freeradbiomed.2018.05.071.
209. Nishida, C.R.; Ortiz de Montellano, P.R. Reductive Heme-Dependent Activation of the N -Oxide Prodrug AQ4N by Nitric Oxide Synthase. *J. Med. Chem.* **2008**, *51*, 5118–5120, doi:10.1021/jm800496s.
210. Lavaggi, M.L.; Cabrera, M.; González, M.; Cerecetto, H. Differential Enzymatic Reductions Governing the Differential Hypoxia-Selective Cytotoxicities of Phenazine 5,10-Dioxides. *Chem. Res. Toxicol.* **2008**, *21*, 1900–1906, doi:10.1021/tx800199v.
211. Pochapsky, T.C.; Wong, N.; Zhuang, Y.; Futcher, J.; Pandelia, M.-E.; Teitz, D.R.; Colthart, A.M. NADH reduction of nitroaromatics as a probe for residual ferric form high-spin in a cytochrome P450. *Biochim. Biophys. Acta - Proteins Proteomics* **2018**, *1866*, 126–133, doi:10.1016/j.bbapap.2017.04.003.
212. Mauk, A.G.; Scott, R.A.; Gray, H.B. Distances of electron transfer to and from metalloprotein redox sites in reactions with inorganic complexes. *J. Am. Chem. Soc.* **1980**, *102*, 4360–4363, doi:10.1021/ja00533a012.
213. Xia, C.; Misra, I.; Iyanagi, T.; Kim, J.J.P. Regulation of interdomain interactions by calmodulin in inducible nitric-oxide synthase. *J. Biol. Chem.* **2009**, *284*, 30708–30717, doi:10.1074/jbc.M109.031682.
214. Hurley, J.K.; Morales, R.; Martínez-Júlvez, M.; Brodie, T.B.; Medina, M.; Gómez-Moreno, C.; Tollin, G. Structure–function relationships in Anabaena ferredoxin/ferredoxin:NADP+ reductase electron transfer: insights from site-directed mutagenesis, transient absorption spectroscopy and X-ray crystallography. *Biochim. Biophys. Acta - Bioenerg.* **2002**, *1554*, 5–21, doi:10.1016/S0005-2728(02)00188-3.
215. Pladziewicz, J.R.; Carney, M.J. Reduction of ferricenium ion by horse heart ferrocytochrome c. *J. Am. Chem. Soc.* **1982**, *104*, 3544–3545, doi:10.1021/ja00376a068.
216. He, Y.; Haque, M.M.; Stuehr, D.J.; Lu, H.P. Single-molecule spectroscopy reveals how calmodulin activates NO synthase by controlling its conformational fluctuation dynamics. *Proc. Natl. Acad. Sci.* **2015**, *112*, 11835–11840, doi:10.1073/pnas.1508829112.
217. Campbell, M.G.; Smith, B.C.; Potter, C.S.; Carragher, B.; Marletta,

M.A. Molecular architecture of mammalian nitric oxide synthases. *Proc. Natl. Acad. Sci.* **2014**, *111*, E3614–E3623, doi:10.1073/pnas.1413763111.

218. Gao, Y.T.; Smith, S.M.E.; Weinberg, J.B.; Montgomery, H.J.; Newman, E.; Guillemette, J.G.; Ghosh, D.K.; Roman, L.J.; Martasek, P.; Salerno, J.C. Thermodynamics of Oxidation-Reduction Reactions in Mammalian Nitric-oxide Synthase Isoforms. *J. Biol. Chem.* **2004**, *279*, 18759–18766, doi:10.1074/jbc.M308936200.

SANTRAUKA

Flavininiai fermentai sudaro apie 3% visų fermentų, jie aptinkami visų grupių organizmuose ir pasižymi itin didele funkcijų gausa: redukcijos ekvivalentų pernaša fotosintezėje, DNR reparacija, aplinkos taršalų ir ksenobiotikų detoksifikacija, apoptozė, ląstelių signalai ir kt. Fermentų sudėtyje esantis flavinas yra flavino mononukleotido (FMN) arba flavino adenino dinukleotido (FAD) pavidalo, paprastai jungiasi nekovalentiškai.

Dažnu atveju flavininiai fermentai yra susiję su oksidacijos – redukcijos reakcijomis, kurių metu jie funkcionuoja pernešdami elektronus į tolimesnius taikinius. Tokių fermentų sudėtyje esančius flavinus oksiduoja ne tik jų gamtiniai elektronų akceptoriai, bet ir įvairūs nefiziologiniai elektronų akceptoriai, tokie kaip aplinką teršiantys nitroaromatiniai junginiai ar ksenobiotiniai chinonai. Taip pat itin svarbu paminėti tai, kad flavino prostetinė grupė geba transformuoti tarp vienelektroninės ir dvielektroninės redukcijos.

Prooksidantiniai ksenobiotikai – medžiagos, randamos organizme, tačiau paprastai organizmo negaminamos – dehidrogenazių – elektrontransferazių gali būti redukuojamos. Šių žemo potencialo oksidatorių redukcijos metu susidaro radikalų anijonai, kuriuos futilinio redokso ciklo metu reoksiduoja aplinkos deguonis, kas ir lemia jų citotoksiškumą oksidacinio streso pagrindu.

Šiame darbe buvo tirti trys dehidrogenazėms – elektrontransferazėms priskiriami fermentai, priklausantys dviems skirtingoms grupėms: Fe-S baltymų reduktazėms (*Pf*FNR, *Rp*FNR) ir hemo baltymų reduktazėms (nNOS). Jų reakcijos su nefiziologiniais oksidatoriais ir ksenobiotikais yra čia pristatomų mechanistinių tyrimų, kurių rezultatais remiantis daromos išvados apie fermentinės ksenobiotikų redukcijos mechanizmus bei specifines kiekvieno fermento savybes, pagrindas.

Tikslas ir uždaviniai

Pagrindinis darbo tikslas yra dviejų tipų dehidrogenazių – elektrontransferazių (Fe-S baltymų reduktazių (*Pf*FNR ir *Rp*FNR) ir hemo baltymų reduktazių (nNOS)) katalizuojamos elektronų pernašos mechanizmų charakterizavimas bei šios vienelektroninės redukcijos įvertinimas ir palyginimas tarp fermentų.

Tikslui pasiekti iškelti šie uždaviniai:

1. *Pf*FNR ir *Rp*FNR katalizuojamos ksenobiotikų redukcijos tyrimas ir šių fermentų atliekamos katalizės palyginimas su gerai ištirta *An*FNR ir *So*FNR katalizuojama redukcija;

2. Naujo, į tioredoksino reduktazę panašių, tipo *Rp*FNR redokso savybių charakterizavimas, ypatingą dėmesį skiriant semichinonui;
3. nNOS katalizuojamos ksenobiotikų redukcijos tyrimas, ypatingą dėmesį skiriant kalmodulino vaidmeniui bei galimam hemo vaidmeniui;
4. Dehidrogenazių – elektrontransferazių katalizuojamos vienelektroninės ksenobiotikų redukcijos reakcijų greičio konstantų panaudojimas apytiksliam jų vienelektroninės redukcijos potencialų ir elektronų pernašos atstumų šiose reakcijose įvertinimas.

Darbo svarba ir mokslinis naujumas

1. Parodyta, kad nNOS aktyvumas ksenobiotikų bioaktyvacijoje gali būti panašus į P-450R. Pirmą kartą parodyta, kad nNOS hemas (Fe^{2+}-NO kompleksas) gali turėti vaidmenį oksidatorių redukcijos procese;
2. Elektronų pernašos atstumai, apskaičiuoti pagal išorinės sferos elektronų pernašos modelį, yra artimi anksčiau paskelbtoms homologiškų fermentų elektronų pernašos vertėms;
3. Parodyta, kad dehidrogenazės – elektrontransferazės gali būti pasitelkiamos norint apytiksliai nustatyti $ArNO_2$ ir ArN→O vienelektroninės redukcijos potencialus, o apskaičiuotos potencialų vertės skiriasi ne daugiau nei 30 mV nuo išmatuotųjų;
4. *Plasmodium falciparum* apikoplastuose lokalizuota *Pf*FNR yra potencialus naujų antimaliarinių vaistų taikinys. Darbe pateikiami rezultatai suteikia įžvalgų į prooksidantinių ksenobiotikų, kurie gali būti laikomi kaip oksidacinį stresą pirmuoniui sukeliantys vienelektroninės redukcijos metu, redukcijos mechanizmus;
5. Modelinio *Rhodopseudomonas palustris* TrxR tipo *Rp*FNR katalizuojamų redokso reakcijų detalus tyrimas ir kiekybinė gautų rezultatų analizė leido nustatyti redokso potencialus ir semichinono stabilizaciją, o gautos vertės yra panašios į plastidinių *So*FNR ir *An*FNR atitinkamas vertes.

Ginamieji teiginiai

1. Dehidrogenazės – elektrontransferazės redukuoja chinonus, nitroaromatinius junginius ir aromatinius *N*-oksidus *ping-pong* mechanizmu. Visais atvejais oksidatorių reaktyvumas (log k_{cat}/K_m) didėja didėjant vienelektroninės redukcijos potencialui (E_7^1). Nitroaromatinių junginių reaktyvumas yra sistemingai žemesnis, nei chinonų ar aromatinių *N*-oksidų su analogiškais vienelektroninės redukcijos potencialais. Greitį limituojanti stadija yra oksidacinė pusiau-reakcija;

2. Šios fermentinės reakcijos neprieštarauja išorinės sferos elektronų pernašos modeliui, o reaktyvumas gali būti pasitelkiamas skaičiuojant apytikslius elektronų pernašos atstumus;
3. Kai kurių klasių oksidatorių nuostoviosios stadijos greičio konstantos gali būti naudojamos apytiksliam jų vienelektroninės redukcijos potencialų įvertinimui.

Medžiagos ir metodai

Darbe naudoti fermentai feredoksino:NADP+ oksidoreduktazės, išskirtos iš *Plasmodium falciparum* (*Pf*FNR, išskirta dr. A. Aliverti (Italija)) ir *Rhodopseudomonas palustris* (*Rp*FNR, išskirta dr. D. Seo (Japonija)), bei neuroninė NO sintazė, išskirta iš žiurkių (nNOS, išskirta dr. J.-L. Boucher (Prancūzija)). Darbe naudotos medžiagos įsigytos iš Sigma-Aldrich arba susintetintos dr. J. Šarlausko, dr. V. Miškinienės arba dr. E. Davioud-Charvet (Prancūzija) grupės.

Stacionariosios stadijos kinetiniai tyrimai atlikti spektrofotometriškai, reakcijų parametrai k_{cat} ir k_{cat}/K_m esant fiksuotai NADPH koncentracijai gauti po duomenų glaudinimo parabolės lygtimi, jie atitinka susikirtimo su y ašimi tašką ir nuolydį Lineweaver – Burk koordinatėse. Fermentinė NADPH oksidacija terpėje esant elektronų akcceptoriaus vertinta pagal $\Delta\varepsilon_{340}$ = 6.2 $mM^{-1}cm^{-1}$. Gautos greičių vertės koreguotos atsižvelgiant į oksidazinį fermentų aktyvumą.

Nestacionariosios stadijos kinetiniai tyrimai atlikti sustabdytos srovės metodu aerobinėmis sąlygomis, matavimus atliekant 460 – 800 nm bangos ilgio intervale.

Deguonies suvartojimo tyrimai atlikti naudojant Klarko elektrodą matuojant deguonies redukcijos srovę.

Fotoredukcijos tyrimai atlikti anaerobinėmis sąlygomis, fotosensitizatoriais naudoti 5-deaza-FMN ir EDTA. Fotoredukcija atlikta trumpais intervalais apšviečiant reakcijos mišinį šviesos šaltiniu naudojant kaitrinę lempą.

Rezultatai ir jų aptarimas

Stacionariosios stadijos kinetikos tyrimų metu varijuojant juglono – itin aktyvaus nefiziologinio elektronų akceptoriaus – koncentraciją gauta eilė lygiagrečių tiesių rodo dehidrogenazėms – elektrontransferazėms būdingą *ping-pong* mechanizmą, kitaip sakant, oksidacinė ir redukcinė pusiau-reakcijos vyksta nepriklausomai viena nuo kitos. Remiantis ankstesniais

tyrimais, kur parodytas vienelektroninis chinonreduktazinis *Pf*FNR aktyvumas, buvo tiriama, ar tai galioja ir nitroaromatiniams junginiams bei aromatiniams *N*-oksidams. Vienelektroninė nitroaromatinių junginių redukcija parodyta į terpę pridėjus citochromo *c*, kurio fermentas tiesiogiai redukuoti negali. Esant terpėje nitroaromatinio junginio, citochromo *c* redukcijos greitis siekė 140 – 195% NADPH oksidacijos greičio, o superoksiddismutazė slopino citochromo *c* redukciją 15 – 25%. Paraleliai atliekant deguonies suvartojimo ir spektrinių pokyčių $ArNO_2$ redukcijos metu tyrimus stebėtas redoksciklinimas, o *Pf*FNR katalizuojamas stabilių reakcijos produktų susidarymas prasideda, kai $[O_2]$ = 40 – 50 μM. ArN→O atveju, naudojant TPZ ir jo darinius, NADPH oksidacija vyko lygiagrečiai su O_2 sunaudojimu. Cyt *c* redukcijos greitis siekia 180 – 190% NADPH oksidacijos greičio, o SOD slopinimas siekia 40 – 65%: $1e^-$ srautas ArN→O atveju yra 90 – 95%.

Substratinis *Pf*FNR specifiškumas vertintas tiriant trijų grupių (Q, $ArNO_2$ ir ArN→O) žemo potencialo elektronų akceptorių redukciją. Struktūrinis specifiškumas nestebėtas, kita vertus, matoma katalitinio efektyvumo konstantos (k_{cat}/K_m) logaritmo priklausomybė nuo vienelektroninės redukcijos potencialo. $ArNO_2$ atveju stebima tiesinė priklausomybė, o Q ir ArN→O formuoja bendrą „seriją“, kuriai būdinga parabolinė priklausomybė. Matomas reaktyvumo skirtumas aiškintinas elektronų savimainų konstantų skirtumais: chinonų ir aromatinių *N*-oksidų atveju jos siekia $\approx 10^8$ $M^{-1}s^{-1}$, tuo tarpu nitroaromatinių junginių atveju šios konstantos yra $\approx 10^6$ $M^{-1}s^{-1}$.

Plazmodionas (PD) ir jo dariniai pasižymi antimaliariniu aktyvumu, kuris, kaip manoma, kyla iš bioredukcinę aktyvaciją sukeliančio redoksciklinimo. Modelinių chinonų atveju egzistuoja priklausomybė tarp reaktyvumo ir $1e^-$ redukcijos potencialo, tačiau PD darinių atveju šie potencialai nėra žinomi, o dėl prasto junginių tirpumo negalima naudoti įprastai tokiais atvejais pasitelkiamos pulsinės radiolizės. Šių junginių potencialiai buvo apytiksliai nustatyti matuojant O_2 suvartojimo greitį oksiduojant askorbatą, kai terpėje yra chinono. Atlikus stacionariosios kinetikos tyrimus nustatytas PD ir jo darinių reaktyvumas buvo aukštesnis, nei analogiško E_7^1 modelinių chinonų; $1e^-$ srautas siekė 75 – 95%, o didėjant potencialui mažėjo jautrumas SOD slopinimui.

Slopinimo tyrimų metu tirta transhidrogenazinė reakcija: NADPH redukuojant 3-AcADP molekulę stebimas konkurentinis slopinimas atsiranda dėl to, kad 3-AcADP užima piridino nukleotido jungimosi vietą redukuotoje fermento formoje. Slopinimas reakcijos produktu $NADP^+$ yra dvejopas. NADPH atžvilgiu stebimas konkurentinis slopinimas, o juglono atžvilgiu

stebimas bekonkurentinis slopinimas. Iš to seka, kad, pirma, 3-AcADP ir chinonai oksiduoja skirtingas FNR redokso formas, kurių gimiringumas NADPH yra skirtingas, ir, antra, dvejopas slopinimas rodo specifinį *ping pong* atvejį, kai $NADP^+$ glaudžiai jungiasi su oksiduota fermento forma, tuo tarpu su $2e^-$ redukuota forma jungiasi silpnai arba nesijungia apskritai. Taigi kaip ir FNR, išskirtų iš špinatų ar *Anabaena*, atveju, greitį riboja FADH semichinono oksidacija.

Fiziologinis FNR oksidatorius yra feredoksinas (Fd), o gimiringumas tarp FNR ir Fd mažėja didėjant joninei tirpalo jėgai, kadangi Fd paviršiuje gausu neigiamai įkrautų aminorūgščių, o FNR paviršiuje – teigiamai įkrautų. Tyrimų metu buvo vertinta elektrostatinių sąveikų įtaka. Krūvį turinčių elektronų akceptorių atveju stebima varpo formos priklausomybė nuo joninės jėgos, ką galima paaiškinti tuo, kad oksidatoriai sąveikauja tiek su neigiamai įkrautu Glu314, tiek su teigiamai įkrautu Lys287, kuris, beje, yra šalia izoaloksazino žiedo ir dalyvauja susidarant sąveikai tarp Fd ir FNR.

Fd būdingas stimuliacinis Q ir $ArNO_2$ redukcijos efektas, matomas kaip dvifaziškumas atvirkštinėse koordinatėse. Lėtosios fazės maksimalūs greičiai yra panašūs į cyt *c* redukcijos greičius esant atitinkamai Fd koncentracijai. Kitaip sakant, tokia stimuliacija rodo, kad Fd gali būti alternatyvus nefiziologinio oksidatoriaus redukcijos kelias, šį redukuojant per redukuotą Fd, galimai dėl geriau prieinamo aktyvaus centro. Kita vertus, panaši aktyvacija stebėta ir Adx/AdxR ar *An*Fd/*An*FNR porų atveju, taigi gali būti, kad tai yra bruožas, būdingas šiai fermentui grupei.

Nestacionariosios stadijos kinetikos tyrimų metu kontroliniuose eksperimentuose be Q stebima greita FAD redukcija ir lėta reoksidacija deguonimi ties 460 nm, bet kartu stebimas ir tarpinio junginio, absorbuojančio 600 nm ilgio šviesą, susidarymas. Pridėjus chinono, reoksidacija pagreitėja apie 100 kartų, kas rodo nykstamą O_2 įtaką reoksidacijos kinetikai eksperimentinėmis sąlygomis. Laikant, kad FAD redukcija atitinka maksimalų sugerties pokytį ties 460 nm, kai terpėje nėra chinono, gautos greičių konstantos yra panašios į stacionariosios kinetikos sąlygomis gautąsias atitinkamas konstantas. Redukuoto FNR reoksidacijos limituojanti stadija ko gero yra FAD semichinono oksidacija. Stebėta produkto akumuliacija 600 nm regione. Be to, absorbcija virš 700 nm nėra būdinga FAD semichinonui, ko gero atspindi kitų tarpinių produktų, pavyzdžiui FAD•-NADP(H) komplekso susidarymą.

Nitroaromatinių junginių atveju egzistuojanti tiesinė priklausomybė gali būti pasitelkiama apytiksliai vertinant vienelektroninės redukcijos potencialą. Iš šio ir ankstesnių tyrimų metu atliktų skaičiavimų su dehidrogenazėmis –

elektrontransferazėmis matyti, jog apskaičiuoti junginių $1e^-$ redukcijos potencialai nuo išmatuotųjų skiriasi ne daugiau nei per 30 mV, taigi apskaičiuotos nežinomo potencialo junginių $1e^-$ redukcijos potencialų vertės laikytinos realistiškomis. Be to, atliktų tyrimų su nežinomo potencialo ArN→O metu taip pat parodyta, kad junginių reaktyvumą lemia ne struktūrinis specifiškumas, o elektronakceptorinės jų savybės. Kelių fermentinių sistemų log k_{cat}/K_m priklausomybių nuo E_7^1 vidurkio naudojimas leidžia apytiksliai įvertinti nežinomus potencialus.

Stacionariosios kinetikos sąlygomis atliktų tyrimų su *Rp*FNR metu gautiems rezultatams būdingos analogijos su *Pf*FNR: *ping-pong* mechanizmas rodo nepriklausomas vieną nuo kitos redukcinę ir oksidacinę pusiau-reakcijas, o substratinio specifiškumo tyrimo metu stebimas panašus „profilis“, kai Q ir ArN→O formuoja vieną „seriją“ su būdinga paraboline priklausomybe nuo redukcijos potencialo, tuo tarpu atitinkamo redukcijos potencialo $ArNO_2$ mažiau reaktyvūs, jų reaktyvumas pasižymi tiesine priklausomybe nuo potencialo. Nustatytas vienelektroninis srautas chinonų atveju siekė >50%, o nitroaromatinių junginių atveju jis buvo >90%.

Slopinimo reakcijos produktu $NADP^+$ rezultatai panašūs į *Pf*FNR tyrimuose stebėtus, tačiau juglono atžvilgiu *Rp*FNR atveju stebimas nekonkurentinis slopinimas. Slopinimo tyrimai rodo, kad dominuojantis slopinimo mechanizmas yra reakcijos produkto konkurencija su NADPH dėl jungimosi prie oksiduotos fermento formos.

Nestacionariosios kinetikos sąlygomis stebima greita FAD redukcija NADPH ties 460 nm ir lėta reoksidacija deguonimi. Tuo pat metu susidaro ir 600 nm ilgio šviesą absorbuojantis tarpinis produktas. Chinono pridėjimas į reakcijos mišinį pagreitina reoksidaciją daugiau nei viena eile. Oksidacijos greičių konstantos, gautos nestacionariosios kinetikos tyrimų metu, panašios į stacionariosios kinetikos sąlygomis gautąsias. Kadangi ir reoksidacija ties 460 nm, ir tarpinio produkto nykimas ties 600 nm vyksta tuo pačiu greičiu, $FADH^•$ oksidacija gali būti laikoma greitį limituojančia redukcijos stadija. Tarpinių produktų sugerties charakteristikos taip pat analogiškos *Pf*FNR, stebimas pradinis sugerties augimas 500 – 725 nm intervale, vėliau atsiranda ir nyksta plati sugerties juosta 600 – 700 nm intervale.

Potenciometrinės analizės metu fermento redukcijos potencialas nustatytas iš 3-AcADP^+/3-AcADPH poros. Remiantis Haldane principu ir Nernst lygtimi, jis lygus −0.276 V. Fotoredukcija buvo atliekama anaerobiozės sąlygomis. Neutralaus semichinono susidarymas stebėtas 550 – 650 nm intervale iš augančios sugerties. Apskaičiuotas stabilizavimas siekė 26.5%. Gautas *Rp*FNR redokso potencialas savo verte panašus į *Pf*FNR,

−0.280 V. Semichinono stabilizavimas panašus į *So*FNR ir *An*FNR. Nors *Rp*FNR neturi *So*FNR būdingos Ser96/Glu312 atitinkančios poros, remiantis analogijomis iš gimininginų fermentų galimi aukšto semichinono stabilumo paaiškinimai galėtų būti, pavyzdžui, π – π stekingas tarp izoaloksazino ir terminalinio Tyr328.

NO sintazė pasirinkta siekiant pratęsti mūsų skyriuje prieš dešimtmetį pradėtus tyrimus, ypatingą dėmesį skiriant kalmodulino vaidmeniui. Substratinio nNOS specifiškumo profilis su tirtais Q, $ArNO_2$ ir ArN→O atitinka stebėtą *Pf*FNR ir *Rp*FNR atveju: tiesinė reaktyvumo priklausomybė nuo E_7^1 $ArNO_2$ atveju ir parabolinė priklausomybė Q ir ArN→O atveju. Pridėjus kalmodulino, stebimas reaktyvumo išaugimas, kai kurių junginių atveju net iki šimto kartų.

Elektrostatinės sąveikos yra svarbios FMN elektronų pernašos reakcijoms tiek dėl FMN ir FAD domenų asociacijos, tiek ir dėl komplekso su hemo domenu formavimosi. Tyrimai su neutraliu durochinonu rodo didžiausią k_{cat} esant didelei joninei jėgai. CaM veikia taip, kad maksimali k_{cat} pasiekiama esant mažesnei tirpalo joninei jėgai. k_{cat}/K_m taip pat didėja didėjant joninei tirpalo jėgai, tačiau taip pat pastebėtina tai, kad joninė jėga sumažina aktyvuojantį CaM efektą. Tai, kad joninės jėgos efektas didesnis neigiamai įkrautiems elektronų akceptoriams, rodo oksidatorių sąveiką su neigiamai įkrautu FMN domenu. Kitaip sakant, tokie efektai rodo, pirma, konformacinių FMN domeno pokyčių svarbą redukcijai, ir, antra, joninės jėgos mimikrinį efektą imituojant kalmoduliną.

Slopinimo tyrimų, atliktų su reakcijos produktu $NADP^+$ ir redoks-neaktyviu 2′,5′-ADP, metu durochinono reduktazės reakcijoje stebėtas konkurentinis slopinimas NADPH atžvilgiu, kas rodo naudotų slopiklių ir NADPH jungimąsi toje pačioje vietoje prie oksiduotos fermento formos. Durochinono atžvilgiu stebėtas bekonkurentinis slopinimas.

Nestacionariosios kinetikos tyrimų metu buvo stebimi sugerties pokyčiai ties 340, 397, 436 ir 485 nm, kas leido sekti, atitinkamai, NADPH oksidaciją, hemo redukciją, Fe^{2+}-NO komplekso susidarymą ir flavinų redukciją. Pirma, po greitos flavinų redukcijos vyksta lėta reoksidacija deguonimi. Kadangi sugerties pokyčių amplitudė ties 397 nm ir 485 nm yra panaši, galima manyti esant didelio flavinų indėlio į spektrinius pokyčius. Sugerties pokyčiai ties 436 nm tokiomis sąlygomis taip pat priskirtini flavinų redukcijai, kadangi Fe^{2+}-NO komplekso susidarymo atveju tikimasi sugerties išaugimo. Tai, kad po redukcijos sugertis į pradinį lygį negrįžta, rodo stabilų vienu elektronu redukuotą FMN-FAD. Terpėje esant CaM ir tetrahidrobiopterino, stebimas reakcijos greičio išaugimas. Pridėjus durochinono, fermento reoksidacija

pagreitėja >10 kartų tiek kontrolinėmis sąlygomis, tiek ir esant CaM ir H_4B. Pridėjus arginino, matomas sugerties augimas ties 436 nm, tai rodo Fe^{2+}-NO komplekso susidarymą. Procesai vyksta dvifaziškai, o turnoverio metu 67% hemo yra Fe^{2+}-NO formos. Durochinonas tiek pagreitina reoksidaciją, tiek ir sumažina sugerties pokyčių amplitudę ties 485 nm. Paraleliai su redukuoto FAD-FMN reoksidacija, jis oksiduoja ir hemo Fe^{2+}-NO formą. Remiantis šių tyrimų metu apskaičiuotomis greičio konstantų vertėmis galima teigti, jog hemo vaidmuo redukuojant išorinius elektronų akceptorius nėra žymus, pagrindiniu elektronų donoru išlieka $FMNH_2$.

Norint apskaičiuoti elektronų pernašos atstumą *Pf*FNR katalizuojamoje reakcijoje galima taikyti išorinės sferos elektronų pernašos modelį. Elektronų pernašos atstumas metaloproteinuose su neorganiniais kompleksais priklauso nuo elektronų savimainų konstantos k_{11} vertės. Toks R_p verčių apytikslis apskaičiavimas buvo pritaikytas analizuojant vienelektroninę P-450R, FNR iš *Anabaena* ir NOS oksidaciją chinonais, nitroaromatiniais junginiais ir neorganiniais kompleksais. Flavininių baltymų atveju neatmestina galimybė, kad gautos vertės yra padidintos dėl izoaloksazino žiedo dimetilbenzeno dalies ekspozicijos tirpikliui, tad šios vertės „vidiniam“ flavininių fermentų reaktyvumui apibrėžti turėtų būti naudojamos atsargiai. 15 lentelėje (98 psl.) pateikiami palyginamieji duomenys tarp šiame darbe nustatytų elektronų pernašos atstumų ir ankstesniuose tyrimuose gautų rezultatų. *Pf*FNR ir *Rp*FNR atveju elektronų pernašos atstumai yra didesni nei P-450R ir yra panašūs į gautuosius tiriant *An*FNR, o tai rodo, kad abiejų plastidinių ferredoksinreduktazių FAD izoaloksazino žiedas yra prieinamas mažos molekulinės masės oksidatoriams nepriklausomai nuo skirtumų izoaloksazino aplinkoje.

IŠVADOS

1. *P. falciparum* ir *R. palustris* feredoksino:$NADP^+$ oksidoreduktazių katalizuojama ksenobiotikų redukcija kiekybiškai yra panaši į plastidinės FNR iš *Anabaena* katalizuojamą, o greitį ribojanti stadija yra FAD semichinono oksidacija.
2. *P. falciparum* feredoksinas padidina ksenobiotikų redukciją katalizuojant FNR suteikdamas alternatyvų kelia jų redukcijai, su jam būdinga didesne redukcijos greičio konstanta, bet mažesniu maksimaliu apsisukimų skaičiumi.
3. Pirmą kartą buvo atlikta potenciometrinė naujos, tioredoksino reduktazės tipo, *Rp*FNR analizė, nustatyti redokso potencialas ($E_7^0 = -0.276$ V) ir

santykinai aukštas semichinono stabilumą (26.5% pusiausvyros sąlygomis), kas yra panašu į kitas FNR.

4. Pirmą kartą parodytas neuroninės NO sintazės hemo Fe^{2+}-NO komplekso vaidmuo ksenobiotikų redukcijoje: šis kompleksas paima nedidelę dalį elektronų srauto išorinių elektronų akceptorių redukcijai.
5. Joninės jėgos poveikio nNOS kinetikai tyrimai rodo, kad, esant aukštai joninei jėgai, vyksta fermento konformaciniai pokyčiai, palengvinantys krūvį turinčių elektronų akceptorių priėjimą prie aktyviojo centro.
6. Parodyta, kad dehidrogenazės – elektrontransferazės gali būti naudojamos norint apytiksliai nustatyti nitroaromatinių junginių ir aromatinių *N*-oksidų vienelektroninės redukcijos potencialus.
7. Apskaičiuoti elektronų pernašos atstumai *Pf*FNR ir *Rp*FNR yra panašūs į tuos, kurie buvo apskaičiuoti *An*FNR atveju ir siekia apie 5 Å chinonų bei nitroaromatinių junginių atveju. Elektronų pernašos atstumai nNOS (~3 Å) pridėjus kalmodulino yra panašūs į citochromo P-450 reduktazės.

ACKNOWLEDGEMENTS

First and foremost, I would like to thank my supervisor Habil. Dr. Narimantas Čėnas for this journey that has started back in the last year of my Bachelor's studies. His immense experience, patience, guidance and support were invaluable for my ongoing growth as a scientist.

I would also like to extend my gratitude to everyone in the Department of xenobiotics biochemistry, both for help and support during these studies.

My gratitude goes to Profs. Florence Lederer and Elisabeth Davioud-Charvet, who I had the opportunity to work with during my short internships in France, for their advice and experience shared.

Many thanks to Profs. Alessandro Aliverti, Daisuke Seo and Jean-Luc Boucher for them supplying the enzymes that were used in this work. Many thanks to Dr. Jonas Šarlauskas for the synthesized materials. My thanks go to Prof. Saulius Klimašauskas for allowing me to use the stopped-flow apparatus in his department while ours was under repairs.

And last but not least, I would like to thank my family and friends, both for their support and encouragement when things looked bleak and being there for me in the times of need.

PUBLICATIONS

1. Šarlauskas, J.; Nemeikaitė-Čėnienė, A.; Marozienė, A.; Misevičienė, L.; **Lesanavičius, M.;** Čėnas, N. Enzymatic single-electron reduction and aerobic cytotoxicity of tirapazamine and its 1-oxide and nor-oxide metabolites. *Chemija*. **2018**, 29(4), 273-280; doi:10.6001/chemija.v29i4.3843
2. Marozienė, A.; **Lesanavičius, M.;** Davioud-Charvet, E.; Aliverti, A.; Grellier, P.; Šarlauskas, J.; Čėnas, N. Antiplasmodial activity of nitroaromatic compounds: correlation with their reduction potential and inhibitory action on *Plasmodium falciparum* glutathione reductase. *Molecules*. **2019**, 24, 4509; doi:10.3390/molecules24244509
3. Nemeikaitė-Čėnienė, A.; Šarlauskas, J.; Misevičienė, L.; Marozienė, A.; Jonušienė, V.; **Lesanavičius, M.;** Čėnas, N. Aerobic cytotoxicity of aromatic *N*-oxides: the role of NAD(P)H:quinone oxidoreductase (NQO1). *Int. J. Mol. Sci.* **2020**, 21, 8754; doi:10.3390/ijms21228754
4. **Lesanavičius, M.;** Aliverti, A.; Šarlauskas, J.; Čėnas, N. Reactions of *Plasmodium falciparum* ferredoxin:$NADP^+$ oxidoreductase with redox cycling xenobiotics: a mechanistic study. *Int. J. Mol. Sci*. **2020**, 21, 3234; doi:10.3390/ijms21093234
5. Cichocki, B.A.[1]; Donzel, M.[1]; Heimsch, K.C.[1]; **Lesanavičius, M.[1];** Feng, L.; Montagut, E.J.; Becker, K.; Aliverti, A.; Elhabiri, M.; Čėnas, N.; Davioud-Charvet, E. *Plasmodium falciparum* ferredoxin-$NADP^+$ reductase-catalyzed redox cycling of plasmodione generates both predicted key drug metabolites: implictaion for antimalarial drug development. *ACS Infect. Dis.* **2021**, 7(7), 1996-2012; doi:10.1021/acsinfecdis.1c00054
6. **Lesanavičius, M.;** Boucher, J.-L.; Čėnas, N. Reactions of recombinant neuronal nitric oxide synthase with redox cycling xenobiotics: a mechanistic study. *Int. J. Mol. Sci.* **2022**, 23, 980, doi:10.3390/ijms23020980
7. **Lesanavičius M.;** Seo, D.; Čėnas, N. Thioredoxin reductase-type ferredoxin: $NADP^+$ oxidoreductase of *Rhodopseudomonas palustris*: potentiometric characteristics and reactions with nonphysiological oxidants. *Antioxidants*. **2022**, 11, 1000, doi:10.3390/antiox11051000

[1] - these authors are considered as equally contributed first-authors and are listed alphabetically

CONFERENCES[2]

1. **Lesanavičius, M**.; Aliverti, A.; Šarlauskas, J.; Čėnas, N. Electron transfer reactions of *Plasmodium falciparum* ferredoxin-NADP(+) reductase with nonphysiological oxidants. XVth international conference of the Lithuanian biochemical society, 2018 06 26 – 29, Dubingiai, Lithuania. Poster presentation.
2. Šarlauskas, J.; **Lesanavičius, M**.; Aliverti, A.; Čėnas, N. Reduction of nitroaromatic explosives by *Plasmodium falciparum* ferredoxin reductase: estimation of their single-electron reduction potentials. 21st International seminar New Trends in Research of Energetic Materials (NTREM 2018), 2018 04 18 – 20, Pardubice, Czech Republic. Poster presentation.
3. **Lesanavičius, M**.; Aliverti, A.; Šarlauskas, J.; Čėnas, N. Single-electron reduction of aromatic *N*-oxides by *Plasmodium falciparum* ferredoxin:$NADP^+$ oxidoreductase. XVII Young Research Fellow Meeting 2020, 2020 01 29 – 31, Caen, France. Poster presentation.
4. Nemeikaitė-Čėnienė, A.; Šarlauskas, J.; Jonušienė, V.; Misevičienė, L.; Marozienė, A.; **Lesanavičius, M**.; Čėnas, N. QSARs in prooxidant aerobic cytotoxicity of heteroaromatic N-oxides: Role of flavoenzyme-catalyzed single-electron reduction. Ninth international conference on radiation in various fields of research, 2021 06 14 – 18, Herceg Novi, Montenegro. Poster presentation.
5. **Lesanavičius, M**.; Boucher, J.-L.; Čėnas, N. The ‚outer-sphere' electron-transfer reactions of nitric oxide synthase with prooxidant xenobiotics. 20th International Symposium on Flavins & Flavoproteins, 2021 09 05 – 09, Graz, Austria. Poster presentation.
6. Cichocki, B.A.; Khobragade, V.; Donzel, M.; **Lesanavičius, M**.; Blandin, S.; Aliverti, A.; Čėnas, N.; Elhabiri, M.; Davioud-Charvet, E. A class of valuable (pro-)activity-based protein profiling probes: application to the redox-active antiplasmodial agent, plasmodione – Implication for antimalarial drug development, 20th International Symposium on Flavins & Flavoproteins, 2021 09 05 – 09, Graz, Austria. Poster presentation.

[2] Presenting authors are underlined

CURRICULUM VITAE

Personal information

Name, Surname	Mindaugas Lesanavičius
Date of birth	1987 01 30
e-mail address	mindaugas.lesanavicius@gmail.com mindaugas.lesanavicius@gmc.vu.lt

Education

2011 – 2015	Vilnius University, BSc in biochemistry
2015 – 2017	Vilnius University, MSc in biochemistry

Work experience

2021 10 – now	Vilnius University, junior scientist
2017 06 – 2022 07	Vilnius University, specialist

Skills acquired

Steady-state and presteady-state (stopped-flow, flash photolysis) enzyme kinetics assays (Cary60 UV-Vis, SX-20 spectrophotometers and accompanying software packages). Oxygen consumption assays. Electrochemistry. Enzyme-based biosensors. Enzyme purification. Derivation of rate equations. Basics in Wolfram language.

Academic visits

Laboratoire de Chimie Physique, Universite Paris-Sud, 91405 Orsay Cedex, France, 2018 10 14 – 27. Presteady-state kinetics. The use of stopped-flow methods for enzyme kinetics.

Universite de Strasbourg, Strasbourg, France, 2019 11 04 – 17. Investigation of plasmodione derivatives. Steady-state assays.

National Academy of Sciences, Lviv, Ukraine, 2017. Purification of flavocytochrome b_2 and its application in biosensors.

Languages

Lithuanian – native speaker; English – excellent; Russian, German, Latin – basics.

Online presence

Google Scholar, orcID, Scopus

NOTES

NOTES

NOTES

Vilniaus universiteto leidykla
Saulėtekio al. 9, III rūmai, LT-10222 Vilnius
El. p. info@leidykla.vu.lt, www.leidykla.vu.lt
bookshop.vu.lt, journals.vu.lt
Tiražas 15 egz.